PhD-FSTM-2024-007

The Faculty of Science, Technology and Medicine

DISSERTATION

Presented on 18/01/2024 in Luxembourg

to obtain the degree of

DOCTEUR DE L'UNIVERSITE DU LUXEMBOURG
EN INFORMATIQUE

by

Clément LACOSTE
Born on 20 February 1995 in Cagnes-sur-mer, France

RESOURCE DIMENSIONING OF BROADBAND SATELLITE RETURN NETWORKS AFFECTED BY RAIN FADE

Dissertation defense committee

Dr. Symeon Chatzinotas, Dissertation Supervisor
Professor and Head of SIGCOM, SnT, University of Luxembourg
Dr. Bhavani Shankar Mysore Rama Rao, Chairman
Assistant Professor, SnT, University of Luxembourg
Dr. Wallace Alves Martins, Vice-Chairman
Professor, ISAE-SUPAERO, Université de Toulouse, France
Dr. Giulio Colavolpe, Member
Professor, University of Parma, Italy
Dr. Athanasios D. Panagopoulos, Member
Professor, National Technical University of Athens, Greece

Resource dimensioning of broadband satellite return networks affected by rain fade

Clément Lacoste

Abstract

The use of Ka-band in satellite links has made rain attenuation a major concern in satellite network design. Fade mitigation techniques come at the expense of higher satellite resource consumption, such as bandwidth and power. An accurate estimation of this consumption is essential for the satellite service providers' business case, product strategy, and overall service pricing. However, the spatial correlation of rain fade introduces a high level of model complexity, and no method is currently available to compute its impact on resource consumption. Focusing on the return link of satellite broadband networks, this dissertation proposes a satellite resource dimensioning process that accounts for such a correlation in several scenarios, depending on the network's adaptability to rain fade.

Firstly, we investigate nonadaptive network scenarios and answer the following question: how can the long-term bandwidth requirement of the network be minimized, given a set of ground terminals, modulations and codings, and discrete bandwidths? We formally define the long-term carrier allocation problem and analyze current practical solutions. We subsequently investigate two other potential solutions, found to be more bandwidth-efficient: one based on heuristics and another based on mixed integer linear programming. Finally, we look at the impact of several parameters on the performance of those three methods. Overall, we observe marginal reductions in bandwidth, however, significant ($\geq$10%) gains are reached for networks with low numbers of terminals and low committed information rates.

Secondly, we investigate semi-adaptive network scenarios with the introduction of adaptive coding and modulation. However, these technologies come at the cost of higher complexity when designing the network's carrier plan and user terminals. Taking into account those issues is even more important when the satellite link uses frequencies in Ka-band and above, where rain attenuation is a major concern. To consider such phenomena, we reformulate the previously presented solutions to factor in spatially correlated attenuation time series, in the form of a mixed integer linear programming optimization problem. The numerical results for

a test scenario in Europe show significant bandwidth improvements.

Lastly, we investigate fully-adaptive network scenarios and introduce multibeam aspects. We formulate a quantile estimation problem based on the broadband service level agreements. Then, we solve this problem for a given confidence relative interval using spatially correlated rain fade sample generators. Finally, we provide numerical results for residential and enterprise broadband satellite scenarios, allowing us to determine the underestimation and overestimation of satellite resource consumption made by optimistic (independent) and pessimistic (fully correlated) rain fade assumptions, respectively. Results show that for both assumptions, the satellite resource consumption can be significantly underestimated or overestimated, thus proving the importance of considering the spatial correlation of rain fade in the satellite resource dimensioning problem.

Acknowledgements

First of all, I would like to thank my academic supervisors, Prof. Symeon Chatzinotas, Prof. Wallace Alves Martins, and Dr. Nicola Maturo, for their support and guidance. I am truly grateful for the culture of goodwill, curiosity, and freedom that surrounded me during my research, which undeniably brought significant personal and professional development. For this, I am also thankful to my past and present colleagues at SnT.

I would like to give a special thanks to my industrial supervisor Luis Emiliani from the Société Européenne des Satellites (SES), whose experience and passion for satellite communication systems have always been an inspiration for me. I would also like to thank Prof. Lorenzo Luini from Politecnico di Milano (Polimi), Dr. Xavier Boulanger from the Centre National d'Études Spatiales (CNES), and Dr. Julien Queyrel from the Office National d'Études et de Recherches Aérospatiales (ONERA) for their invaluable help with tropospheric attenuation models.

Last, but certainly not least, I would like to express my gratitude and love for my family and friends, whose support carried me through the ups and downs of this life-changing journey.

Clément Lacoste

Luxembourg, Nov 2023

Preface

This Ph.D. research project was carried out from December 2019 to December 2023, in the SIGCOM research group at the Interdisciplinary Centre for Security, Reliability and Trust (SnT), University of Luxembourg, under the supervision of Prof. Symeon Chatzinotas, Prof. Wallace Alves Martins (ISAE-SUPAERO), Dr. Nicola Maturo (ESA) and Mr. Luis Emiliani (SES S.A.). The time-to-time evaluation of the Ph.D. project was duly performed by the CET members constituting the supervisors and co-supervisors.

Support of the project

This work is supported by the Luxembourg National Research Fund (FNR) RELICA project, ref. 14610745, with industrial partner SES S.A. The views expressed in this work are those of the author and do not reflect the views of SES S.A. Additionally, the substantial support from SIGCOM is also gratefully acknowledged. The numerical simulations presented in this dissertation were carried out using the HPC facilities of the University of Luxembourg [1].[1]

Declaration

Except where acknowledged in the customary manner, the material presented in this dissertation is, to the best of the author's knowledge, original and has not been submitted in whole or part for a degree in any university.

[1] see http://hpc.uni.lu (visited on 24/11/2023).

Contents

1 Introduction **1**

1.1 Motivation . . . 1

1.1.1 The need for rural connectivity . . . 1

1.1.2 The role of satellite broadband . . . 2

1.1.3 Satellite broadband service pricing . . . 2

1.2 Dissertation outline . . . 4

1.3 Publication list . . . 5

1.3.1 Journals included in the dissertation . . . 5

1.3.2 Journal not included in the dissertation . . . 6

2 Background and contributions **7**

2.1 Broadband satellite networks . . . 7

2.1.1 Overview of satellite networks . . . 7

2.1.2 Overview of broadband satellite networks . . . 12

2.1.3 Service level agreement . . . 13

2.2 Satellite resource dimensioning . . . 15

2.2.1 Overview . . . 15

2.2.2 The impact of rain . . . 16

2.2.3 State of the art . . . 21

2.3 Dissertation contributions . . . 23

2.3.1 Constant coding and modulation . . . 23

2.3.2 Adaptive coding and modulation with static carrier plan . . . 24

2.3.3 Adaptive coding and modulation with adaptive carrier plan . . . 24

3 Constant coding and modulation **26**

3.1 Scenario description . . . 26

3.2 Carrier allocation . . . 27

3.2.1 Problem formulation . . . 28

3.2.2 Intuitive approach . . . 30

3.2.3 Mixed integer linear programming approach . . . 31

3.2.4 Heuristic approach . . . 32

3.2.5 Reducing the number of FMT modes in the network . . . 37

3.2.6 Complexity analysis . . . 38

3.3 Performance evaluation . . . 38

3.3.1 Simulation parameters . . . 39

3.3.2 Impact of the number of terminals and CIR . . . 41

3.3.3 Impact of the number of FMT modes . . . 43

3.4 Discussion . . . 43

3.5 Conclusion . . . 45

4 Adaptive coding and modulation with static carrier plan **47**

4.1 Scenario description . . . 47

4.2 Problem formulation . . . 50

4.2.1 FMT mode request time series . . . 51

4.2.2 Outage constraint through order relation . . . 52

4.3 Optimization problem . . . 54

4.3.1 Mixed integer linear programming . . . 54

4.3.2 Worst-case method . . . 56

4.4 Numerical results . . . 57

4.4.1 Test scenario . . . 57

4.4.2 Bandwidth performance . . . 60

4.4.3 Worst terminal outage . . . 61

4.5 Discussions . . . 63

4.5.1 MILP solver implementation . . . 63

4.5.2 Variability of rain . . . 63

4.5.3 RRM policy . . . 64

4.5.4 Heterogeneity for QoS and number of terminals . . . 64
4.6 Conclusion . . . 65

5 Adaptive coding and modulation with adaptive carrier plan 66
5.1 Scenario and assumptions . . . 67
5.1.1 SLA and QoS definitions . . . 67
5.1.2 Traffic SLA . . . 68
5.1.3 Availability SLA . . . 70
5.1.4 Network assumptions . . . 72
5.1.5 Satellite payload assumptions . . . 72
5.1.6 Link budget assumptions . . . 73
5.2 Formulation of the resource demand . . . 73
5.2.1 Transmission at a given rate . . . 74
5.2.2 Expression of the bandwidth demand . . . 76
5.2.3 Expression of the power demand . . . 77
5.2.4 Balanced FMT mode . . . 78
5.2.5 Ground station requirements . . . 79
5.2.6 Resource demand at system level . . . 80
5.3 Equivalent bandwidth quantile problem . . . 81
5.3.1 Computation of link outage time . . . 82
5.3.2 Expression of congestion outage time . . . 83
5.3.3 Formulation of the quantile problem . . . 83
5.4 Monte Carlo process . . . 84
5.4.1 Estimation of the bandwidth CDF . . . 85
5.4.2 Monte Carlo sampling . . . 86
5.4.3 Binomial confidence interval . . . 87
5.4.4 Confidence interval with given relative precision . . . 89
5.5 Scenario for numerical results . . . 91
5.5.1 Network parameters . . . 91
5.5.2 Basic link budget model . . . 93
5.5.3 Interference model . . . 96
5.5.4 Composite link budget model . . . 100

5.5.5 Satellite parameters . . . 100
5.5.6 Ground segment parameters . . . 104
5.5.7 Generation of rain samples . . . 107
5.6 Numerical applications . . . 108
5.6.1 Validation of Monte Carlo method . . . 108
5.6.2 Benchmarks . . . 110
5.6.3 Satellite resource comparison . . . 111
5.7 Discussions and conclusions . . . 115
5.7.1 Discussion on complexity . . . 115
5.7.2 Conclusions . . . 116

6 Conclusion and further work **117**
6.1 Conclusions . . . 117
6.2 Unsuccessful attempts . . . 118
6.2.1 Dirichlet distribution . . . 118
6.2.2 Machine learning . . . 119
6.3 Future work . . . 119

A Examples of traffic characterization **121**
A.1 Conversational audio/video . . . 121
A.2 Transactions . . . 122
A.3 Bulk . . . 122

B Computation of mode probability **124**
B.1 Monotonicity of $\bar{k}_n^{\mathrm{ci}}$ . . . 124
B.2 Detailed procedure . . . 126
B.3 Summarized procedure . . . 128

Bibliography **128**

List of Figures

1.1 Illustration of the satellite revenue chain. 3
1.2 Illustration of the dissertation contents. 5

2.1 Illustration of a satellite network. 8
2.2 Illustration of a ground station's components. 8
2.3 Illustration of transparent satellite payload. 10
2.4 Illustration of star and mesh topologies. 11
2.5 Illustration of the SRD process dependencies. 15
2.6 Attenuation as a function of frequency for a terminal located at (47.66°N, 5.45°E) and for an availability of 99.9%. 16
2.7 BER as a function of the SNR for the 8-PSK 2/3 ModCod scheme presented in [32]. 18
2.8 SE as a function of the SNR for a packet error rate of 10^{-7} and DVB-S2 ModCod schemes, as presented in [34]. 19
2.9 Illustration of the carrier plan, with the RRM algorithm executed every N superframes. 20

3.1 Representation of committed service slots for carrier type (k, l) with $Z_{k,l}^{\max} = 3$ and $N_{k,l} = 2$. 29
3.2 Illustration of Algorithm 1, blue squares represent re-allocated terminals. . . 34
3.3 Snapshot of the generated terminals (red = boat, blue = plane, other = terrestrial). 39
3.4 Histogram of terminal repartition among FMT modes. 41
3.5 Relative gain of B^{ilp} compared to B^{it} in function of number of terminals and R^{ci}. 42
3.6 Relative gain of B^{ilp} compared to B^{hr} in function of number of terminals and R^{ci}. 42

3.7 Proportion of unoccupied slots in the intuitive carrier plan as a function of the number of terminals and R^{ci}. 43
3.8 Impact of the restriction of the number of FMT modes on the bandwidth ($R^{\mathrm{ci}} = 2$ kbps, $N = 1,000$). 44

4.1 Illustration of the FMT mode demand and carrier plan, with $N = 4$ terminals and $K = 3$ FMT modes. 49
4.2 Illustration of Eq. (4.5) for ${}^{\uparrow}k_n\left(a_{n,t}\right) = 3$ 51
4.3 Complementary CDFs of (a) rain rate and (b) rain attenuation, averaged over terminals, obtained with ITU recommendations [64] and [30] (black solid curve) and with the MultiEXCELL [65] samples (red solid curve), as well as minimum and maximum (resp. min/max red dotted curves) CCDFs across all terminals obtained with MultiEXCELL samples. 57
4.4 Population density used for the terminal generation (right, inside red rectangle) as well as rain map example (left) over generated terminals (black dots) . . . 58
4.5 Relative bandwidth gain $(B^{\mathrm{wc}} - B^{\mathrm{milp}})/B^{\mathrm{wc}}$ and solver gap $(B^{\mathrm{milp}} - B^{\mathrm{lb}})/B^{\mathrm{milp}}$ as a function of p^{out} with (a) BOE and (b) EOB scenarios. 61
4.6 Evolution of B^{milp} and B^{wc} as a function of p^{out} with (a) BOE and (b) EOB scenarios. 62
4.7 Comparison of p^{wto} for the worst case and the MILP methods as a function of requested p^{out}, with (a) BOE and (b) EOB scenarios. 63

5.1 Illustration of the chapter's contents. 66
5.2 Illustration of the multibeam BSM return network scenario. The satellite-dependent path is delimited by the *satellite-independent service access point* (SI-SAP) interfaces. 68
5.3 Illustration of the bandwidth vs. PEB (i.e., power) demand tradeoff for a transmission at committed rates. Here, $k_n^{\mathrm{msr}}\left(\mathbf{a}_{n,t}^{\mathrm{tot}}\right) = 5$. 78
5.4 Illustration of the resource demand model at the terminal level 79
5.5 Tree of possible outage causes 84
5.6 Illustration of cases where $P\left(b^{\mathrm{eq,TD}}\left(\mathbf{A}_{t^{\mathrm{sup}}:T}^{\mathrm{tot}}\right) - b^{\mathrm{eq,TD}}\left(\mathbf{A}_{t^{\mathrm{inf}}:T}^{\mathrm{tot}}\right) \leq \delta^{\mathrm{B}} \cdot b^{\mathrm{eq,cs}}\right) \approx 1$ (up) and $P\left(b^{\mathrm{eq,TD}}\left(\mathbf{A}_{t^{\mathrm{sup}}:T}^{\mathrm{tot}}\right) - b^{\mathrm{eq,TD}}\left(\mathbf{A}_{t^{\mathrm{inf}}:T}^{\mathrm{tot}}\right) \leq \delta^{\mathrm{B}} \cdot b^{\mathrm{eq,cs}}\right) \ll 1$ (down). . . 90

5.7 Example of beam footprint over France. The dotted black ellipse shows the 4.3-dB contour. 102
5.8 Example of population coverage over Europe. Black ellipses represent the 4.3-dB contour. 105
5.9 Comparison of the average power needed among terminals to satisfy the clear sky (blue) and fade (red) requirements, for residential and enterprise scenarios. 114

B.1 Illustration of the joint probability space 127

List of Tables

2.1 BSM access network scenarios showed in [21] 12

3.1 Simulation link parameters 40

4.1 Simulation link parameters 59

4.2 DVB-RCS2 FMT mode parameters 59

5.1 List of private satellite broadband offers in France on 04/09/2023 92

5.2 DVB-RCS2 ModCod parameters 94

5.3 Parameters for results scenario 103

5.4 Statistics obtained with the validation method. 109

5.5 Comparison of bandwidth, absolute values in MHz, $\Delta^{\min}$ in % of $b^{\min}$. 112

5.6 Comparison of average annual rain probability P_n^{rain} and average uplink attenuation $\bar{F}_{A_n}^{-1}(p_{s_n}^{\text{adv}})$ for an exceedance probability $p_{s_n}^{\text{adv}} = 0.5\%$. 113

Abbreviations

ACM	Adaptive coding and modulation
ACP	Adaptive carrier plan
ATM	Asynchronous transfer mode
BER	Bit error rate
BOE	Bandwidth over equipment
BSM	Broadband satellite multimedia
CAPEX	Capital expenditure
CCDF	Complementary cumulative distribution function
CCM	Constant coding and modulation
CDF	Cumulative distribution function
CINR	Carrier-to-interference-plus-noise ratio
CIMR	Carrier-to-intermodulation ratio
CIR	Committed information rate
CNR	Carrier-to-noise ratio
CPO	Carrier plan optimization
DVB-RCS	Digital video broadcasting - return channel via satellite
DVB-S	Digital video broadcasting via satellite
EIRP	Equivalent isotropic radiated power
EOB	Equipment over bandwidth
ETSI	European Telecommunication Standard Institute
FMT	Fade mitigation technique
GEO	Geostationary orbit
HEO	High Earth orbit
IBO	Input back-off
IP	Internet protocol

ITU	International Telecommunication Union
Ka	Kurz-above
Ku	Kurz-under
LEO	Low Earth orbit
MEO	Medium earth orbit
MF-TDMA	Multi-frequency time-division multiple access
MILP	Mixed integer linear programming
NSR	Northern Sky Research
OBO	Output back-off
OPEX	Operational expenditure
PEB	Power-equivalent bandwidth
QoS	Quality of service
RRM	Radio resource management
SatCom	Satellite communication
SCP	Static carrier plan
SI-SAP	Satellite-independent service access point
SLA	Service level agreement
SNR	Signal-to-noise ratio
SP	Service package
SRD	Satellite resource dimensioning
SVM	Support-vector machine
VSAT	Very small aperture terminal

Notations

$\mathbf{A}$	Denotes a matrix.
$\mathbf{a}$	Denotes a row vector.
$\mathcal{C}$	Denotes a set.
$\mathbb{R}_+$	The set of strictly positive real numbers.
$\mathcal{I}_N$	The set of integers from 1 to $N \in \mathbb{N}$.
$\lvert\mathcal{C}\rvert$	The cardinality of set $\mathcal{C}$.
$\lceil x \rceil$	Least integer greater than or equal to $x \in \mathbb{R}$.
$\lfloor x \rfloor$	Greatest integer smaller than or equal to $x \in \mathbb{R}$.
$\mathbb{1}_A$	The indicative function of the statement A, equal to one if A is true, zero otherwise.
$\mathbb{E}(X)$	The expected value of the random variable X.
$\mathbf{a}^\intercal$	Transpose of vector $\mathbf{a}$.

Chapter 1

Introduction

1.1 Motivation

1.1.1 The need for rural connectivity

The idea of universal Internet access is nowadays a very real objective of the United Nations. Among the seven Advocacy targets of the Broadband Commission defined by the *International Telecommunications Union* (ITU) report [2], the following two establish clear objectives for worldwide Internet access:

- Target 2: "By 2025, entry-level broadband services should be made affordable in developing countries at less than 2 percent of monthly gross national income (GNI) per capita."
- Target 3: "By 2025, Broadband-Internet user penetration should reach: a) 75 percent worldwide, b) 65 percent in developing countries, c) 35 percent in least developed countries."

The report acknowledges that connecting rural areas is essential to meet these objectives. It is further explained in [3, pp. 6-7], which states that the percentage of Internet penetration for urban populations is 82% vs. 46% for rural populations worldwide.

Aside from personal Internet access, certain commercial and institutional applications require rural connectivity, such as:

- Remote point-of-sales, such as retail stores, rental services, or gas stations, which require credit card authentication.

- Banking, used for stock exchange and ATM services.
- Energy, such as oil and gas extraction on remote sites or supervisory control and data acquisition networks.
- Onboard connectivity for planes, boats, and trains.
- Military and government projects.

1.1.2 The role of satellite broadband

Satellite broadband is a natural solution to bring Internet access in rural areas, due to the ubiquitous nature of its coverage [4, Section 1]. According to the 2023 *Northern Sky Research* (NSR) industry report [5], the satellite broadband market generated around 7 billion dollars of revenue in 2022. Moreover, the report forecasts a sharp increase in satellite capacity demand over the next 10 years, especially in developing regions of the globe.

However, satellite broadband is currently far from being the go-to solution for rural connectivity. The NSR report estimates that over 400 million households could benefit from satellite services, but only a fraction are currently using satellite broadband. Competitive service pricing is highlighted as a "key variable" to the growth of satellite broadband revenues. This concurs with observations made in the European Commission report [6]: over the 12 examples of rural broadband deployments, only one chose satellite broadband as a (partial) solution. The report mentions the following drawbacks for satellite solutions: high latency (mostly dependent on the satellite's orbit), unreliability (due to weather sensitivity), and high cost.[1] Thus, it is crucial for satellite service providers to achieve good quality of service at the lowest price possible.

1.1.3 Satellite broadband service pricing

The price of offered services in broadband satellite networks is influenced by multiple actors in the revenue chain, from the satellite manufacturer to the satellite service provider [7], as shown in Fig. 1.1. The cost of a satellite network can be divided into two components: the *operational expenditure* (OPEX) and the *capital expenditure* (CAPEX). From the perspective of a satellite service provider, the former relates to recurring costs throughout the network's

[1] The report redirects to the link https://geolinks.com/best-rural-internet-options/ (visited on 14/11/2023) for a list of pros and cons of various connectivity solutions.

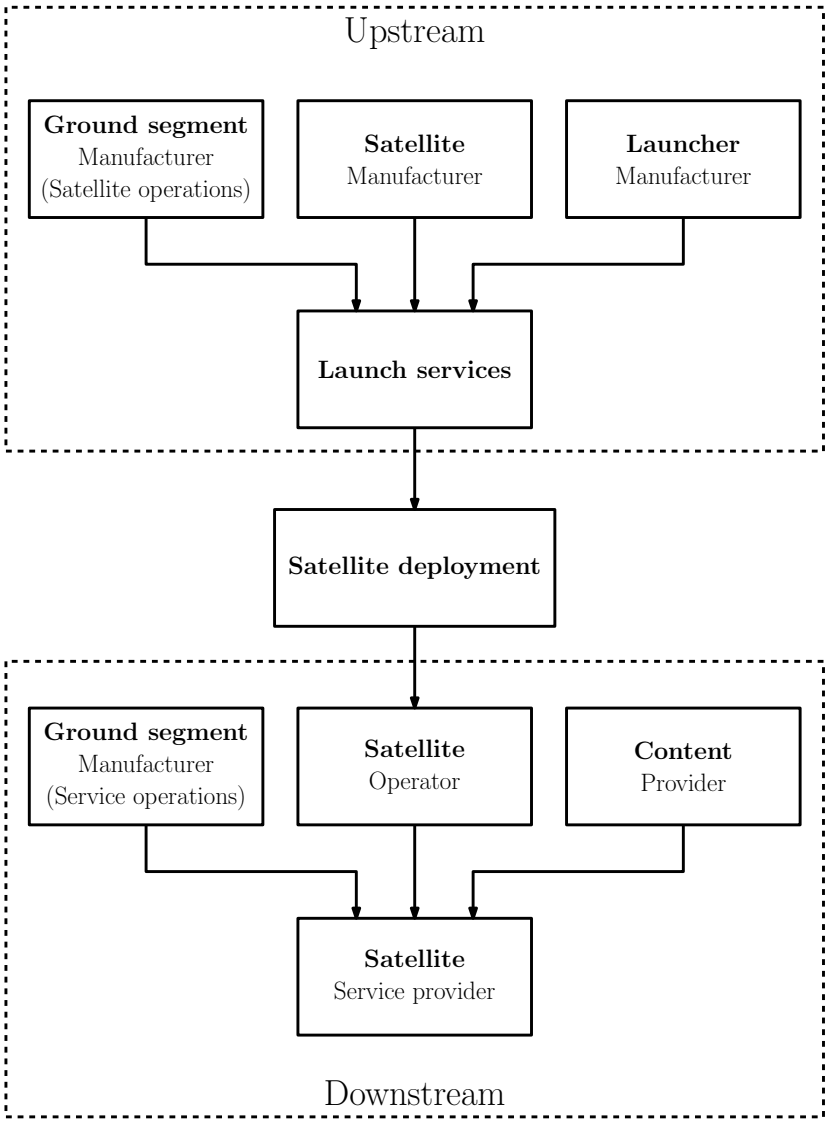

Figure 1.1: Illustration of the satellite revenue chain.

lifetime (e.g., lease of satellite resources, ground station maintenance), while the latter refers to one-time expenses, usually necessary for the service activation (e.g., ground station purchase and installation).

One of the main OPEX components is the lease of satellite resources necessary to operate a network with given requirements. The satellite resources influencing the cost of the lease are typically the transponder bandwidth and power [8, Section 1.3.1] [9, Chapter 13], [10, p. 29]. Determining the appropriate amount of satellite resources for a given network is done through a process that we call *satellite resource dimensioning* (SRD) in this dissertation, although other denominations exist, such as network sizing or network planning.

One key part of such a process is to determine the impact of rain fade on the system's performance. Indeed, for networks operating in the Ka-band and beyond, the attenuation of the radio signal due to rain can reach high values [11]. *Fade mitigation techniques* (FMTs) are needed to avoid the degradation of the quality of service below acceptable level [12]. However, some FMTs, such as *adaptive coding and modulation* (ACM) [13], will maintain the service quality in case of rain fade by increasing the satellite resource consumption compared to non-rainy conditions. Thus, the vulnerability to rain fade implies that the dimensioning process should factor in a resource margin, depending on the desired quality of service.

1.2 Dissertation outline

In this dissertation, we focus on the impact of rain fade on the dimensioning of satellite return link resources, in the context of broadband satellite networks. The dissertation is organized as follows:

- Chapter 2 presents the technical background needed to understand the SRD problem. It introduces in Section 2.2.2 two FMTs that have a deep impact on the SRD problem: the first one is the adaptability of the coding and modulation scheme, and the second one is the adaptability of the carrier plan. Finally, a literature review of existing solutions is presented and the contributions of this dissertation are highlighted.

- Chapter 3 investigates the SRD problem in the context of *constant* (i.e., nonadaptable) *coding and modulation* scheme (CCM) and *static* (i.e., nonadaptable) *carrier plan* (SCP). Starting from simple service requirements, a carrier allocation problem is formulated and several solutions of varying complexity are compared through numerical simulations.

- Chapter 4 investigates the SRD problem in the context of ACM scheme and SCP. The spatial correlation of rain is introduced in the SRD problem using synthetic rain fade simulators. An optimization problem is presented to solve the SRD problem and is compared to existing solutions through numerical simulations.

- Chapter 5 investigates the SRD problem in the context of ACM and *adaptive carrier plan* (ACP). More complex assumptions are made in this chapter, including the service requirements, the satellite resource demand model, and the introduction of multibeam

aspects. A method to solve the SRD problem within a given confidence interval using synthetic rain fade simulators is presented and validated through numerical simulations.

- Finally, Chapter 6 presents the general conclusions and the future lines of work.

Fig. 1.2 illustrates the dissertation contents and the related publications listed in Section 1.3.1.

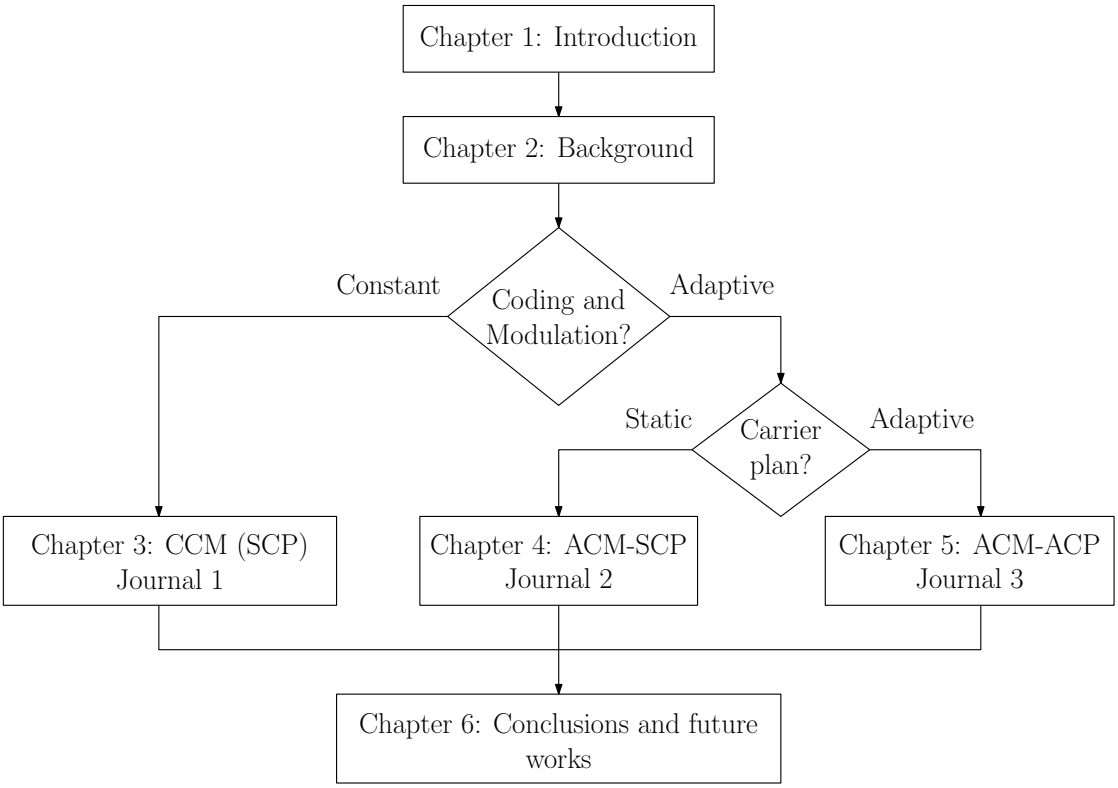

Figure 1.2: Illustration of the dissertation contents.

1.3 Publication list

1.3.1 Journals included in the dissertation

The work presented in this dissertation has led to the publication of three journal articles that are fully covered in this dissertation:

1. C. Lacoste, N. Maturo, S. Chatzinotas, L. Emiliani, "Optimization of the return link carrier planning for a constant coding, modulation satellite network," *Frontiers in Communications, Networks,* vol. 2, p. 52, Oct. 2021, ISSN: 2673-530X. DOI: 10.3389/frcmn.2021.744998, *(published).*

2. C. Lacoste, W. A. Martins, S. Chatzinotas, L. D. Emiliani, "Inbound carrier plan optimization for adaptive VSAT networks," *IEEE transactions on aerospace and electronic systems*, vol. 59, no. 2, pp. 1–16, 2023, ISSN: 0018-9251. DOI: 10.1109/TAES.2022.3194502, *(published)*.

3. C. Lacoste, W. A. Martins, S. Chatzinotas, L. D. Emiliani, "Resource dimensioning of broadband satellite return networks affected by spatially-correlated rain fade," *IEEE transactions on aerospace and electronic systems*, 2023, *(submitted)*, preprint on TechRxiv: https://doi.org/10.36227/techrxiv.24106125.v1.

1.3.2 Journal not included in the dissertation

The following publication was written during the Ph.D., but was not included in the dissertation for the sake of consistency:

1. G. Fontanesi, F. Ortíz, E. Lagunas, V. Monzon Baeza, M. Á. Vázquez, J. A. Vásquez-Peralvo, M. Minardi, H. N. Vu, P. J. Honnaiah, C. Lacoste, Y. Drif, T. S. Abdu, G. Eappen, J. Rehman, L. M. Garcés-Socorrás, W. A. Martins, P. Henarejos, H. Al-Hraishawi, J. C. Merlano Duncan, T. X. Vu, and S. Chatzinotas, "Artificial intelligence for satellite communication, non-terrestrial networks: A survey," *IEEE Communications Surveys, Tutorials*, 2023, *(submitted)*, preprint on ArXiv: https://doi.org/10.48550/arXiv.2304.13008.

Chapter 2

Background and contributions

2.1 Broadband satellite networks

In this section, we present the background knowledge needed to understand what broadband satellite networks consist of.

2.1.1 Overview of satellite networks

Satellite networks are primarily characterized by the orbit of the satellites. Circular Earth-centered orbits are usually categorized into three altitude regions (above mean sea level) [8, Chapter 2]:

- *Low Earth orbit* (LEO) for less than 2,000 km of altitude.
- *Medium Earth orbit* (MEO) between 2,000 and 35,786 km.
- *High Earth orbit* (HEO)[1] for more than 35,786 km.

One special orbit at 35,786 km of altitude, called *geostationary orbit* (GEO), offers the specific advantage of matching the satellite's orbital period with the Earth's rotation period, thus the satellite's coverage appears fixed from a fixed observer viewpoint on the Earth. Another advantage compared to LEOs and MEOs is the larger field of view of the satellite, covering around one-third of the Earth's surface. Because of these particularities, the GEO has been historically the most utilized orbit for telecommunication systems [14, Chapter 3]. However, the NSR industry report [5] highlights that non-GEO solutions[2] have increasingly gained a

[1] HEO is sometimes used for *highly elliptical orbit*, see [8, Section 2.2.1] for more details.
[2] See [15, Section II.A] for a survey on non-geostationary satellite Internet.

larger share of the total broadband satellite market over the past few years. Nonetheless, we will focus on the more mature GEO broadband networks in this dissertation.

Fig. 2.1 illustrates the main hardware components typically found in satellite networks. These are divided into two categories: the ground segment, in blue, and the space segment, in red. Note that we will focus on the return link in this dissertation. The reasons for this choice are explained further down in Section 2.2.2.

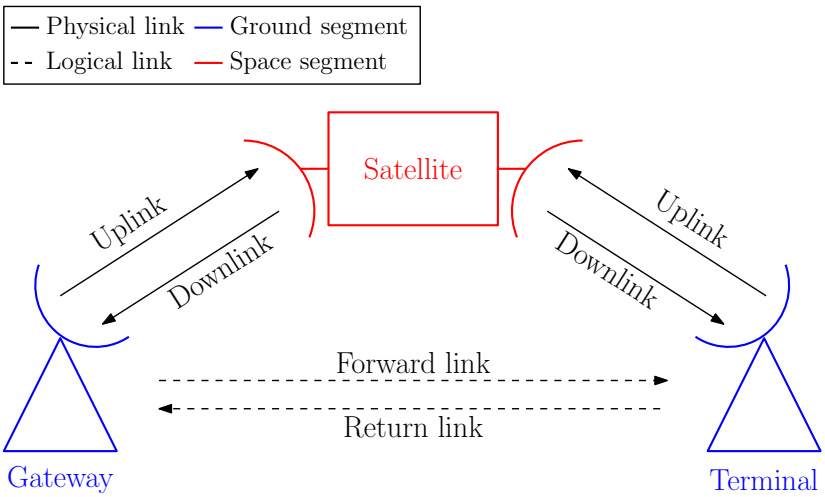

Figure 2.1: Illustration of a satellite network.

The ground segment

Both the gateway and the terminals are ground stations. A typical ground station is organized as illustrated in Fig. 2.2 [8, Section 8.1]. Gateways are usually equipped with larger antenna

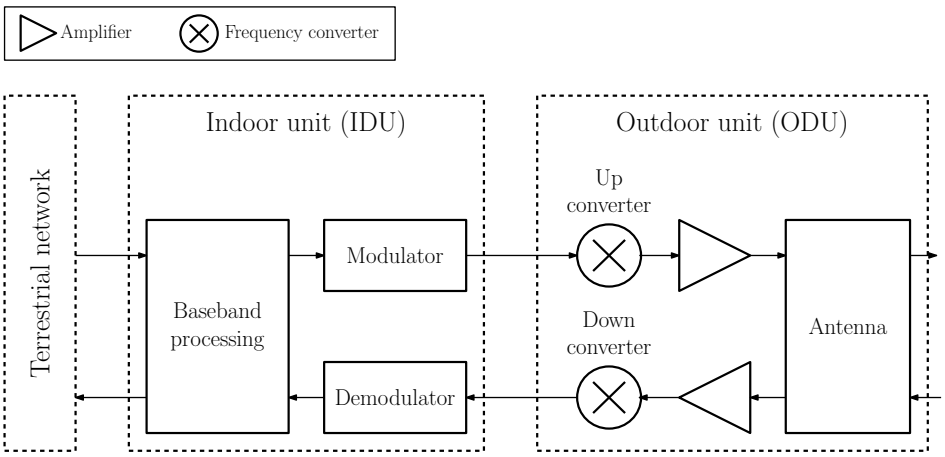

Figure 2.2: Illustration of a ground station's components.

diameters and higher power amplifiers than terminals. The gateway is connected to the network providing the services (e.g., Internet via Internet exchange points), while the terminal is connected to the users' local area network.

The space segment

The space segment is composed of the satellite, which consists of the payload and the platform [8, Section 1.3]. The payload consists of all the satellite equipment dedicated to the radio transmissions, while the platform consists of all the remaining satellite equipment that supports the payload operations. Typical platform subsystems are:

- Attitude and orbit control.
- Propulsion.
- Electric power supply.
- Telemetry, tracking, and command.
- Thermal control.
- Structure.

In this dissertation, we will assume the payload is "transparent", i.e., it does not demodulate and regenerates the received signal.

The satellite payload has two resources available for allocation: bandwidth and power. These resources are usually distributed inside the satellite payload among several independent chains called "transponders" [8, Section 1.3.2]. Each transponder corresponds to a physical amplification chain, as illustrated in Fig. 2.3.

Two pieces of equipment influence the available resources. The bandpass filter determines the bandwidth allocated to the transponder, and the amplifier determines the power allocated to the transponder. Traditionally, the transponder configuration is fixed and determines its capacity. Hence, the physical equipment itself is leased, with the billing being based on the resource that is proportionally used the most [8, Section 1.3.1], [9, Chapter 13]. However, with the recent advances in adaptive payload technologies such as multiport amplifiers [16] and digital transparent processors [17], it can be more relevant for modern satellite systems to look at the aggregated satellite resources. In such a case, the aggregated bandwidth is defined

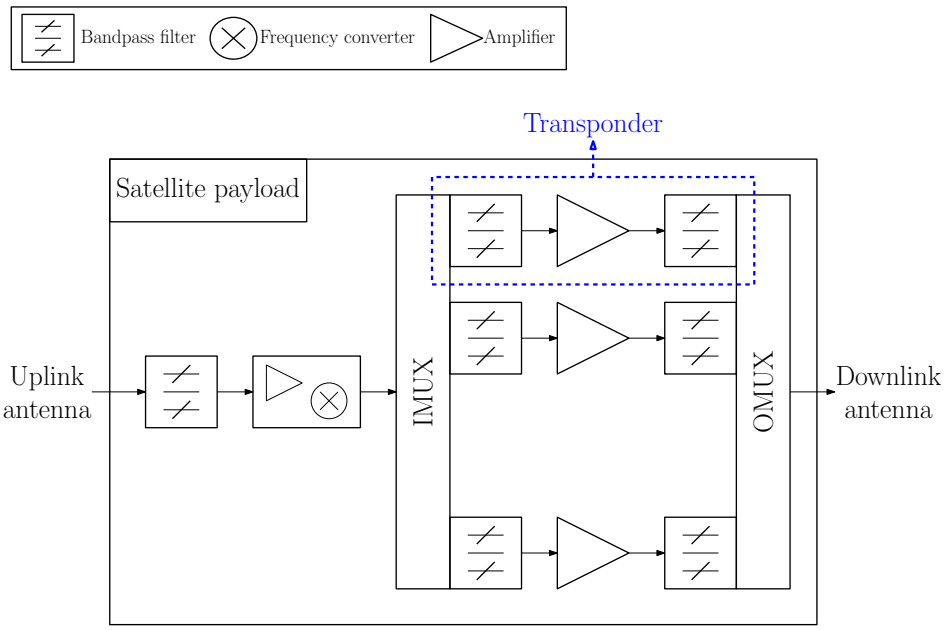

Figure 2.3: Illustration of transparent satellite payload.

as the radio spectrum multiplied by the frequency reuse factor, while the aggregated power is defined as the sum of active amplifiers' output power.

The price of satellite resources is determined by the satellite operator and is driven by the cost of radio spectrum license and orbital position plus the cost of building, launching, deploying, and operating the satellite [9, Chapter 13]. The majority of these expenses happen at the satellite's beginning of life and the pricing of resources is determined to compensate for these expenses throughout the expected lifetime of the satellite, usually 15 years for GEO satellites.

Satellite network topologies

The logical connections between ground stations usually follow either a star or mesh topology, as illustrated in Fig. 2.4 [18, Section 4.7]. Terminals connected in a star topology only communicate with the gateway, while terminals connected in a mesh topology communicate directly with each other.[3] Two terminals can communicate using the star topology only through the intermediacy of the gateway. Thus, the mesh network has the advantage of lower delay for terminal-to-terminal communications. However, gateways often have significantly

[3]In the mesh topology case, the definition of forward and return links depends on the terminal point of view, although the forward name is sometimes attributed to the link that requires the highest rate, e.g., in the case of a data transfer.

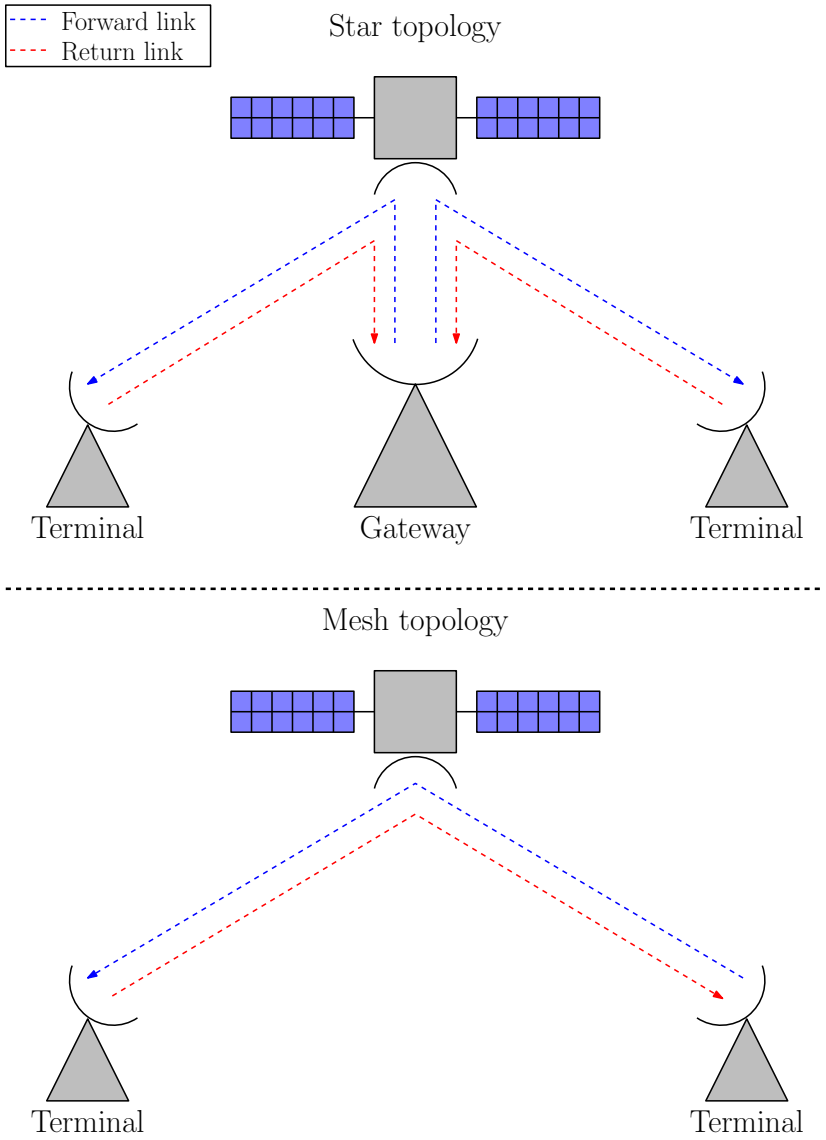

Figure 2.4: Illustration of star and mesh topologies.

more transmission capabilities (antenna size and amplification power) than terminals. This allows to reduce the transmission requirements, and consequently the cost, of terminals using star networks. Due to this cost advantage, star networks are well-suited for satellite networks with gateways serving a massive number of terminals, such as broadcast television or residential broadband access [9, Chapter 8]. On the other hand, mesh topology networks are only found for specific enterprise and government applications that require point-to-point connectivity. Star topology networks are the most prevalent topology for GEO satellite networks and we focus on those in this dissertation.

2.1.2 Overview of broadband satellite networks

Broadband satellite networks designate satellite networks capable of supporting interactive (i.e., forward and return links) multimedia applications. With the growth of broadband networks, the *European Telecommunication Standard Institute* (ETSI) has surveyed existing satellite broadband networks in [19] and [20]. The general acronym *broadband satellite multimedia* (BSM) network was proposed to designate such networks. Since then, the ETSI has published and continues to publish technical reports and specifications regarding BSM networks. These documents help us understand the core aspects and challenges of BSM networks. The technical report [21] gives an overview of the services, roles, and equipment related to the BSM context.

BSM scenarios

The BSM scenarios as defined in [21, Section 4.2] are presented in Table 2.1.[4] We can see that

Access network scenarios	**Point-to-point**	**Multicast**	**Broadcast**
Corporate intranet	Corporate VSAT[a] network Site interconnections	Corporate Multicast Data distribution Video conferencing	Datacasting TV broadcast (private)
Corporate Internet	Internet access via corporate ISP[b] or via third party ISP	IP multicast RT[c] streaming ISP caching	ISP caching
SME[d] intranet	Small VSAT network	SME multicast	
SME Internet	Internet access via third party ISP	IP multicast RT streaming ISP caching	ISP caching
SOHO[e]	Internet access via ISP Company access via VPN[f]	IP multicast RT streaming ISP caching	ISP caching
Residential	Internet access via ISP	IP multicast RT streaming ISP caching	ISP caching

[a] VSAT: *very small aperture terminal.*
[b] ISP: *Internet service provider.*
[c] RT: *real-time.*
[d] SME: *small and medium-sized enterprises.*
[e] SOHO: *small office/home office.*
[f] VPN: *virtual private network.*

Table 2.1: BSM access network scenarios showed in [21]

[4] See https://www.ses.com/find-service for a more up-to-date overview of BSM satellite scenarios (visited on 04/12/2023)

BSM networks must support a wide range of services for different types of clients. It is thus not surprising that BSM networks are implemented in different ways based on which services should be delivered to the client. Therefore, it is crucial to establish a reference framework to translate service needs into BSM network requirements. This is typically the role of a document called the *service level agreement* (SLA).

2.1.3 Service level agreement

The ITU defines in [22, Section 5.1] the SLA as follows:

> "A service level agreement is a formal agreement between two or more entities that is reached after a negotiating activity with the scope to assess service characteristics, responsibilities and priorities of every part.
>
> A SLA may include statements about performance, billing, service delivery but also legal and economic issues.
>
> The part of SLA which refers to the *quality of service* (QoS) is called QoS Agreement and includes formal program agreed between two entities to monitoring, measuring and deciding QoS parameters. The goal is to reach the QoS agreed with end user and then obtain its satisfaction."

General service quality characteristics are presented in [23, Annex A.5] and are:

- Speed: It characterizes the aspects of temporal efficiency associated with a function. It is defined by measurements made on sets of time intervals.
- Accuracy: It characterizes the degree of correctness with which a particular function is realized. This type of parameter is based on either the ratio of incorrect realizations on total attempts or the rate of incorrect realizations during an observation period.
- Reliability (or dependability): It expresses the degree of certainty with which a function is performed. This type of parameter is based on either the ratio of failures on total attempts or the rate of failures during an observation period.

Based on these recommendations, the definition of QoS characteristics is quite wide, in order to accommodate for the vast variety of services present in broadband networks. More refined QoS metrics are found in [24] and [25], however, they reveal a large variation of

QoS characteristics depending on the service's nature. It should also be noted that BSM actors sometimes use QoS metrics outside of the standard frameworks. Finally, note that with the progress made in adaptive resource allocation technologies and the emergence of satellite-as-a-service models, changes to traditional SLA frameworks are being proposed [26, Section 7.5].

In this dissertation, in order to make assumptions as generic as possible, basic QoS requirements are assumed [26, Section 7.1]. They consist of a percentage of time, called service availability, during which a *committed information rate* (CIR) must be delivered at a given *bit error rate* (BER). More insights into the role of SLAs in the SRD process are given in Chapter 5.

Actors of broadband satellite networks

Several roles for BSM network actors are presented in [21, Section 5]:

- The satellite operator deploys and operates the satellite platform. It sells transponder capacity to satellite network operators.
- The satellite network operator deploys and operates the satellite network. It leases satellite transponders and provides the associated ground segment equipment. It offers a given coverage and bandwidth to network access providers.
- The network access provider manages and operates the network access elements in the satellite terminals and one or more gateways. It buys the services of one or more satellite network operators and sells bulk transmission resources to the service providers for use by their subscribers. The network access provider is linked to each service provider by a contract specifying the SLA.
- The service provider manages and operates the related service provider elements in the satellite terminals and one or more gateways. They buy bulk capacity from the network access provider and resell that capacity to their subscribers.
- The subscriber buys services from one or more service providers. The subscriber can subscribe to services for one or several satellite terminals, and each satellite terminal can serve one or more end users.
- The user is the entity that makes use of the services.

Based on the roles listed, it becomes clear that the cost of the transponder capacity lease on the network access provider's side impacts the price of the SLA contracted with the service providers. This, in turn, impacts the price the service provider charges to its subscribers. Thus, there is an indirect relationship between the price of services and the amount of transponder capacity needed to deliver these services. Determining the capacity amount given the services is the objective of the SRD process.

2.2 Satellite resource dimensioning

In this section, we introduce the background knowledge relative to the SRD problem and present the current state of the art.

2.2.1 Overview

The goal of the SRD process is to determine the amount of transponder capacity needed to deliver the satellite services, given the SLA [9, Chapter 9]. Fig. 2.5 illustrates the dependencies of this process. It is in the best interest of the network access provider and the service provider that the SRD is done as precisely as possible. On the one hand, underestimating the satellite resource amount cannot guarantee the satisfaction of the contracted SLA, and a violation of SLA will have to be compensated by the service provider, for example by granting a credit

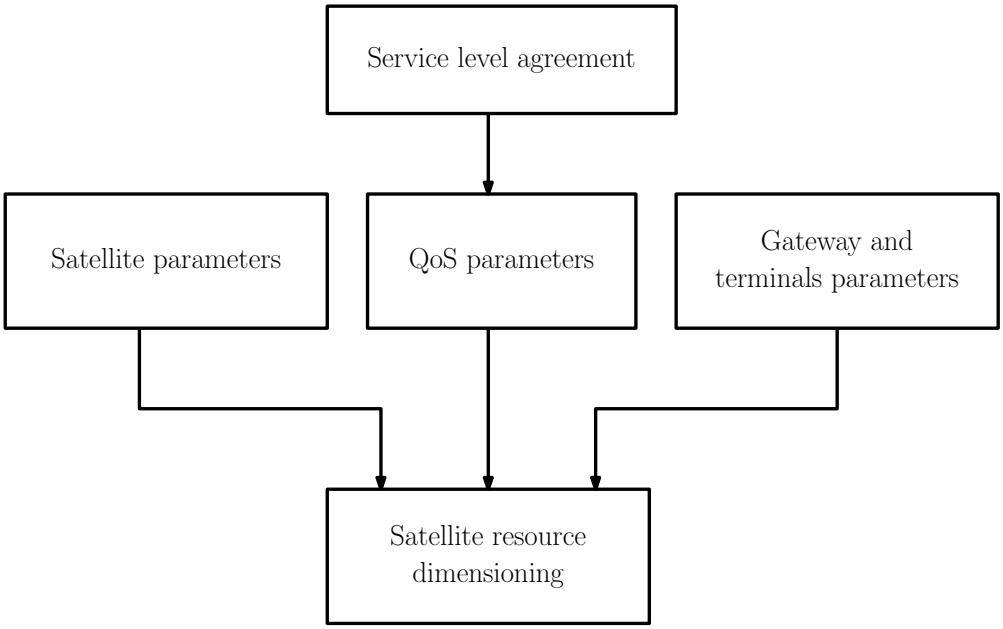

Figure 2.5: Illustration of the SRD process dependencies.

to the customer [26, Section 7.1]. On the other hand, overestimating said amount will drive prices up, making the services unattractive in the face of a competitive market.

2.2.2 The impact of rain

More spectrum is available in less occupied spectrum regions, mainly higher frequency bands such as Ku, Ka, and now Q/V bands. Such bands are of high interest to broadband satellite actors [27]. However, using higher frequency bands comes with several technological challenges [28]. Among them is the attenuation induced by tropospheric phenomena.

Due to the complexity of such phenomena, the attenuation induced by rain is usually assumed to be a random variable. A vast literature of rain attenuation models for satellite communication applications is available [29]. The most popular model is the statistical ITU model presented in [30]. Given a desired availability percentage and various radio link parameters, the model computes the attenuation from various tropospheric phenomena (rain, clouds, gases, scintillation) that are not exceeded for the corresponding percentage of time. This approach allows BSM actors to measure the impact of rain attenuation on the availability percentage expressed in the SLA, which also accounts for other causes of outage.

Fig. 2.6 shows the total tropospheric attenuation and the rain attenuation obtained by the ITU model [30] for a terminal located at (47.66°N, 5.45°E) and for an availability of 99.9%. The rain is the major contributor to the total attenuation in the Ku and Ka bands, while

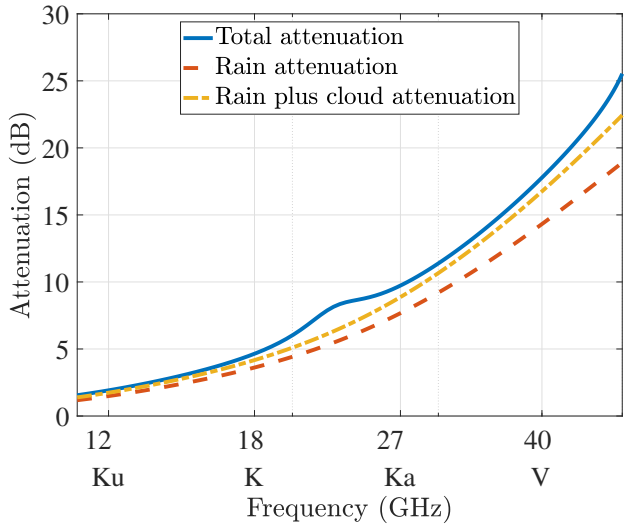

Figure 2.6: Attenuation as a function of frequency for a terminal located at (47.66°N, 5.45°E) and for an availability of 99.9%.

the clouds' attenuation becomes important beyond the V band. V band satellite links are currently at an experimental stage [31]. Therefore, we chose to focus on the Ka-band and the impact of rain attenuation in this dissertation.

Fade mitigation techniques

The tropospheric attenuation above the Ku band can reach significant values and cause severe degradation of the link's quality. Some protection against fade events is thus required. Traditionally, a power margin is added to the link budget to compensate for such fade events [8, Section 5.8]. However, the attenuation in the Ka-band reaches such high values that having a permanent high power margin in the satellite link becomes impractical.

With the rise of adaptive satellite links, and given the stochastic nature of tropospheric phenomena, FMTs are implemented in Ka-band satellite links. The authors of [12] present a survey on FMTs, organized into three main categories:

- EIRP control techniques. Examples are uplink power control and beam shaping.
- Adaptive transmission techniques. Examples are ACM and data rate reduction.
- Diversity protection schemes. Examples are site diversity or frequency diversity.

Implementing each FMT technique comes at a cost, thus not all techniques are found in all satellite networks. The well-known DVB-RCS2 [32] standard gives us an idea of what is usually found in BSM return links. The standard proposes the implementation of ACM inside a *multi-frequency time-division multiple access* (MF-TDMA) scheme. We will see that the adaptability of both *modulation and coding* (ModCod) and MF-TDMA schemes plays an important role in SRD.

Adaptive coding and modulation

The BER is a function of the *signal-to-noise ratio* (SNR), of which the expression depends on the ModCod scheme used by the transmission [8, Chapter 4]. The general behavior is that the BER decreases when the SNR increases (see Fig. 2.7). Thus, given a ModCod scheme, we can determine the minimum SNR required to achieve a specific BER. Such an SNR value is called the activation threshold of the ModCod scheme.

In the presence of a fade event, the SNR will decrease. Thus, for a given ModCod scheme, the BER will potentially rise above acceptable levels. To prevent this, ACM proposes to

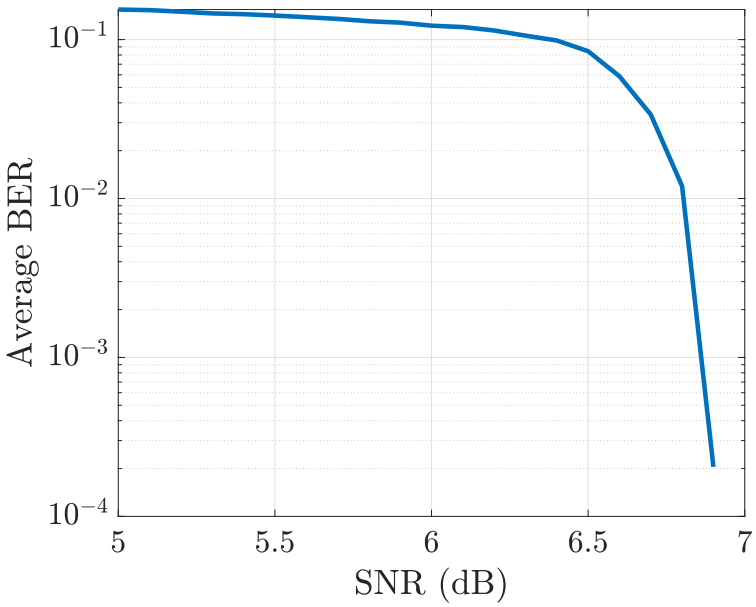

Figure 2.7: BER as a function of the SNR for the 8-PSK 2/3 ModCod scheme presented in [32].

dynamically change the ModCod scheme of the transmission to one with a lower activation threshold [33, Section 2.3.2]. The new ModCod scheme is said to be more "robust" or power efficient. However, using a more robust ModCod scheme comes with the tradeoff of decreasing the *spectral efficiency* (SE), i.e., the information rate per Hz (see Fig. 2.8). Thus, when switching to a more robust ModCod scheme, the bandwidth must be increased to maintain the information rate above the committed level.

In summary, the ACM technology allows maintaining a constant bitrate and BER in the presence of fade at the expense of higher satellite resource consumption than in non-rainy conditions. In the presence of ACM, it is crucial that the rain attenuation is accounted for in SRD to ensure the satisfaction of the SLA. In opposition to the ACM technology, CCM refers to links that are unable to adapt their ModCod schemes to attenuation conditions. In this dissertation, we provide solutions to the SRD problem for networks using both CCM (Chapter 3) and ACM (Chapters 4 and 5) technologies.

Adaptability of the carrier plan

The number of terminals in BSM networks can be high, and simultaneous transmission of several terminals on the return link is likely. To avoid interference, an access method is put in

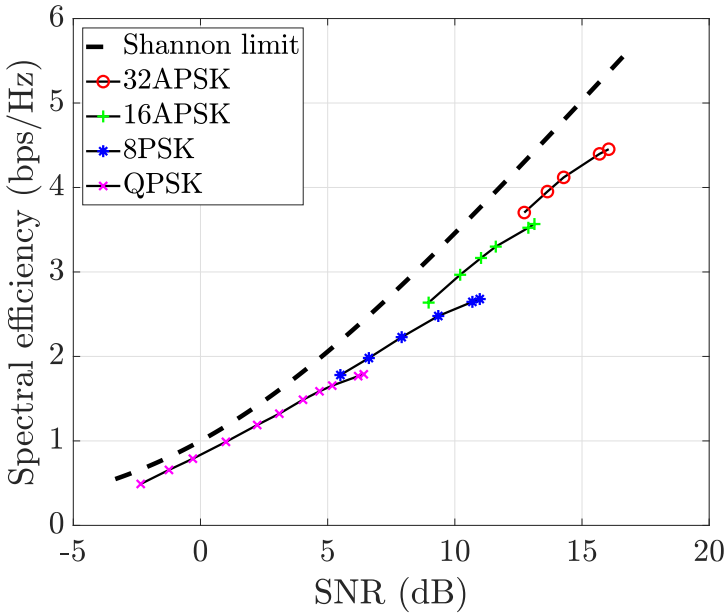

Figure 2.8: SE as a function of the SNR for a packet error rate of 10^{-7} and DVB-S2 ModCod schemes, as presented in [34].

place. A popular access method for satellite return links is the MF-TDMA method presented in the DVB-RCS2 standard [32]. The MF-TDMA decomposes the time-frequency domain in units called time slots. Time slots are aggregated in time and frequency to form frames, which in turn are aggregated in the same way to form super-frames, as illustrated in Fig. 2.9.[5]

In order to transmit, a terminal has to send a transmit request. Then, the *demand assigned multiple access* (DAMA) algorithm is in charge of finding in the following super-frame the frames and time slots appropriate for the terminal's transmission. The frame and time slot allocation is communicated to the terminal via the time-burst time plan sent every super-frame. It is important to note that the time slots constituting a frame are of the same type, which includes the ModCod scheme expected to be used for this time slot type. In this context, the ModCod schemes are often referred to under the more general denomination of FMT modes, or simply modes. The frame and time slot types repartition in the super-frames, which we will refer to as the *carrier plan*, is managed by the *radio resource management* (RRM) algorithm.

Contrarily to the DAMA algorithm, the RRM algorithm usually updates the carrier plan at time scales greater than the super-frame duration [35]. This limitation comes from the fact that all terminals must be informed of structure changes. If done frequently, the transmission

[5]Frames are not represented in the figure for the sake of simplification, as the standard specifies that resources should be allocated following the super-frame time period.

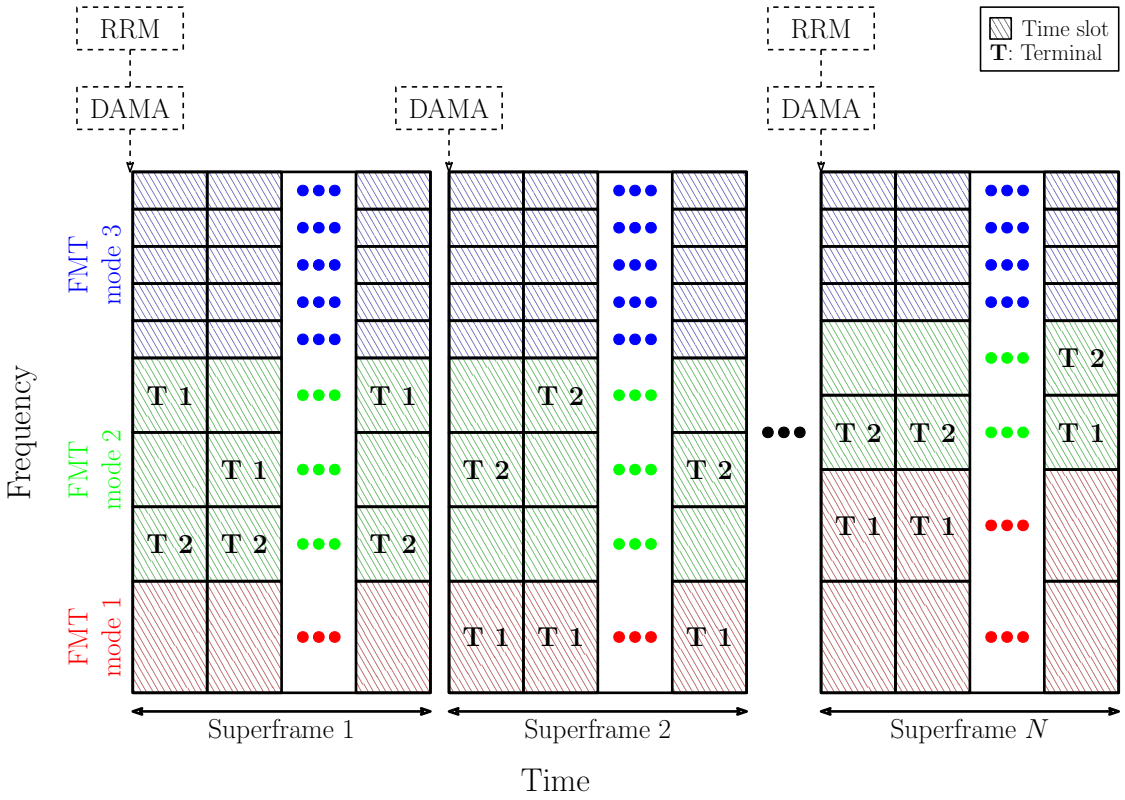

Figure 2.9: Illustration of the carrier plan, with the RRM algorithm executed every N superframes.

of structure updates can decrease the efficiency of the forward link. The more frequently the RRM algorithm is able to update the carrier plan, the more adaptive the carrier plan is. Ideally, the carrier plan would be adaptive enough to adapt to changes in FMT mode demands due to fade events while having minimum impact on the forward link capacity. Efficient RRM algorithms in such conditions have been investigated in the academic literature under the more generic term of dynamic bandwidth allocation [36, Chapter 7]. We refer to this adaptation hypothesis as ACP.

In practice, we see instances of BSM networks where ACM is enabled but the carrier plan is either static or is not adaptive enough to adapt to fade events [37, Section 2.3]. In opposition to ACP, we refer to these cases as SCP. In such a case, terminals can be denied the use of certain FMT modes if all time slots of the corresponding type are already allocated. Therefore, the adaptability of the carrier plan also impacts the satellite resource consumption and must be considered in the SRD. In this dissertation, we provide solutions to the SRD problem for both SCP (Chapters 3 and 4) and ACP (Chapter 5) scenarios. As this type of multiple access technology is mostly found on return links, we will focus on those in this

dissertation.

2.2.3 State of the art

Several methods to solve the SRD problem are found in academic and industrial literature.

Analytic methods

A commonly seen methodology in the SRD literature computes satellite resources with the assumption that all terminals operate under their worst fade conditions *simultaneously* [9], [38]–[40]. This method is inherited from older dimensioning methods in networks using CCM and SCP. In such a case, the amount of satellite resources allocated to each terminal is predetermined and should be assessed individually. The total amount of satellite resources is given by the sum of individual amounts. While having the advantage of simplicity, great care must be taken when using such a method on networks using ACM and/or ACP. This approach implicitly assumes that there is a complete correlation of fade between all stations in the network, and will predict higher resource margins than necessary for arbitrarily correlated rain fade, which in reality depends on the distance between terminals [41]. Thus, the amount of satellite resources is overestimated, and consequently the services' pricing. It is said that the design is "oversized" given the SLA. Given the high values of rain attenuation beyond the Ku-band, the risk of significant oversizing is not negligible.

More recent work in [42] has tried to solve a related problem by estimating the outage-capacity *cumulative distribution function* (CDF) of a multibeam satellite return link using a lognormal rain fade model. However, while the provided models give a good approximation of the outage capacity CDF at very low (less than -10 dB) and very high (greater than 10 dB) *signal-to-noise ratio* (SNR), they fall short in the intermediate range. It should also be noted that the low SNR approximation uses the central limit theorem assuming independent and identically distributed rain fade. Thus, the results of this work also do not cover the case of arbitrarily correlated rain fade.

On the industry side, satellite operators and network providers have developed ad hoc solutions. These are not available in the public domain,[6] however, we noted that the assumption of uncorrelated fade is often made to simplify design processes and maintain competitive

[6]Several products (https://www.idirect.net/products/satellite-network-calculator/) and tutorial (https://www.idirect.net/products/training/) are found online (visited on 24/11/2023).

pricing. Assuming uncorrelated fading comes at the risk of underestimating the amount of satellite resources and failing to satisfy the SLA. It is said that the design is "undersized" given the SLA.

In summary, there are no analytical solutions to the problem of SRD in the presence of arbitrarily correlated rain fade. The existing methods either overestimate or underestimate the satellite resource margins and the gap to optimality is unknown. The empirical choice of companies to assume uncorrelated rain fade suggests that the oversizing induced by the traditional approach is significant enough to hinder competitiveness.

Simulation-based dimensioning

The term *simulation-based dimensioning* refers to dimensioning methods that rely on simulating the behavior of the network to obtain estimates of its resource needs. Such methods have been enabled thanks to the development of spatially correlated rain fade time series generators [43]. A detailed list of such rain fade simulators has been presented in [44].

The application of rain fade simulators to compute network-scale statistics has been firstly explored for the forward link in [45] and [46], demonstrating the potential for resource dimensioning applications.

Such applications have come a few years later. Joint terminal fade statistics have been used to compare ACM and variable coding and modulation technologies in a multibeam video broadcast satellite scenario [47], and the software SISTAR was used to produce numerical results. The authors of [48] have proposed a simulation-based optimization approach by using the capacity simulator presented in [49], which itself uses the rain fade simulator presented in [50]. Although relying on simulation-based methods, these two contributions do not give a thorough insight into how the rain fade simulators were used for their dimensioning problems.

An attempt to provide a general methodology has been carried out by the authors of [51]. They have tried to solve the return link dimensioning problem in the context of ACM with SCP. They have focused on using a *mixed integer linear programming* (MILP) formulation to solve a *carrier plan optimization* (CPO) problem in the context of limited sets of carrier bandwidths and FMT modes. However, the proposed MILP formulation only provides guarantees on the link availability, not on the QoS. The approach also fails to take into account spatial correlation, as the optimization variables are based only on individual terminal's attenuation *complementary CDFs* (CCDFs).

2.3 Dissertation contributions

The work carried out in [51] gave the impulse of the Ph.D. project described in this dissertation. Starting from here, the goal was to propose a solution to the problem of SRD in the presence of arbitrarily correlated rain fade. Given the shortcomings of [51], it was decided to split the problem into several parts of increasing complexity and contribution based on the assumptions made on the adaptability of the ModCod scheme and the carrier plan. Since CCM does not benefit from the use of ACP, three combinations are possible:

- CCM with SCP.
- ACM with SCP.
- ACM with ACP.

Each of the following chapters of this dissertation solves the SRD problem assuming one of the above possibilities. Each chapter includes the work of one of the three journal contributions listed in Chapter 1, in chronological order.

2.3.1 Constant coding and modulation

Chapter 3 focuses on SRD in the context of CCM and SCP. The aim of this contribution was to adapt the work in [51] by reformulating the MILP problem to obtain an SLA-compliant and bandwidth-optimal carrier plan. The decision was taken to focus on nonadaptive networks to avoid considering the spatial correlation of rain fade, thus simplifying the problem. This simplification was deemed acceptable as CCM satellite networks continue to be used and deployed in frequency bands that do not require adaptation, such as the C band. Other simplifications include assuming that terminals transmit at constant power spectral density and not considering the satellite power in the resource optimization problem.

The contributions of this work are summarized as follows:

- A mathematical formulation of the CPO problem based on simple SLAs, focusing on the bandwidth resource.
- A benchmark method based on the current industry's techniques.
- A MILP formulation that solves the CPO problem.

- A low-complexity heuristic method that allows us to understand the specificities of the CPO problem.
- A resource-efficient method to reduce the number of available FMT modes.
- A comprehensive performance analysis focusing on the uplink link budget.

2.3.2 Adaptive coding and modulation with static carrier plan

Once the SRD problem was solved for the CCM scenario, we decided to move on to the ACM with SCP scenario, with the same aim of solving the CPO problem. The introduction of adaptability to rain fade came with the need to model its spatial correlation. We took the simulation-based approach presented in Section 2.2.3 and assumed available a synthetic rain fade simulator. Some simplifications of the previous work were carried on to this work, such as the SLA formulation, the focus on the bandwidth resource, and the assumption that terminals transmit at constant power spectral density.

The contributions of this work are summarized as follows:

- An adaptation of the CPO problem presented in Chapter 3 in the presence of ACM and spatially-correlated rain attenuation.
- A MILP problem formulation that solves the CPO problem.
- A comparison against the state-of-the-art methods presented in Section 2.2.3 in a test scenario in Europe, using the MultiEXCELL model for the generation of rain attenuation.

2.3.3 Adaptive coding and modulation with adaptive carrier plan

The final scenario to consider was ACM with ACP. Due to the adaptability of the carrier plan, there is no CPO problem to solve, and only the amount of satellite resources needs to be determined. Thus, this part focused more on statistical aspects than optimization and aimed at predicting the amount of satellite resources within a given confidence interval. This scenario is the most futuristic one of the three and brought a desire to increase the complexity of the scenario in several aspects, such as the SLA formulation, considering power in the resource-demand model, considering fixed power terminal emissions, and the introduction of multibeam aspects. The link budget model of the numerical results was also complexified by adding the downlink and various interference components.

The contributions of this work are summarized as follows:

- A detailed explanation of translating service-level requirements into an SRD problem, with a resource-demand model that considers both bandwidth and power.
- A Monte Carlo methodology to approximate the problem's solution with arbitrary precision and confidence level.
- A quantitative comparison among clear sky, uncorrelated, arbitrarily correlated, and fully correlated rain fade assumptions.

Chapter 3

Constant coding and modulation

This chapter focuses on solving the CPO problem in the context of CCM return links. In Section 3.1, we introduce the CCM return link scenario and assumptions. In Section 3.2, we present a mathematical formulation of the CPO problem and constraints, and present three ways to solve it: an intuitive solution which will be our benchmark, a MILP problem formulation, and finally a heuristic solution. Then, in Section 3.3.1, we introduce a simulation scenario in Europe, and in Section 3.3, we provide the results for the different optimization methods. Section 3.4 introduces some discussions around the results. Finally, Section 3.5 concludes the chapter.

3.1 Scenario description

Our scenario considers that N terminals distributed over a given area require BSM services. We make the following assumptions for the return path SLA:

- The CIR, in bps, denoted R^{ci}, is identical for all terminals.
- The BER is the same across services.
- The service outage probability, denoted p^{out}, is identical for all terminals.

Furthermore, we make the assumption that the terminal's modem supports:

- K FMT modes, ordered by increasing activation thresholds $\{\theta(1), ..., \theta(K)\}$ for the desired BER. We will note $\eta^{\text{spe}}(k)$ the spectral efficiency of FMT mode k, in bps/Hz, and assume $\eta^{\text{spe}}(k)$ increases with $\theta(k)$.

- L channel/carrier bandwidths, in Hz, ordered increasingly in the set $\mathcal{B}^{\mathrm{c}} = \{B_1^{\mathrm{c}}, ..., B_L^{\mathrm{c}}\}$.

We assume terminals transmit at constant *EIRP spectral density* (EIRP_0), in W/Hz,[1] across the carrier bandwidths in $\mathcal{B}^{\mathrm{c}}$ and that a link budget model allows the computation of the *carrier-to-interference-plus-noise ratio* (CINR), denoted γ_n, of each terminal n given the outage probability p^{out}.

Contrarily to [46] and [51], in this work the carrier plan will be designed for CCM, implying:

- Each terminal is assigned to one carrier and cannot change over time.
- Each carrier is assigned one FMT mode and bandwidth and cannot change over time.

Thus, all terminals assigned to the same return link carrier will use the same FMT mode. Nevertheless, the carrier allocation problem tackled in this chapter is equivalent to the one described in [51] as the terminal's capacity to change carriers was not used in the problem-solving. We assume that all terminals can support the most robust FMT mode, i.e.:

$$\gamma_n \geq \theta\,(1) \qquad \forall\ n \in \mathcal{I}_N\,, \tag{3.1}$$

and that the smallest carrier information rate is greater than R^{ci}, i.e.:

$$B_1^{\mathrm{c}} \cdot \eta^{\mathrm{spe}}\,(1) \geq R^{\mathrm{ci}}\,. \tag{3.2}$$

3.2 Carrier allocation

In this section, we will translate the scenario into mathematical constraints. We will then show three ways of solving the problem: an intuitive solution that will be our benchmark, a MILP problem formulation, and finally a heuristic.

We need to assign to each combination of FMT mode and bandwidth, called carrier type, a cluster of terminals such that all of them can support the FMT mode. The resulting number of terminals assigned to each carrier type, and subsequently the number of carriers needed to serve them, constitute what is called the carrier plan, from which we can compute the total bandwidth of the network (assuming the bandwidth of a carrier is proportional to its

[1] EIRP spectral densities are often used by satellite operators to measure intersystem interference and check ITU regulation compliance; see [52].

bandwidth). Our goal is then to find the optimal carrier plan that will minimize the total bandwidth. Let us first note for each terminal n the FMT mode index k_n^{tgt} such that:

$$\theta\left(k_n^{\text{tgt}}\right) \leq \gamma_n < \theta\left(k_n^{\text{tgt}}+1\right) . \tag{3.3}$$

If carrier bandwidths can take values in a continuous set $\mathcal{B}^{\text{c}} = [B_1^{\text{c}}, B_L^{\text{c}}]$, we can easily calculate the minimum bandwidth for each terminal:

$$B_n^{\min} = \frac{R^{\text{ci}}}{\eta^{\text{spe}}\left(k_n^{\text{tgt}}\right)} \qquad [\text{Hz}] . \tag{3.4}$$

Hypothesis (3.2) guarantees that $B_n^{\min} \in \mathcal{B}^{\text{c}}$. We can then deduce the carrier plan minimum bandwidth:

$$B^{\min} = \sum_{n=1}^{N} B_n^{\min} . \tag{3.5}$$

However, the type of ground and satellite equipment, and the system capabilities, might limit the choice of supported bandwidths to a discrete set $\mathcal{B}^{\text{c}} = \{B_1^{\text{c}}, ..., B_L^{\text{c}}\}$.[2] In this case, determining the optimal carrier plan is not trivial.

3.2.1 Problem formulation

To build the carrier plan, we need to determine for each carrier type (k, l), combining k with B_l^{c}, the number of carriers $X_{k,l}$ needed to deliver R^{ci} to the set of terminals $\mathcal{N}_{k,l}$, defined as:

$$X_{k,l} = \left\lceil \frac{N_{k,l}}{Z_{k,l}^{\max}} \right\rceil , \tag{3.6}$$

with $N_{k,l} = |\mathcal{N}_{k,l}|$ being the number of terminals, $\lceil \cdot \rceil$ being the ceil function, and $Z_{k,l}^{\max}$ being the maximum number of terminals one carrier of type (k, l) can serve at committed rate, equal to:

$$Z_{k,l}^{\max} = \left\lfloor \frac{B_l^{\text{c}} \cdot \eta^{\text{spe}}(k)}{R^{\text{ci}}} \right\rfloor , \tag{3.7}$$

with $\lfloor \cdot \rfloor$ being the floor function. Equivalently, $Z_{k,l}^{\max}$ can be interpreted as the number of committed service slots available in one carrier of type (k, l). Because of condition (3.2), the inequality $Z_{k,l}^{\max} \geq 1$ is always verified. A graphical representation of the capacity of a carrier

[2] See for example the MDM2510 Satellite Modem datasheet:
https://www.vsat.fr/index.php?controller=attachment&id_attachment=30 (visited on 24/11/2023).

of type (k, l) is given in Fig. 3.1 , in which we took as an example $Z_{k,l}^{\max} = 3$ and $N_{k,l} = 2$.

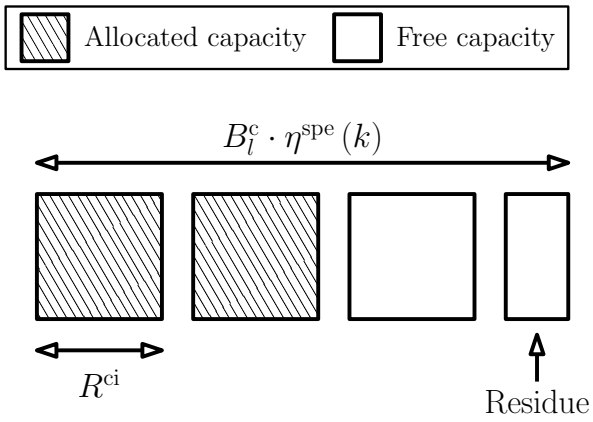

Figure 3.1: Representation of committed service slots for carrier type (k, l) with $Z_{k,l}^{\max} = 3$ and $N_{k,l} = 2$.

To obtain a valid carrier plan, we need the following constraint on $\mathcal{N}_{k,l}$:

$$\theta(k) \leq \min_{n \in \mathcal{N}_{k,l}} \left(\theta\left(k_n^{\mathrm{tgt}}\right)\right). \tag{3.8}$$

Furthermore, $X_{k,l}$ must comply with the following constraint for a given $\mathcal{N}_{k,l}$:

$$\frac{B_l^{\mathrm{c}} \cdot \eta^{\mathrm{spe}}(k) \cdot X_{k,l}}{N_{k,l}} \geq R^{\mathrm{ci}}. \tag{3.9}$$

Finally, to ensure that all terminals are served by one and only one carrier, the carrier plan must satisfy:

$$\mathcal{N}_{k_1,l_1} \cap \mathcal{N}_{k_2,l_2} = \emptyset \qquad \forall (k_1, k_2) \in \mathcal{I}_K^2\,,\ \forall (l_1, l_2) \in \mathcal{I}_L^2\,,\ (k_1, l_1) \neq (k_2, l_2)\,, \tag{3.10}$$

and

$$\sum_{k=1}^{K} \sum_{l=1}^{L} N_{k,l} \geq N\,. \tag{3.11}$$

As they stand, those constraints are a direct translation of our informal problem and can hardly be used inside optimization solvers.

Let us define $\mathcal{N}_{k,l}^{\mathrm{ini}}$ as:

$$\mathcal{N}_{k,l}^{\mathrm{ini}} = \begin{cases} \left\{ n \in \mathcal{I}_n \mid k_n^{\mathrm{tgt}} = k \right\} & \text{if } l = L\,, \\ \varnothing & \text{otherwise}\,. \end{cases} \tag{3.12}$$

We define accordingly $N_{k,l}^{\text{ini}} = \left|\mathcal{N}_{k,l}^{\text{ini}}\right|$ and $X_{k,l}^{\text{ini}} = \left\lceil N_{k,l}^{\text{ini}} / Z_{k,l}^{\max} \right\rceil$. We are then able to reformulate the constraints (3.8), (3.9), (3.10), and (3.11) into:

$$\sum_{i=k}^{K}\sum_{j=1}^{L} X_{i,j} \cdot Z_{i,j}^{\max} \;\leq\; \sum_{i=k}^{K}\sum_{j=1}^{L} X_{i,j}^{\text{ini}} \cdot Z_{i,j}^{\max} \qquad \forall\, k \in \{2,\ldots,K\}\,, \tag{3.13}$$

and

$$\sum_{i=1}^{K}\sum_{j=1}^{L} X_{i,j} \cdot Z_{i,j}^{\max} \;\geq\; N\,. \tag{3.14}$$

Note that constraints are now expressed in a linear form, which is appropriate for linear optimization solvers. Let us represent the carrier plan as a $K \times L$ matrix $\mathbf{X}$, with $X_{k,l}$ being the (k,l) entry. Then, we can express the CPO problem as the following constrained combinatorial optimization problem:

$$\underset{\mathbf{X}}{\text{minimize}} \qquad \sum_{k=1}^{K}\sum_{l=1}^{L} B_l^{\text{c}} \cdot X_{k,l}\,, \tag{3.15a}$$

$$\text{subject to} \qquad (3.13) \text{ and } (3.14)\,. \tag{3.15b}$$

3.2.2 Intuitive approach

One would intuitively think, as we saw with (3.4) and (3.5), that assigning terminal n to the carrier type $\left(k_n^{\text{tgt}}, l^{\text{opt}}\right)$, with l^{opt} such that:

$$l^{\text{opt}} = \underset{l\in[1,L]}{\arg\min}\, X_{k_n^{\text{tgt}},l} \cdot B_l^{\text{c}}\,, \tag{3.16}$$

would lead to an optimal carrier plan. This method is optimal when $\mathcal{B}^{\text{c}}$ is continuous, but it is not when $\mathcal{B}^{\text{c}}$ is a discrete set.

Proof. For instance, let us assume that for the carrier type (k_1, l_1), using FMT mode k_1 and bandwidth $B_{l_1}^{\text{c}}$, N_{k_1,l_1} is such that:

$$N_{k_1,l_1} = g_{k_1,l_1} \cdot Z_{k_1,l_1}^{\max} + h_{k_1,l_1}\,, \qquad 0 < h_{k_1,l_1} < Z_{k_1,l_1}^{\max}\,. \tag{3.17}$$

Let us also assume that for the carrier type (k_2, l_2), with $\eta^{\text{spe}}(k_2) < \eta^{\text{spe}}(k_1)$, N_{k_2,l_2} is such that:

$$N_{k_2,l_2} = g_{k_2,l_2} \cdot Z_{k_2,l_2}^{\max} + h_{k_2,l_2}\,, \qquad 0 < h_{k_2,l_2} + h_{k_1,l_1} < Z_{k_2,l_2}^{\max}\,. \tag{3.18}$$

By assigning all terminals to their most spectrally efficient FMT mode, we would have to create $g_{k_1,l_1}+1$ carriers for (k_1,l_1) and $g_{k_2,l_2}+1$ carriers for (k_2,l_2), with a total bandwidth equal to:

$$B_1 = (g_{k_1,l_1}+1)\cdot B^{\mathrm{c}}_{l_1} + (g_{k_2,l_2}+1)\cdot B^{\mathrm{c}}_{l_2} \qquad [\mathrm{Hz}]\ . \tag{3.19}$$

Yet because $0 < h_{k_2,l_2} + h_{k_1,l_1} < Z^{\max}_{k_2,l_2}$, we can reassign h_{k_1,l_1} terminals from (k_1,l_1) to (k_2,l_2), and thus have:

$$N_{k_1,l_1} = g_{k_1,l_1}\cdot Z^{\max}_{k_1,l_1}\ , \tag{3.20a}$$

$$N_{k_2,l_2} = g_{k_2,l_2}\cdot Z^{\max}_{k_2,l_2} + h_{k_2,l_2} + h_{k_1,l_1}\ . \tag{3.20b}$$

Therefore, we need only g_{k_1,l_1} carriers for (k_1,l_1) and $g_{k_2,l_2}+1$ carriers for (k_2,l_2), with a total bandwidth equal this time to:

$$B_2 = g_{k_1,l_1}\cdot B^{\mathrm{c}}_{l_1} + (g_{k_2,l_2}+1)\cdot B^{\mathrm{c}}_{l_2} \qquad [\mathrm{Hz}]\ , \tag{3.21}$$

and thus $B_1 > B_2$, proving that a more bandwidth efficient solution exists. □

3.2.3 Mixed integer linear programming approach

Solving optimization problems with linear constraints can be done by writing them as matrix operations and feeding them to a linear programming solver, which is a well-explored topic [53]. However our optimization variables $X_{k,l}$ have to be integers, and thus we need to use a specific branch of the linear programming problem class called MILP [54]. This class of problem is NP-hard due to its combinatorial nature, however, techniques have been discovered to solve certain cases [55]. It is first necessary to reformulate the optimization problem with matrix operations. Let:

$$q \equiv (k,l) \ \text{ with } q = (k-1)\cdot L + l\ , \tag{3.22a}$$

$$Q = K\cdot L\ , \tag{3.22b}$$

$$\mathbf{X} = [X_1, ..., X_Q]\ . \tag{3.22c}$$

The optimization function $b(\mathbf{X})$ we want to minimize can then be written as a vector

multiplication:

$$b(\mathbf{X}) = \mathbf{b}^\intercal \cdot \mathbf{X}\,, \qquad \mathbf{b} = \begin{pmatrix} \mathbf{b}_1^{\mathrm{c}} \\ \vdots \\ \mathbf{b}_K^{\mathrm{c}} \end{pmatrix}, \qquad \mathbf{b}_k^{\mathrm{c}} = \begin{pmatrix} B_1^{\mathrm{c}} \\ \vdots \\ B_L^{\mathrm{c}} \end{pmatrix}. \tag{3.23a}$$

We then need to express (3.13) and (3.14) with a matrix $\mathbf{A}$ and a vector $\mathbf{y}$ such that $\mathbf{A} \cdot \mathbf{X} \leq \mathbf{y}$. This is possible by using:

$$\mathbf{A} = \begin{pmatrix} -Z_1^{\max} & -Z_2^{\max} & \cdots & -Z_{Q-1}^{\max} & -Z_Q^{\max} \\ & Z_2^{\max} & \cdots & Z_{Q-1}^{\max} & Z_Q^{\max} \\ & & \ddots & \vdots & \vdots \\ & 0 & & Z_{Q-1}^{\max} & Z_Q^{\max} \\ & & & & Z_Q^{\max} \end{pmatrix}, \tag{3.24}$$

and:

$$\mathbf{y} = \begin{pmatrix} -N \\ y_2 \\ \vdots \\ y_Q \end{pmatrix}, \qquad y_q = \sum_{j=q}^{Q} X_j^{\mathrm{ini}} \cdot Z_j^{\max}\,. \tag{3.25}$$

We can then use a MILP solver to solve the following optimization problem:

$$\underset{\mathbf{X}}{\text{minimize}} \qquad b(\mathbf{X})\,, \tag{3.26a}$$

$$\text{subject to} \qquad \mathbf{A} \cdot \mathbf{X} \leq \mathbf{y}\,. \tag{3.26b}$$

3.2.4 Heuristic approach

While MILP solutions can solve the optimization problem, they do not allow us to get a good understanding of the core mechanics at play in our problem. To remedy this issue we propose to look into a heuristic solution.

Looking back at Section 3.2.2 we can identify two issues that prevented the intuitive approach from reaching the minimum bandwidth: unoccupied slots and residual bandwidth, which are graphically represented in Fig. 3.1. The residue is the remainder of the modulo operation of $R(l) \cdot \eta^{\mathrm{spe}}(k)$ by R^{ci}, and because this portion of the carrier cannot deliver R^{ci},

it is wasted every time a new carrier is created. Thus, we need to minimize the number of unused slots and the total residue. The two following heuristics, that can be combined, aim to solve those two issues.

Minimizing the residue

Each carrier of type (k, l) has a residual throughput per terminal $\rho_{k,l}$ equal to:

$$\rho_{k,l} = \frac{B_l^{\mathrm{c}} \cdot \eta^{\mathrm{spe}}(k)}{Z_{k,l}^{\max}} - R^{\mathrm{ci}} \qquad [\mathrm{bps}]\ . \tag{3.27}$$

A possible optimization is to allocate terminals in priority to bandwidths that minimize $\rho_{k,l}$. In order to achieve that, we must re-arrange for each FMT mode k the set of bandwidths $[B_1^{\mathrm{c}}, ..., B_l^{\mathrm{c}}]$ into a vector $[B_{\sigma_k(1)}^{\mathrm{c}}, ..., B_{\sigma_k(L)}^{\mathrm{c}}]$, with $\sigma_k(\cdot)$ a re-arrangement of the indexes such that $\rho_{k,\sigma_k(1)} > \rho_{k,\sigma_k(2)} > ... > \rho_{k,\sigma_k(L-1)} > \rho_{k,\sigma_k(L)}$.

Carrier filling

To minimize the number of unused slots, we need to keep only the filled carriers of a given carrier type, i.e. the ones without unused slots, and then move the terminals of the remaining unfilled carriers to other carrier types. Formally speaking, the goal is to find $N'_{k,l}$ such that:

$$X'_{k,l} \cdot Z_{k,l}^{\max} - N'_{k,l} = 0\,, \tag{3.28}$$

while ensuring that as many terminals as possible still get the most efficient FMT mode they can afford. Considering we already initialized the problem by assigning each terminal n to the carrier type $\left(k_n^{\mathrm{tgt}}, L\right)$, (3.28) can be reached for almost all carrier types by following Algorithm 1, which moves the extra terminals from the largest carrier types to the smallest ones (in terms of capacity). An illustration of this algorithm is given in Fig. 3.2 , in which the algorithm starts by setting $N_{K,L}^{\mathrm{tm}} = 0$ and iterates on the carrier type (K, L) with $Z_{K,L}^{\max} = 4$ and $N_{K,L}^{\mathrm{ini}} = 6$. It computes the total number of terminal $N_{K,L} = N_{K,L}^{\mathrm{ini}} + N_{K,L}^{\mathrm{tm}} = 6$, and then the number of carriers that can be filled $X'_{K,L} = \lfloor 6/4 \rfloor = 1$. Finally it computes the number of terminals that can stay $N'_{K,L} = X'_{K,L} \cdot Z_{K,L}^{\max} = 4$ in (K, L), and the rest $N_{K,L-1}^{\mathrm{tm}} = N_{K,L} - N'_{K,L} = 2$ is moved to the carrier type $(K, L-1)$. The algorithm then iterates on the carrier type $(K, L-1)$ with $Z_{K,L-1}^{\max} = 3$, $N_{K,L-1}^{\mathrm{ini}} = 5$ and $N_{K,L-1}^{\mathrm{tm}} = 2$. Those steps are repeated until $C_{1,1}$ is reached. For this carrier type, we cannot reallocate the remaining terminals $N_{1,1}^{\mathrm{tm}}$ to

Algorithm 1 Carrier filling

$N^{\text{tm}}_{K,L} \leftarrow 0$; ▷ Number of terminals moved to carrier type (K, L)
for $k = K, k \geq 1, k--$ **do**
  for $l = L, l \geq 1, l--$ **do**
    $N_{k,l} \leftarrow N^{\text{ini}}_{k,l} + N^{\text{tm}}_{k,l}$
    $X'_{k,l} \leftarrow \left\lfloor \frac{N_{k,l}}{Z_{k,l}} \right\rfloor$
    $N'_{k,l} \leftarrow X'_{k,l} \cdot Z_{k,l}$
    if k=1 & l=1 **then**
      $N^{\text{tm}}_{1,1} \leftarrow N_{k,l} - N'_{k,l}$
    else
      if l=1 **then**
        $N^{\text{tm}}_{k-1,L} \leftarrow N_{k,l} - N'_{k,l}$
      else
        $N^{\text{tm}}_{k,l-1} \leftarrow N_{k,l} - N'_{k,l}$
      end if
    end if
  end for
end for

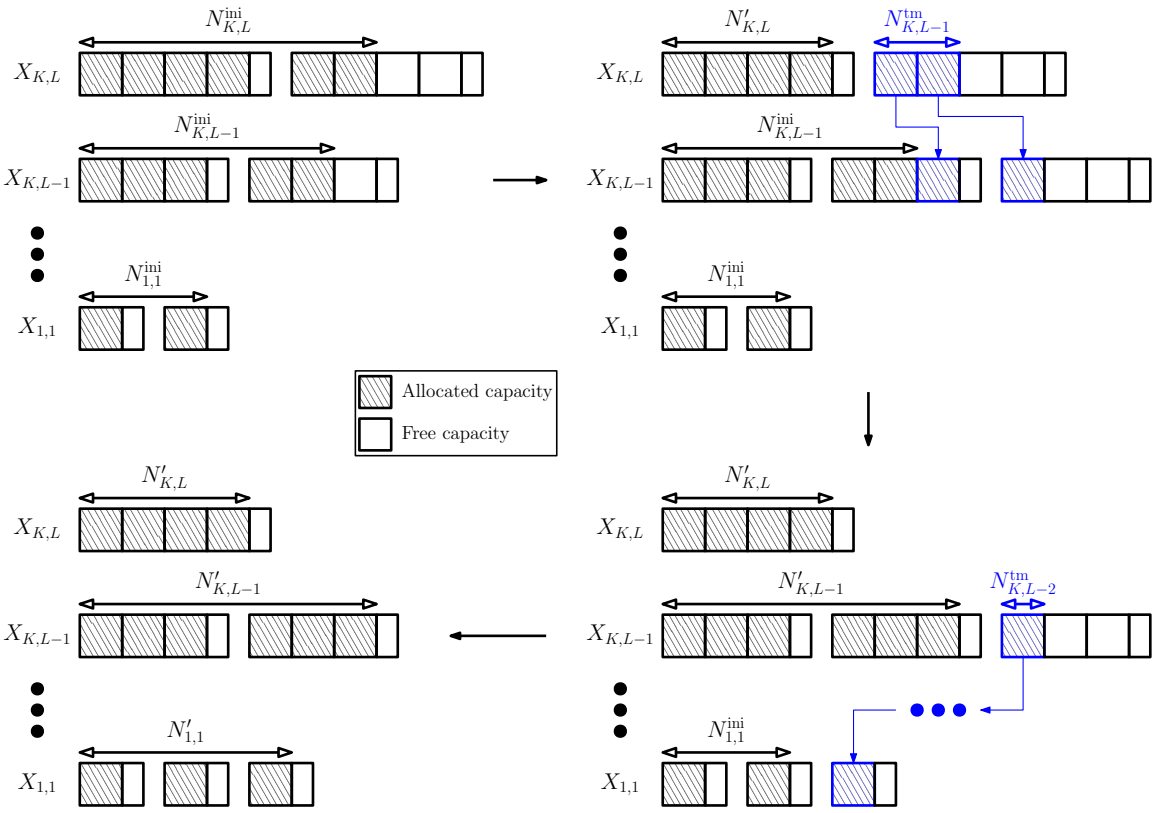

Figure 3.2: Illustration of Algorithm 1, blue squares represent re-allocated terminals.

another carrier type with a higher ρ or a lower spectral efficiency. If some terminals need to

be moved, we will instead move them to the carrier type $\left(1, l^{\text{opt}}\right)$ s.t.

$$l^{\text{opt}} = \underset{l \in \mathcal{I}_L}{\arg\min}\, X'_{1,l} \cdot B^{\text{c}}_l \,. \tag{3.29}$$

and then compute $X'_{1,l^{\text{opt}}}$ as:

$$X'_{1,l^{\text{opt}}} = \left\lceil \frac{N'_{1,l^{\text{opt}}} + N^{\text{tm}}_{1,1}}{Z^{\max}_{1,l^{\text{opt}}}} \right\rceil \,. \tag{3.30}$$

In this specific case, the heuristic will behave exactly like the intuitive process described in Section 3.2.2. It is possible to combine the minimization of residue with the carrier filling algorithm by replacing all the l indexes with $\sigma_k(l)$ in Algorithm 1.

Constraints compliance

We need to make sure the heuristic solution complies with constraints (3.13) and (3.14). Let us prove that (3.13) is satisfied. We first need to prove:

$$N^{\text{tm}}_{k,l} = \sum_{j=l+1}^{L} N^{\text{ini}}_{k,j} - N'_{k,j} + \sum_{i=k+1}^{K} \sum_{j=1}^{L} N^{\text{ini}}_{i,j} - N'_{i,j} \qquad \forall k \geq 2 \,. \tag{3.31}$$

Proof. Let's prove (3.31) by induction:

- Base case:
$$N^{\text{tm}}_{K,L} = 0 = \sum_{j=L+1}^{L} N^{\text{ini}}_{K,j} - N'_{K,j} + \sum_{i=K+1}^{K} \sum_{j=1}^{L} N^{\text{ini}}_{i,j} - N'_{i,j} \,. \tag{3.32}$$

- Induction: Let us assume (3.31) is true for carrier type (k, l). Let us prove it is true for carrier type $(k, l-1)$.

$$N^{\text{tm}}_{k,l-1} = N_{k,l} - N'_{k,l} = N^{\text{ini}}_{k,l} + N^{\text{tm}}_{k,l} - N'_{k,l} \,, \tag{3.33}$$

and by using our induction hypothesis we have:

$$N^{\text{tm}}_{k,l-1} = N^{\text{ini}}_{k,l} - N'_{k,l} + \sum_{j=l+1}^{L} N^{\text{ini}}_{k,j} - N'_{k,j} + \sum_{i=k+1}^{K} \sum_{j=1}^{L} N^{\text{ini}}_{i,j} - N'_{i,j} \tag{3.34a}$$

$$= \sum_{j=l}^{L} N^{\text{ini}}_{k,j} - N'_{k,j} + \sum_{i=k+1}^{K} \sum_{j=1}^{L} N^{\text{ini}}_{i,j} - N'_{i,j} \,. \tag{3.34b}$$

Thus, carrier type $(k, l-1)$ also verifies (3.31). We would prove in the same way that (3.31) is also true for carrier type $(k-1, L)$.

□

Let us now demonstrate that (3.13) is verified. For all $k \geq 2$, we have:

$$N'_{k,1} = X'_{k,1} \cdot Z^{\max}_{k,1} = \left\lfloor \frac{N^{\text{ini}}_{k,1} + N^{\text{tm}}_{k,1}}{Z^{\max}_{k,1}} \right\rfloor \cdot Z^{\max}_{k,1} \tag{3.35a}$$

$$\implies N'_{k,1} \leq N^{\text{ini}}_{k,1} + N^{\text{tm}}_{k,1} \tag{3.35b}$$

$$\implies N'_{k,1} \leq N^{\text{ini}}_{k,1} + \sum_{j=2}^{L} N^{\text{ini}}_{k,j} - N'_{k,j} + \sum_{i=k+1}^{K} \sum_{j=1}^{L} N^{\text{ini}}_{i,j} - N'_{i,j} \tag{3.35c}$$

$$\implies N'_{k,1} + \sum_{j=2}^{L} N'_{k,j} + \sum_{i=k+1}^{K} \sum_{j=1}^{L} N'_{i,j} \leq N^{\text{ini}}_{k,L} + \sum_{j=2}^{L} N^{\text{ini}}_{k,j} + \sum_{i=k+1}^{K} \sum_{j=1}^{L} N^{\text{ini}}_{i,j} \tag{3.35d}$$

$$\implies \sum_{i=k}^{K} \sum_{j=1}^{L} N'_{i,j} \leq \sum_{i=k}^{K} \sum_{j=1}^{L} N^{\text{ini}}_{i,j} \tag{3.35e}$$

$$\implies \sum_{i=k}^{K} \sum_{j=1}^{L} X'_{i,j} \cdot Z^{\max}_{i,j} \leq \sum_{i=k}^{K} \sum_{j=1}^{L} X^{\text{ini}}_{i,j} \cdot Z^{\max}_{i,j}, \tag{3.35f}$$

and thus constraint (3.13) is satisfied.

As for (3.14), we need to look at the specific case $(k = 1, l = 1)$. Because of the branching condition, we have:

$$N^{\text{tm}}_{1,1} = \sum_{j=1}^{L} N^{\text{ini}}_{1,j} - N'_{1,j} + \sum_{i=2}^{K} \sum_{j=1}^{L} N^{\text{ini}}_{i,j} - N'_{i,j} \tag{3.36a}$$

$$\implies N^{\text{tm}}_{1,1} = \sum_{i=1}^{K} \sum_{j=1}^{L} N^{\text{ini}}_{i,j} - N'_{i,j} \tag{3.36b}$$

$$\implies \sum_{i=1}^{K} \sum_{j=1}^{L} N'_{i,j} + N^{\text{tm}}_{1,1} = \sum_{i=1}^{K} \sum_{j=1}^{L} N^{\text{ini}}_{i,j} = N\,. \tag{3.36c}$$

Furthermore, at the end of Algorithm 1, we re-allocate $N^{\text{tm}}_{1,1}$ to $N'_{1,l^{\text{opt}}}$ such that:

$$X'_{1,l^{\text{opt}}} = \left\lceil \frac{N'_{1,l^{\text{opt}}} + N^{\text{tm}}_{1,1}}{Z^{\max}_{1,l^{\text{opt}}}} \right\rceil . \tag{3.37}$$

Therefore:

$$\sum_{i=1}^{K}\sum_{j=1}^{L} X'_{i,j} \cdot Z_{i,j}^{\max} \geq N\,, \tag{3.38}$$

and thus constraint (3.14) is satisfied.

3.2.5 Reducing the number of FMT modes in the network

As we saw in the previous sections, the heuristic and MILP methods rely on the diversity of FMT modes and bandwidths to allocate residual throughput to carrier types that would not have been considered otherwise, as more diversity means more options during the optimization process, which leads to smaller bandwidths. A natural consequence is that our solution favors carrier plans with a high number of carrier types, and consequently FMT modes.

However, due to hardware constraints found in CCM networks, there are often costs induced by supporting an FMT mode. Those costs will depend on many network variables, and making an exhaustive list of them would be outside of the scope of this chapter, but the trade-off between the number of FMT modes K and the total bandwidth must be acknowledged. Techniques for FMT set reduction have been investigated in [56], which proposes a solution aimed at optimizing the real-time complexity vs performance trade-off. The mode selection process focuses on the modes' spectral efficiencies and thresholds, however, it does not factor in the carriers' bandwidth, residue, and number of terminals. As we have seen in the previous sections, these aspects play a role in the computation of the network's bandwidth, and consequently its cost.

Our idea is, given the final number of desired FMT modes, to start with the carrier plan computed by the different algorithms, and then decide which FMT modes should be removed in order to minimize the bandwidth increase. This is done iteratively: for each iteration, we must find the index k^{tbr} of the FMT mode to be removed, and then re-allocate the $N_{k^{\text{tbr}}} = \sum_{l=1}^{L} N_{k^{\text{tbr}},l}$ terminals to the receiving carrier type (k^{rec}, L), with $k^{\text{tbr}} > k^{\text{rec}}$.

We need to select k^{tbr} and k^{rec} such that they minimize the bandwidth increase, and to do this we need to evaluate the bandwidth cost $B^{\text{cost}}_{k^{\text{tbr}},k^{\text{rec}}}$ of moving terminals from FMT mode k^{tbr} to mode k^{rec}. It can be approximated with the following equation:

$$B^{\text{cost}}_{k^{\text{tbr}},k^{\text{rec}}} = N_{k^{\text{tbr}}} \cdot R^{\text{ci}} \cdot \left(\frac{1}{\eta^{\text{spe}}\left(k^{\text{tbr}}\right)} - \frac{1}{\eta^{\text{spe}}\left(k^{\text{rec}}\right)} \right) \qquad [\text{Hz}]\ . \tag{3.39}$$

This equation is exact only if the constraint of discrete bandwidth is dropped, but it is a

good enough approximation if the spectral efficiencies of the FMT modes are close to equally spaced, which is the case for the mode set we used in our simulations (DVB-RCS2 [32]). For one given k^{tbr}, minimizing $B^{\mathrm{cost}}_{k^{\mathrm{tbr}},k^{\mathrm{rec}}}$ is thus equivalent to minimize $1/\eta^{\mathrm{spe}}\left(k^{\mathrm{tbr}}\right) - 1/\eta^{\mathrm{spe}}\left(k^{\mathrm{rec}}\right)$ and this minimum is reached for $k^{\mathrm{rec}} = k^{\mathrm{tbr}} - 1$. If we compute $B^{\mathrm{cost}}_{k,k-1}$ for each k, we can find k^{tbr} by solving:

$$k^{\mathrm{tbr}} = \underset{k \in \mathcal{I}_K}{\arg\min}\ B^{\mathrm{cost}}_{k,k-1}\,. \tag{3.40}$$

We can then remove the FMT mode k^{tbr}, update the FMT mode population $N_{k^{\mathrm{rec}}}$, and iterate until we reach the desired number of FMT modes. We can finally use the reduced FMT mode set as an input of any of the three methods we described in the previous sections to compute the new carrier plan.

3.2.6 Complexity analysis

The intuitive method requires finding the most spectrally efficient FMT mode k_n^{tgt} for each terminal n which is a $O(N \cdot K)$, and a loop to find the best bandwidth $B^{\mathrm{c}}_{l^{\mathrm{opt}}}$ which is a $O(K \cdot L)$. This process will then be a $O(N)$ at high numbers of terminals. On the heuristic side, the minimization of residues requires sorting K times $\mathcal{B}^{\mathrm{c}}$, which is of length L, and thus is a $O(K \cdot L \cdot \log L)$. The carrier filling algorithm requires finding the most spectrally efficient FMT mode k_n^{tgt} for each terminal which is a $O(N \cdot K)$, and then executes an $K \cdot L$ loop for the terminal re-allocation. Finally, finding $\left(1, l^{\mathrm{opt}}\right)$ is a $O(L)$. For a high number of terminals, the heuristic will then also be a $O(N)$. The complexity of the MILP solver depends on its parameters but is in any case expected to be higher than the intuitive and the heuristic solutions since MILP problems are NP-hard. This matter is discussed in greater detail in Section 3.4. Finally, the FMT mode reduction method requires to compute $B^{\mathrm{cost}}_{k,k-1}$ for each k at the first iteration. Then if more than one FMT mode needs to be removed, we only need to update $B^{\mathrm{cost}}_{k^{\mathrm{rec}},k^{\mathrm{rec}}-1}$ at each iteration. The FMT mode reduction method is then a $O(K)$.

3.3 Performance evaluation

In this section, we will present the satellite link simulation we created to evaluate and compare the minimum bandwidth calculated using the intuitive approach B^{it} described in Section 3.2.2, the MILP approach B^{ilp} described in Section 3.2.3, and the heuristic approach B^{hr} described in Section 3.2.4. We will then look at how the relative performances of those three methods

are impacted by the number of terminals N, by the CIR R^{ci}, and by the number of FMT modes K in the network.

3.3.1 Simulation parameters

User terminal coordinates are generated based on known patterns for terrestrial, maritime, and aerial traffic statistics over Europe (Fig. 3.3), using a traffic simulator developed inside our research center [57]. All terminals are assumed to be fixed terrestrial stations with a 0.85m dish and with an EIRP capability of 51.6 dBW. The uplink frequency is 29.75 GHz, in the Ka band. The CINR for each terminal n is computed with the following link budget formula:

$$\gamma_n = \left(\frac{1}{\left(\frac{C}{N}\right)_n^{\text{ul}}} + \frac{1}{\left(\frac{C}{I}\right)_n^{\text{im}}} + \frac{1}{\left(\frac{C}{N}\right)_n^{\text{dl}}} \right)^{-1}, \tag{3.41}$$

where $(C/N)_n^{\text{ul}}$ is the uplink CNR, $(C/N)_n^{\text{dl}}$ is the downlink CNR and $(C/I)_n^{\text{im}}$ is the *carrier-to-intermodulation-noise ratio* (CIMR). We assumed that the uplink CNR is significantly smaller than the downlink CNR, the CIMR, and the carrier-to-interference ratio from any other interference sources. All link parameters are given in Table 3.1. The uplink CNR was

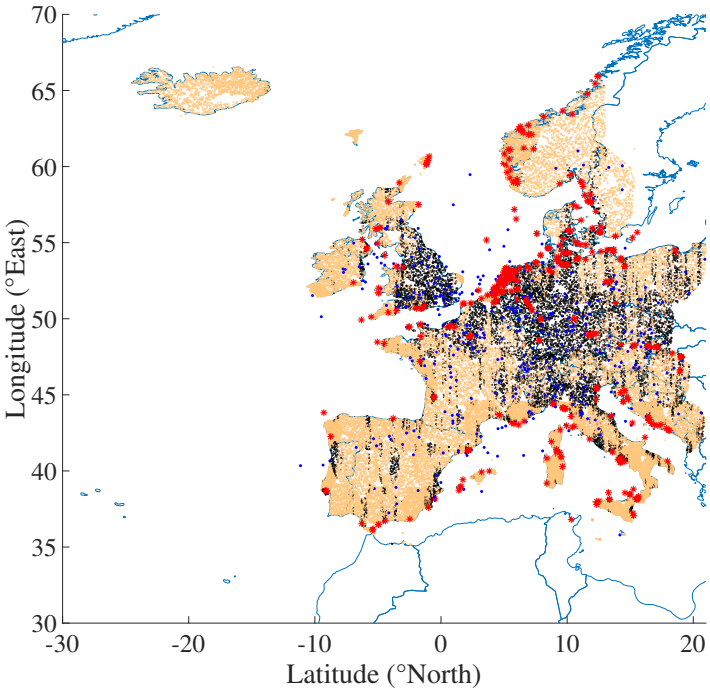

Figure 3.3: Snapshot of the generated terminals (red = boat, blue = plane, other = terrestrial).

Table 3.1: Simulation link parameters

Name	**Value**	**Unit**
Frequency	29.75	GHz
Ground antenna diameter	0.85	m
Ground antenna gain	45.6	dBi
Maximum emission power	4	W
EIRP_0	-13.8	dBW/Hz
Satellite Longitude	28.5	°East
CIMR	20	dB
CNR downlink	30	dB

computed for each terminal's location with the following formula:

$$\left(\frac{C}{N}\right)_n^{\text{ul}} = \text{EIRP}_0 \cdot \frac{1}{L_n^{\text{fs}} \cdot L_n^{\text{atm}}} \cdot \left(\frac{G}{T}\right)_n^{\text{sat}} \cdot \frac{1}{k^{\text{B}}} \,. \tag{3.42}$$

where:

- L_n^{fs} is the free space losses between terminal n and the satellite.
- L_n^{atm} is the atmospheric attenuation at terminal's n location for a 99.5% uplink availability target.
- $(G/T)_n^{\text{sat}}$ is the satellite's figure of merit at terminal's n location.
- k^{B} is the Boltzmann constant.

The atmospheric attenuation is computed using the ITU-R framework [30] which includes the effects of scintillation, clouds, gases, and rain for a given location and link availability.

Once γ_n has been computed, we compute k_n^{tgt}. The set of FMT modes follows the DVB-RCS2 standard [32] with target $\frac{E_s}{N_0}$ thresholds as noted in [48]. Depending on R^{ci}, some FMT modes can be removed from the pool if they do not meet condition (3.2). The discrete set of bandwidths is the same as in [51]. User terminals that either cannot afford the minimum FMT mode or fall out of the service area are taken out of the considered user set. The final mapping of terminals to FMT modes is illustrated in Fig. 3.4 for 150,000 terminals.

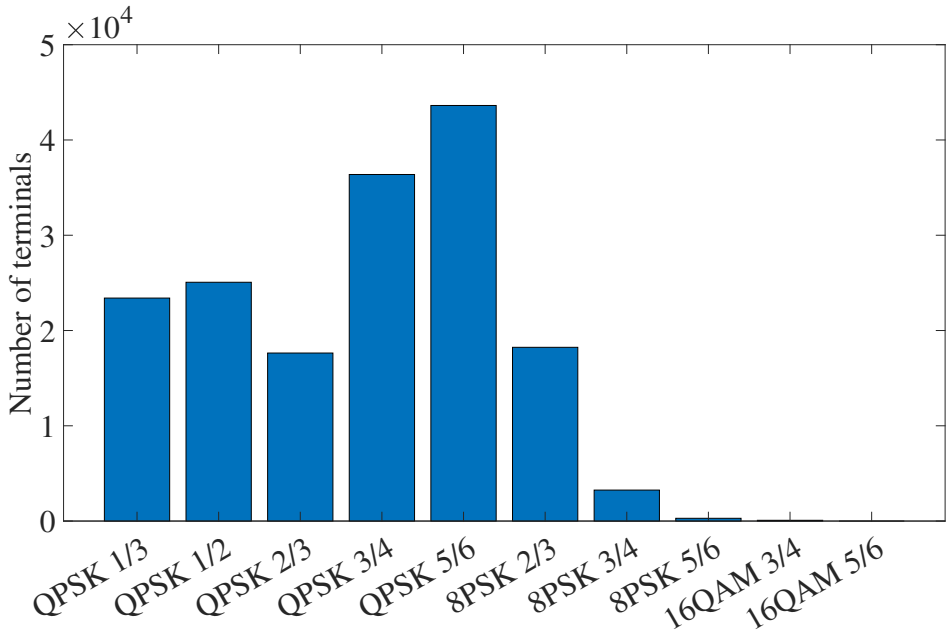

Figure 3.4: Histogram of terminal repartition among FMT modes.

3.3.2 Impact of the number of terminals and CIR

On average the gain of B^{ilp} is marginal ($\approx 2.9\%$) compared to B^{it}, as showed in Fig. 3.5a. Only 3.1% of samples in this figure show a gain greater or equal to 10%. The gain of B^{ilp} w.r.t B^{it} decreases with both N and R^{ci}.

However substantial gains ($\geq 10\%$) are observed for small networks with low CIR. In Fig. 3.5b, we restricted N to the interval [100, 1,000] and R^{ci} to the interval [1, 20]. The average gain increases to 12.9%, with a maximum of 71.4%. Around half (44%) of the samples in this region have a gain greater or equal to 10%. The MILP and the heuristic performances are virtually identical and consequently the previous comparison between B^{ilp} and B^{it} is also valid between B^{hr} and B^{it}. The average gain of B^{ilp} w.r.t. B^{hr} is 0.2%, with a maximum of 25% in very specific cases as shown in Fig. 3.6. A great proportion (96%) of samples in this figure have a gain inferior to or equal to 1%.

Finally, the gains of the MILP and heuristic methods are highly similar to the proportion of unoccupied terminals in the intuitive carrier plan: variations in Fig. 3.7a and 3.7b are almost identical to the ones in Fig. 3.5a and 3.5b. We interpreted this result as proof that the two issues we presented in Section 3.2 play a key role in reaching the optimal bandwidth.

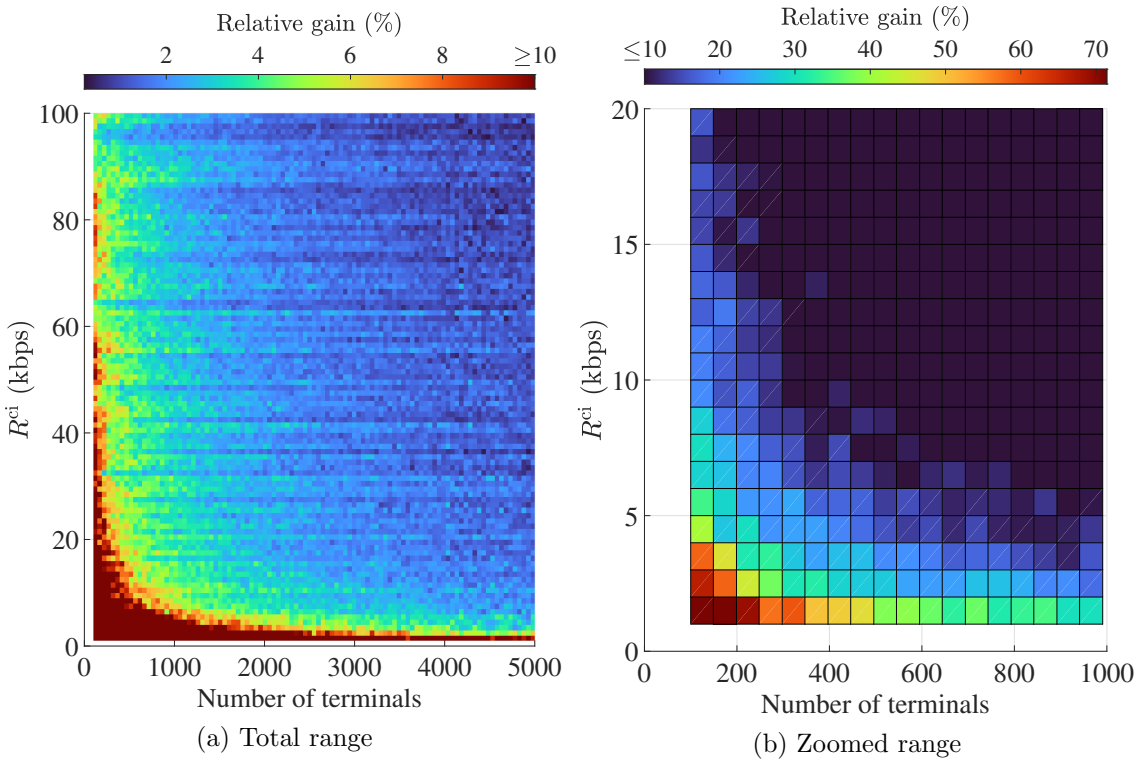

(a) Total range (b) Zoomed range

Figure 3.5: Relative gain of B^{ilp} compared to B^{it} in function of number of terminals and R^{ci}.

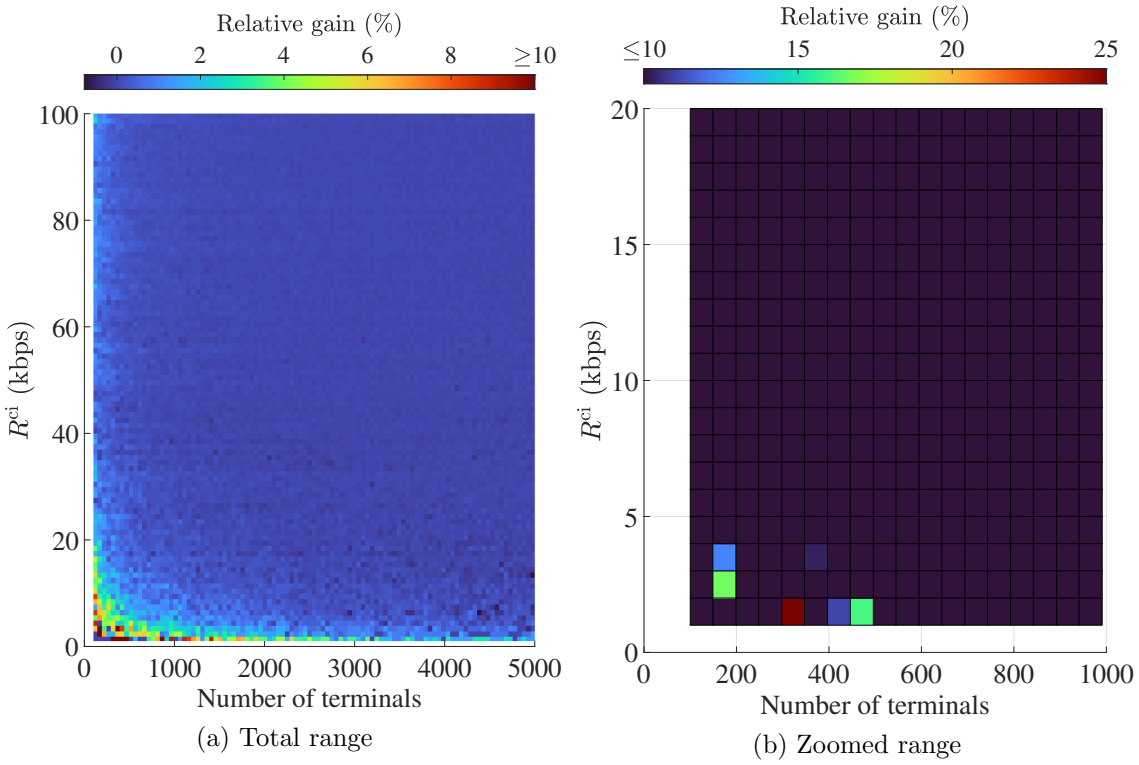

(a) Total range (b) Zoomed range

Figure 3.6: Relative gain of B^{ilp} compared to B^{hr} in function of number of terminals and R^{ci}.

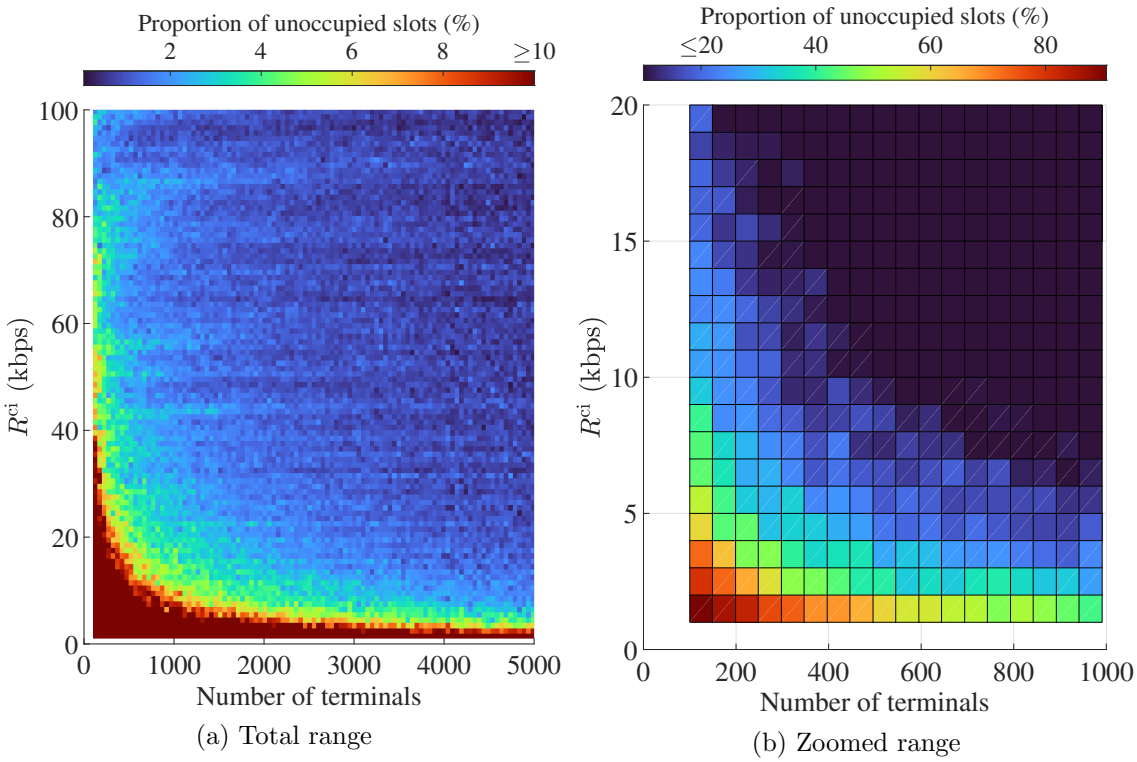

(a) Total range

(b) Zoomed range

Figure 3.7: Proportion of unoccupied slots in the intuitive carrier plan as a function of the number of terminals and R^{ci}.

3.3.3 Impact of the number of FMT modes

The more FMT modes are added to the network, the less the total bandwidth diminishes. As we can see in Fig. 3.8, the blue curve representing the total bandwidth follows a $1/K$ trend for B^{hr} and B^{ilp} and shows negligible improvements once passed the "elbow" of the curve. Depending on the cost of adding one FMT mode, a network designer would be able to determine the optimal operating point. As we can see on the red curve, the gain of B^{ilp} w.r.t. B^{it} increases with K.

3.4 Discussion

The results showed that having a gain similar to the one found in [51], i.e. 82%, was extremely unlikely in a general case. This difference in results can be explained by the difference in the benchmark methods and by the difference in the MILP problem constraints. In the small networks region, our average gain of 12.9% is in line with the 10%-17% bandwidth gain found in [58]. Since CCM networks are usually older than ACM ones, our methods could be useful

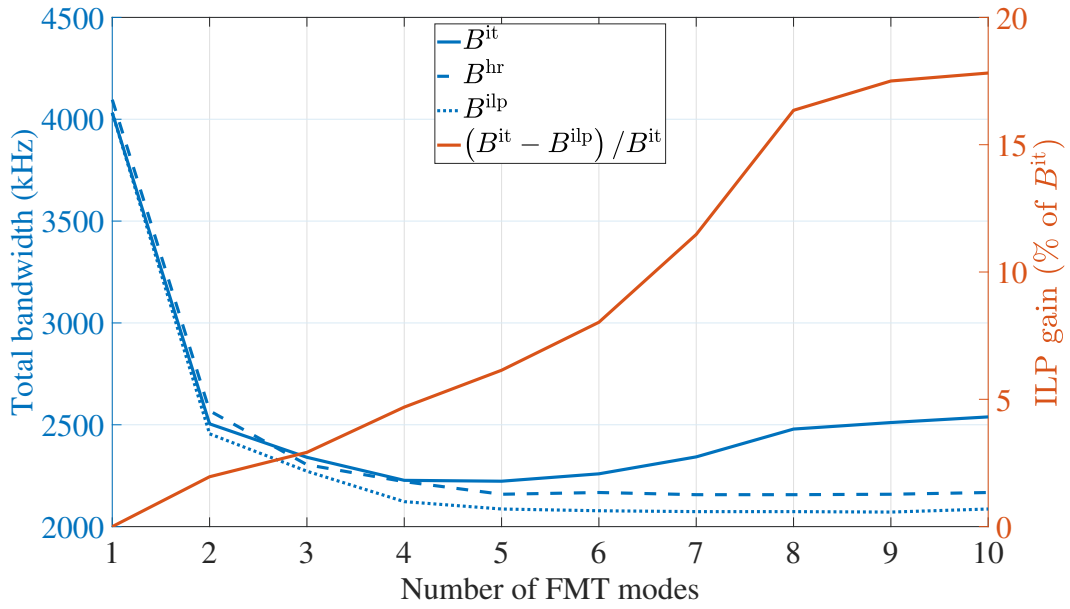

Figure 3.8: Impact of the restriction of the number of FMT modes on the bandwidth ($R^{\text{ci}} = 2$ kbps, $N = 1,000$).

to CCM networks' return links. Section 3.3.3 showed that gains will grow up with K, however, networks with large FMT mode sets are more suited for ACM than CCM, and thus a CCM scenario with significantly more FMT modes would not be realistic. Bandwidth reductions could become substantial for bigger networks in an ACM scenario, which are studied in Chapters 4 and 5. It can also be argued that the performances of the MILP solver depend on its parameters. In our case, the OPTI Toolbox for Matlab[3] was used, which allows using three solvers: the one provided in the Matlab optimization toolbox[4], the *solve constraint integer programs* (SCIP) solver [59] and the *COIN-OR Branch* (CBC) solver [60]. In certain cases the solvers are not able to reach the optimal solution in a reasonable time, thus two stopping conditions were added such that the solver stops if the evaluation function's relative difference with the last iteration is equal or less than 10^{-6} or if the execution time exceeds 5 seconds. The initial lower bound of all $X_{k,l}$ was set to 0 and the initial maximum bound was set to N. The reason for those parameter choices was empirical, allowing the solver to explore enough nodes to give better results than the heuristic while keeping a reasonable execution time to produce Figs. 3.5 and 3.6 (resolution of 100 by 100). With those parameters set, the relative gain difference between the three solvers was within 1.3%, thus only the results from the Matlab toolbox solver were presetend in Section 3.3. Higher gains were reached using more

[3]Available at https://www.controlengineering.co.nz/Wikis/OPTI/ (visited on 24/11/2023).
[4]Available at https://www.mathworks.com/products/optimization.html (visited on 24/11/2023).

processing-heavy parameters, but no major bandwidth gains were observed. On the other hand, using less processing-heavy parameters led to solvers being unable to find a solution in some cases. While the complexity of our different methods was presented for academic purposes, complexity would not necessarily translate into implementation costs. The methods presented are made for the creation and the revision of a network, not for real-time use, thus the execution time seems irrelevant. The only foreseeable costs are integration costs inside the current industry's processes. The integration costs would be quite low as the same inputs and outputs as found in existing processes.

3.5 Conclusion

In this chapter, we presented three methods aimed at building a carrier plan with the smallest bandwidth possible for the return link of a CCM satellite network constrained by discrete bandwidths. We first presented the carrier allocation problem and translated it into a combinatorial optimization problem. We then introduced three different methods to solve the problem: an intuitive benchmark method representative of what is currently being done in the industry, a MILP problem that gives the optimal carrier plan, and a low-complexity heuristic to help us understand the different mechanisms at play. We finally introduced an additional heuristic method to reduce the number of FMT modes in the network while minimizing the bandwidth increase.

We then compared the bandwidth produced by those three methods in a European scenario. In the vast majority of cases (96.9%) the gain of the MILP method w.r.t. the intuitive one was inferior or equal to 10%, which contradicts the findings of [51]. We only saw a significant improvement (12.9% average gain, up to 71.4%) for small networks (less than 1,000 terminals) with a CIR inferior or equal to 20 kbps. The MILP and the heuristic methods showed virtually identical performances, thus the CPO problem is now well understood. Studying the effects of reducing the number of FMT modes present in the network, we showed how a network designer could use the resulting curves to find the optimal trade-off between bandwidth and FMT mode number. We also demonstrated that increasing the dimensionality of the problem will increase the gain of the MILP and heuristic methods w.r.t. our benchmark.

Despite showing marginal improvements overall, the results proved that significant gains can be achieved for networks with small return links at low implementation costs. Moreover, the

translation of the CPO problem opens the way for solving the satellite resource dimensioning problem in the context of ACM-enabled BSM networks.

Chapter 4

Adaptive coding and modulation with static carrier plan

This chapter focuses on solving the CPO problem in the context of ACM return links with SCP. In Section 4.1, we introduce the ACM scenario as well as the carrier plan definition. In Section 4.2, we define the attenuation time series along with other input parameters and show how to formulate a general CPO problem. In Section 4.3, we present a reformulation of the general CPO problem solvable by MILP solvers, as well as a benchmark based on current methods found in the literature. In Section 4.4, we introduce a test scenario in Europe, and we present numerical results comparing our MILP method to the benchmark. In Section 4.5, we discuss some aspects of the two methods and the corresponding results. Finally, Section 4.6 concludes the chapter.

4.1 Scenario description

We consider the return link CPO problem of a single-beam satellite network serving N terminals. We make assumptions similar to Chapter 3 for the return path SLA, i.e.:

- The CIR, in bps, denoted R^{ci}, is identical for all terminals.
- The BER is the same across services.
- The service outage probability, denoted p^{out}, is identical for all terminals.

Our goal is to find a carrier plan that minimizes the network's required satellite transponder bandwidth while ensuring the QoS constraints are satisfied. Given a set of K FMT modes

and a set of bandwidths $\mathcal{B} = \{B_1, ..., B_L\}$, in Hz, we defined in Chapter 3 a carrier plan as a matrix $\mathbf{X}$, with $X_{k,l}$ being the number of carriers associated with FMT mode k and bandwidth B_l. The total bandwidth of the network is computed as:

$$B^{\text{tot}} = \sum_{k=1}^{K} \sum_{l=1}^{L} X_{k,l} \cdot B_l \qquad [\text{Hz}] \ . \tag{4.1}$$

In Chapter 3, we have proposed several solutions that, starting from a given number of terminals $N_k \in \mathcal{I}_N$ using FMT mode k, compute the $X_{k,l}$ values minimizing the total carrier plan bandwidth. Thus, we will focus on computing the optimal $x_k = N_k/N$ in this work, interpreted as the *maximum proportion of terminals* the network will be able to serve with FMT mode k at the committed rate. We then define the (simplified) carrier plan $\mathbf{x}$ as

$$\mathbf{x} = (x_1, \ldots, x_K) \, . \tag{4.2}$$

In this chapter, we assume terminals will be able to adapt the FMT mode used for the transmission depending on the attenuation conditions at their location. Fig. 4.1a illustrates an example of the terminals' requests, with $N = 4$ terminals and $K = 3$ FMT modes. Terminal 4 is in clear sky and can use the most efficient FMT mode. On the other hand, terminals 2 and 3, experiencing moderate fade, can only transmit at committed rate using less spectrally efficient FMT modes. Finally, terminal 1 is facing severe fading and cannot transmit at committed rate.

The carrier plan, however, will not be allowed to change over short periods of time. In Fig. 4.1, we also illustrated an example of such carrier plan with $\mathbf{x} = (x_1, x_2, x_3)$, where $x_1 = x_2 = 1/4$ and $x_3 = 2/4$. This carrier plan can then serve at best one terminal using FMT mode 1, one terminal using FMT mode 2, and two terminals using FMT mode 3, for a total of four terminals. Each represents a time slot of capacity R^{ci}, with the color indicating the FMT mode used for the transmission. For instance, in Fig. 4.1a, terminal 2 is using FMT mode 1, terminal 3 is using FMT mode 2, and terminal 4 is using FMT mode 3. Only one terminal can use FMT mode 3, therefore half of the capacity provisioned for this mode is unused.

In this context, great care must be taken in the composition of the carrier plan to avoid congestion, i.e., to prevent too many terminals from requesting the same FMT mode at the same time. Fig. 4.1b illustrates such a case, as terminals 2 and 3, facing the same rain fade

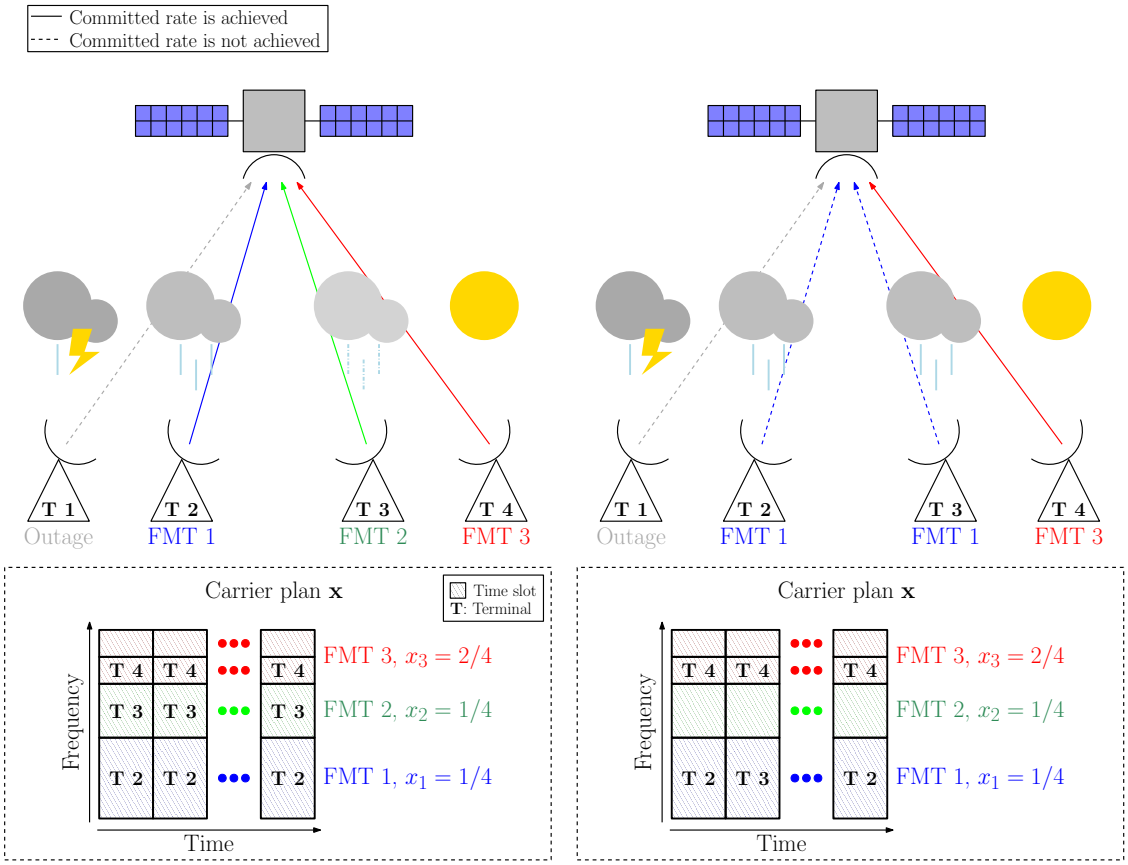

(a) Illustration of outage (terminal 1) due to severe fade conditions.

(b) Illustration of outage (terminals 2 and 3) due to congestion at FMT mode 1.

Figure 4.1: Illustration of the FMT mode demand and carrier plan, with $N = 4$ terminals and $K = 3$ FMT modes.

conditions, request FMT mode 1. However, the carrier plan $\mathbf{x}$, identical to Fig. 4.1a, can only afford one terminal using FMT mode 1. Knowing how the available resources will be distributed among terminals 2 and 3 requires knowing the RRM algorithm behavior (the figure assumes fair distribution by alternating terminals 2 and 3 time slots), however, it is sure that at least one of them will not achieve the committed rate. Thus, the carrier plan composition indirectly influences the satisfaction of the SLA, notably the outage probability p^{out}.

Note that in this case, the spatial correlation of the rain fade between the terminal's locations also plays a role, as it influences the likelihood that multiple terminals request the same FMT mode, and thus the likelihood of congestion. In order to consider the spatial correlation of fade, and given the difficulties of such a task as expressed in Section 2.2.3, we propose in this chapter to take a simulation-based optimization approach. We account for the rain fade and its spatial correlation by means of a time series of spatially correlated

attenuations, assumed given by one of the models presented in Section 2.2.3, and use it as an input of our optimization method.

4.2 Problem formulation

Let us assume given the uplink attenuation time series $a_{n,t}$ faced by the terminal $n \in \mathcal{I}_N$ at time $t \in \mathcal{I}_T$. Then, assuming the same link budget model as in Chapter 3, the CINR $\gamma_n(a_{n,t})$ is computed as follows:

$$\gamma_n(a_{n,t}) = \left[\frac{1}{\left(\frac{C}{N}\right)_n^{\mathrm{ul}}(a_{n,t})} + \frac{1}{\left(\frac{C}{I}\right)_n^{\mathrm{im}}(a_{n,t})} + \frac{1}{\left(\frac{C}{N}\right)_n^{\mathrm{dl}}(a_{n,t})} \right]^{-1}, \tag{4.3}$$

where $(C/N)_n^{\mathrm{dl}}(a_{n,t})$ is the downlink CNR of terminal n, $(C/I)_n^{\mathrm{im}}(a_{n,t})$ is the CIMR, and $(C/N)_n^{\mathrm{ul}}(a_{n,t})$ is the uplink CNR, defined as:

$$\left(\frac{C}{N}\right)_n^{\mathrm{ul}}(a_{n,t}) = (\mathrm{EIRP}_0)_n \cdot \frac{1}{L_n^{\mathrm{fs}} \cdot a_{n,t}} \cdot \left(\frac{G}{T}\right)_n^{\mathrm{sat}} \cdot \frac{1}{k^{\mathrm{B}}}, \tag{4.4}$$

and where:

- $(\mathrm{EIRP}_0)_n$ is the EIRP spectral density of terminal n, in W/Hz, assumed constant over time.
- L_n^{fs} is the free space loss between terminal n and the satellite.
- $(G/T)_n^{\mathrm{sat}}$ is the figure of merit of the satellite at the location of terminal n.
- k^{B} is the Boltzmann constant.

Furthermore, we make the assumption that the terminal's modem supports K FMT modes, ordered by increasing activation thresholds $\{\theta(1), ..., \theta(K)\}$ for the desired BER. We will note $\eta^{\mathrm{spe}}(k)$ the spectral efficiency of FMT mode k, in bps/Hz, and assume $\eta^{\mathrm{spe}}(k)$ increases with $\theta(k)$. The output of our optimization process will be the optimal carrier plan $\mathbf{x}^{\mathrm{opt}} \in [0,1]^K$, which minimizes the system bandwidth under the constraint that terminals must be able to transmit at the committed rate and BER for a proportion of time greater than $1 - p^{\mathrm{out}}$. For the sake of conciseness, we will refer to this constraint as the "outage constraint".

4.2.1 FMT mode request time series

Before diving into the optimization problem, we first need to process the CINR time series in order to extract a time series of FMT mode requests, which we can then use to find the optimal carrier plan. After computing the CINR time series from the attenuation, the following step is to find the index ${}^{\uparrow}k_n\left(a_{n,t}\right)$ of the most spectrally efficient FMT mode ${}^{\uparrow}k_n\left(a_{n,t}\right)$ that the terminal n can use at time t. This is done by comparing the terminal CINR, $\gamma_n\left(a_{n,t}\right)$, against the FMT mode thresholds in order to satisfy the following:

$$ {}^{\uparrow}k_n\left(a_{n,t}\right) = \max\left\{k \in \{0,1,\ldots,K\} \mid \theta\left(k\right) \leq \gamma_n\left(a_{n,t}\right)\right\} , \tag{4.5} $$

with the convention $\theta\left(0\right) = -\infty$, as illustrated in Fig. 4.2. Thus, if ${}^{\uparrow}k_n\left(a_{n,t}\right) = 0$, we know that terminal n is not able to transmit at the committed rate using any FMT mode. We can then determine, for all $k \in \mathcal{I}_K$, the FMT mode request proportion time series, $\hat{x}_k\left(\mathbf{a}_t\right)$, as follows:

$$ \hat{x}_k\left(\mathbf{a}_t\right) = \frac{\left|\left\{n \in \mathcal{I}_N \mid {}^{\uparrow}k_n\left(a_{n,t}\right) = k\right\}\right|}{N} , \tag{4.6} $$

with $\mathbf{a}_t = \left(a_{1,t},\ldots,a_{N,t}\right)$, and:

$$ \hat{\mathbf{x}}\left(\mathbf{a}_t\right) = \left(\hat{x}_1\left(\mathbf{a}_t\right),\ldots,\hat{x}_K\left(\mathbf{a}_t\right)\right) . \tag{4.7} $$

In this chapter, we will use the hat notation to indicate that $\hat{x}_k\left(\mathbf{a}_t\right)$ is a sample computed from the CINR time series. We also define p_n^{link}, the proportion of samples in which terminal n is not able to close the link, as

$$ p_n^{\text{link}} = \frac{\left|\left\{t \in \mathcal{I}_T \mid {}^{\uparrow}k_n\left(a_{n,t}\right) = 0\right\}\right|}{T} . \tag{4.8} $$

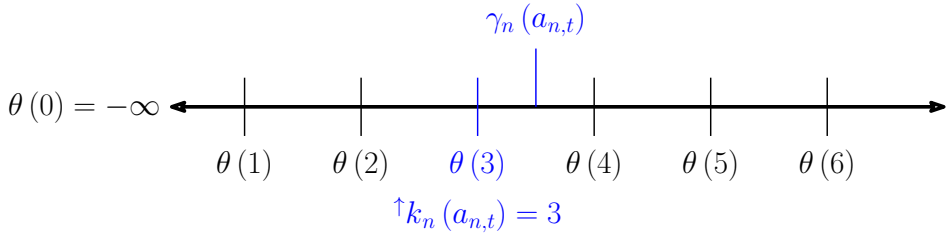

Figure 4.2: Illustration of Eq. (4.5) for ${}^{\uparrow}k_n\left(a_{n,t}\right) = 3$

We assume that, for any terminal n, p_n^{link} is strictly less than p^{out}. Having this condition violated would mean the $(\text{EIRP}_0)_n$ values have not been designed properly in early design steps, and no carrier plan will be able to satisfy the outage constraint.

From a given carrier plan $\mathbf{x}$, we are able to compute the bandwidth needed to deliver R^{ci} to each of the terminal proportions x_k via

$$B(\mathbf{x}) = \sum_{k=1}^{K} \frac{x_k \cdot N \cdot R^{\text{ci}}}{\eta^{\text{spe}}(k)} \qquad [\text{Hz}] \,. \tag{4.9}$$

Our goal is then to find the optimal carrier plan $\mathbf{x}^{\text{opt}} = (x_1^{\text{opt}}, ..., x_K^{\text{opt}})$ solution of the following optimization problem:

$$\underset{\mathbf{x}}{\text{minimize}} \qquad B(\mathbf{x}) \,, \tag{4.10a}$$

$$\text{subject to} \qquad \mathbf{x} \in \mathcal{O} \,, \tag{4.10b}$$

with $\mathcal{O} \subset [0,1]^K$ the viable set of carrier plans that satisfy the outage constraint, which we need to express mathematically.

4.2.2 Outage constraint through order relation

Let us assume we have found $\mathbf{x}^{\text{opt}}$ and have selected it as our network carrier plan. Let us also assume that our network terminals meet fade conditions that lead to an FMT mode demand equal to $\hat{\mathbf{x}}(\mathbf{a}_t)$. In this scenario, the proportion of terminals requesting k is $\hat{x}_k(\mathbf{a}_t)$. If x_k^{opt} is greater or equal to $\hat{x}_k(a_{n,t})$, all the corresponding terminals will have their demand satisfied. However, if x_k^{opt} is less than $\hat{x}_k(a_{n,t})$, the network's carrier plan will not be able to satisfy all terminals' demands. The remaining proportion of terminals $\hat{x}_k(a_{n,t}) - x_k^{\text{opt}}$ will have to seek free capacity in other coordinates of $\mathbf{x}^{\text{opt}}$, i.e., use another FMT mode. As FMT mode usage is conditioned by the terminal CINR, the remaining proportion of terminals can only be re-allocated to x_i^{opt} with $i \in \mathcal{I}_{k-1}$. Having a capacity allocated to every terminal requesting k at time t, including the remaining terminals, is then equivalent to having at least $\hat{x}_k(a_{n,t}) - x_k^{\text{opt}}$ free capacity in the $k-1$ FMT modes between 1 and $k-1$, that is:

$$\sum_{i=1}^{k-1} x_i^{\text{opt}} - \sum_{i=1}^{k-1} \hat{x}_i(a_{n,t}) \geq \hat{x}_k(a_{n,t}) - x_k^{\text{opt}} \,. \tag{4.11}$$

By iterating on k, we deduce that all terminals able to close the link at time t can have a capacity allocated in $\mathbf{x}^{\text{opt}}$ iff

$$\sum_{i=1}^{k} x_i^{\text{opt}} \geq \sum_{i=1}^{k} \hat{x}_i \left(a_{n,t}\right) \qquad \forall k \in \mathcal{I}_K \,. \tag{4.12}$$

We then denote the order relation $\succeq$ as

$$\mathbf{x}^{\text{opt}} \succeq \hat{\mathbf{x}} \left(\mathbf{a}_t\right) \Leftrightarrow \sum_{i=1}^{k} x_i^{\text{opt}} \geq \sum_{i=1}^{k} \hat{x}_i \left(a_{n,t}\right) \qquad \forall k \in \mathcal{I}_K \,, \tag{4.13}$$

and say that $\mathbf{x}^{\text{opt}}$ can accommodate $\hat{\mathbf{x}} \left(\mathbf{a}_t\right)$. This relation is a partial order, but it is not a total order, as it is possible to have both $\mathbf{x}^{\text{opt}} \not\succeq \hat{\mathbf{x}} \left(\mathbf{a}_t\right)$ and $\mathbf{x}^{\text{opt}} \not\preceq \hat{\mathbf{x}} \left(\mathbf{a}_t\right)$, and thus $\mathbf{x}^{\text{opt}} \not\succeq \hat{\mathbf{x}} \left(\mathbf{a}_t\right) \nRightarrow \mathbf{x}^{\text{opt}} \preceq \hat{\mathbf{x}} \left(\mathbf{a}_t\right)$. Note that this order relation is different from the well-known majorization relation [61] since the vector's coordinates are not sorted in descending order.

If $\mathbf{x}^{\text{opt}} \not\succeq \hat{\mathbf{x}} \left(\mathbf{a}_t\right)$, then we know that some terminals will be denied service due to congestion. Knowing exactly which terminals would necessitate precise knowledge of the RRM algorithm. In this work, we decided to provide a solution that is independent of the RRM algorithm, in order to be as general as possible. Thus, we are forced to make the worst-case assumption in which $\mathbf{x}^{\text{opt}} \not\succeq \hat{\mathbf{x}} \left(\mathbf{a}_t\right)$ implies that *all* terminals are denied service.[1]

Given this worst-case assumption, and assuming congestion is the only cause of outage, the only way to ensure the satisfaction of the outage constraint is to have $\mathbf{x}^{\text{opt}}$ accommodating at least $\lceil T \cdot (1 - p^{\text{out}}) \rceil$ samples. Let $\mathcal{A}_{\mathbf{x}}$ denote the set containing all samples accommodated by $\mathbf{x} \in [0,1]^K$ as follows:

$$\mathcal{A}_{\mathbf{x}} = \{t \in \{1, \ldots, T\} \mid \mathbf{x} \succeq \hat{\mathbf{x}} \left(\mathbf{a}_t\right)\} \,. \tag{4.14}$$

Then, the constraint on $\mathbf{x}^{\text{opt}}$ is the following:

$$|\mathcal{A}_{\mathbf{x}^{\text{opt}}}| \geq T \cdot (1 - p^{\text{out}}) \,. \tag{4.15}$$

However, outages are not only caused by congestion but also by link conditions. Without precise information on the RRM algorithms, we need to assume that the set of samples at which a terminal is denied service due to its link's condition is disjoint from the set of time

[1] Section 4.4.3 provides some more insights into the impact of the RRM algorithm.

samples at which this terminal is denied service due to congestion. This implies that $\mathbf{x}^{\text{opt}}$ has to accommodate not just $\lceil T \cdot (1 - p^{\text{out}}) \rceil$ samples, but $\lceil T \cdot (1 - p^{\text{min}}) \rceil$, with p^{min} defined as:

$$p^{\text{min}} = \min \left\{ p^{\text{out}} - p_1^{\text{link}}, \ldots, p^{\text{out}} - p_N^{\text{link}} \right\} . \tag{4.16}$$

The optimal carrier plan then has to satisfy:

$$|\mathcal{A}_{\mathbf{x}^{\text{opt}}}| \geq T \cdot (1 - p^{\text{min}}) . \tag{4.17}$$

We can finally express $\mathcal{O}$ as:

$$\mathcal{O} = \left\{ \mathbf{x} \in [0,1]^K \mid |\mathcal{A}_{\mathbf{x}}| \geq T \cdot (1 - p^{\text{min}}) \right\} , \tag{4.18}$$

and therefore rewrite (4.10) as the following optimization problem:

$$\begin{aligned} \underset{\mathbf{x}}{\text{minimize}} \quad & B(\mathbf{x}) , && \text{(4.19a)} \\ \text{subject to} \quad & |\mathcal{A}_{\mathbf{x}}| \geq T \cdot (1 - p^{\text{min}}) , && \text{(4.19b)} \\ & \mathbf{x} \in [0,1]^K . && \text{(4.19c)} \end{aligned}$$

4.3 Optimization problem

The main difficulty in solving (4.19) resides in efficiently determining if a given $\mathbf{x}$ satisfies (4.19b). In this section, we reformulate (4.19b) with integer constraints, enabling the use of MILP solvers. Then, we introduce a worst-case method that we compare against our MILP formulation in Section 4.4.

4.3.1 Mixed integer linear programming

The optimization problem (4.19) is quite difficult to solve due to the cardinality constraint on $\mathcal{A}_{\mathbf{x}}$ in (4.17), which is non-linear. Drawing inspiration from the work in [62], we can translate the cardinality constraint into an integer constraint. This is done by introducing a binary

optimization variable, $\boldsymbol{\alpha} \in \{0,1\}^T$, as in:

$$|\mathcal{A}_{\mathbf{x}}| \geq T \cdot (1 - p^{\min}) \iff \begin{cases} \sum_{i=1}^{k} x_i \geq \alpha_t \cdot \sum_{i=1}^{k} \hat{x}_i\,(a_{n,t}) & \forall k \in \mathcal{I}_K, \forall t \in \mathcal{I}_T\,, \\ \sum_{t=1}^{T} \alpha_t \geq T \cdot (1 - p^{\min})\,. \end{cases} \tag{4.20}$$

This variable lets the solver decide which samples should be accommodated by $\mathbf{x}$. We can then rewrite the cardinality-constrained optimization problem (4.19) as the following MILP optimization problem:

$$\underset{\mathbf{x},\boldsymbol{\alpha}}{\text{minimize}} \quad B(\mathbf{x})\,, \tag{4.21a}$$

$$\text{subject to} \quad \sum_{i=1}^{k} x_i \geq \alpha_t \cdot \sum_{i=1}^{k} \hat{x}_i\,(a_{n,t}) \qquad \forall k \in \mathcal{I}_K, \forall t \in \mathcal{I}_T\,, \tag{4.21b}$$

$$\sum_{t=1}^{T} \alpha_t \geq T \cdot (1 - p^{\min})\,, \tag{4.21c}$$

$$\mathbf{x} \in [0,1]^K\,, \tag{4.21d}$$

$$\boldsymbol{\alpha} \in \{0,1\}^T\,. \tag{4.21e}$$

This formulation is solvable by standard MILP solvers [63]. The number of constraints grows as $O(K+T)$, as does the size of the optimization variables.

It is important to note that the precision of the solution depends on T and $p^{\min}$. Indeed, as we previously stated, we are looking for a solution that satisfies (4.19b). As we have assumed that $p_n^{\text{link}} < p^{\text{out}}$ for all $n \in \mathcal{I}_N$, then $p^{\min} \in (0,1]$; thus, there exists some $z \in \{0,\ldots,T-1\}$ such that $z/T \leq p^{\min} < (z+1)/T$. Hence, (4.19b) is equivalent to:

$$|\mathcal{A}_{\mathbf{x}^{\text{opt}}}| \geq T \cdot (1 - p^{\min}) \iff |\mathcal{A}_{\mathbf{x}^{\text{opt}}}| \geq \lceil T \cdot (1 - p^{\min}) \rceil \tag{4.22a}$$

$$\iff |\mathcal{A}_{\mathbf{x}^{\text{opt}}}| \geq T - z\,. \tag{4.22b}$$

In the particular case where $0 \leq p^{\min} < 1/T$, then from (4.22) and the fact that $|\mathcal{A}_{\mathbf{x}^{\text{opt}}}| \leq T$ we would have:

$$|\mathcal{A}_{\mathbf{x}^{\text{opt}}}| \geq T \cdot (1 - p^{\min}) \iff |\mathcal{A}_{\mathbf{x}^{\text{opt}}}| = T\,. \tag{4.23}$$

In this case, the solver has to find a solution that accommodates every sample, and it will output the same solution regardless of the value of p^{out}. However, as one can see in Fig. 4.3 in

57, the rain attenuation CCDF, and subsequently the total attenuation, grows exponentially with $\log(1 - p^{\text{out}})$. This exponential behavior has an impact on the size of the bandwidth used by the optimal carrier plan. Thus, having T such that $0 \leq p^{\min} < 1/T$ is an issue, as the bandwidth required to accommodate all samples might be much bigger than what would be really needed for this value of p^{out}. In order to not oversize our carrier plan for a given p^{out} value, we then need to make sure that $T \geq 1/p^{\min}$.

4.3.2 Worst-case method

As a benchmark for our proposal, we consider a worst-case approach as described in the first paragraph of Section 2.2.3, commonly used in the satellite network dimensioning literature. Similarly to the method presented in Chapter 3, it computes the carrier plan $\mathbf{x}^{\text{wc}}$ assuming every terminal n is transmitting using the FMT mode k_n^{tgt}, i.e.:

$$x_k^{\text{wc}} = \frac{\left|\left\{n \in \mathcal{I}_N \mid k_n^{\text{tgt}} = k\right\}\right|}{N} \qquad \forall k \in \mathcal{I}_K \,, \tag{4.24}$$

with k_n^{tgt} computed as:

$$k_n^{\text{tgt}} = \max\left\{k \in \mathcal{I}_K \mid \theta\left(k\right) \leq \gamma_n^{\text{tgt}}\right\}, \tag{4.25}$$

where γ_n^{tgt} is the CINR value exceeded for $1 - p^{\text{out}}\%$ of a given duration (month or year). Traditional satellite resource dimensioning methods would compute γ_n^{tgt} as follows:

$$\gamma_n^{\text{tgt}} = \gamma_n\left(\bar{F}_{a_n}^{-1}\left(p^{\text{out}}\right)\right) \,, \tag{4.26}$$

with $\bar{F}_{a_n}^{-1}$ being the inverse function of the CCDF of a_n, obtained for each terminal by following the ITU model [30] as showed in Fig. 4.3.

Our method assumes available a time series of CINR. Thus, another method to compute γ_n^{tgt} is to use the empirical CDF of γ_n, defined as:

$$F_{\gamma_n}(y) = \frac{1}{T} \cdot \sum_{t=1}^{T} \mathbb{1}_{\gamma_n(a_{n,t}) \leq y} \qquad \forall n \in \mathcal{I}_N \,,\ \forall y \in \mathbb{R}_+ \,. \tag{4.27}$$

The value of $F_{\gamma_n}(y)$ is the proportion of samples in which the CINR of terminal n falls below the value y. We can then compute γ_n^{tgt}, the worst CINR met by terminal n with an outage

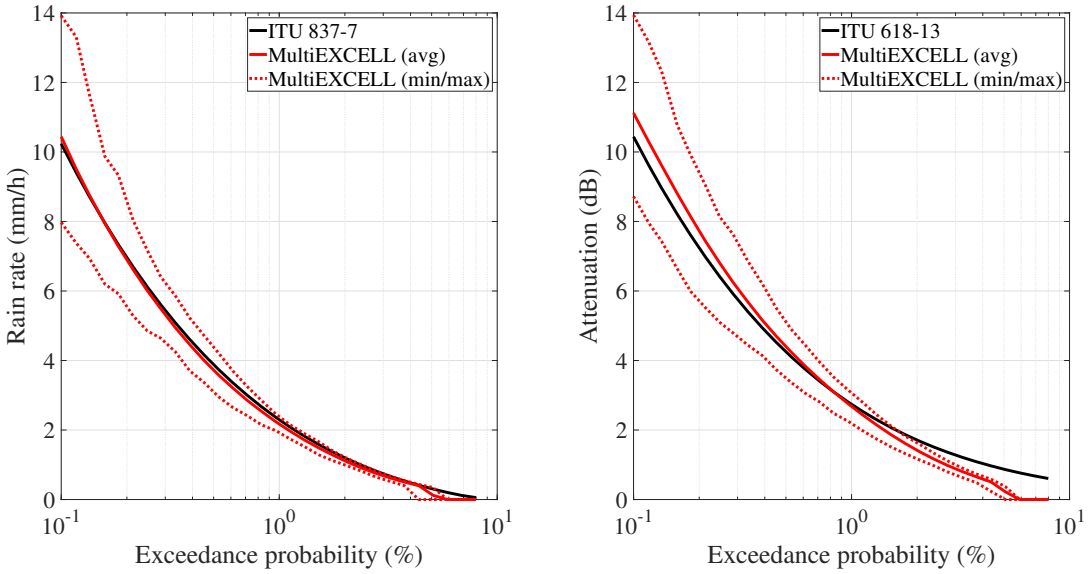

(a) Rain rate CCDF

(b) Rain attenuation CCDF

Figure 4.3: Complementary CDFs of (a) rain rate and (b) rain attenuation, averaged over terminals, obtained with ITU recommendations [64] and [30] (black solid curve) and with the MultiEXCELL [65] samples (red solid curve), as well as minimum and maximum (resp. min/max red dotted curves) CCDFs across all terminals obtained with MultiEXCELL samples.

probability p^{out}, with the generalized inverse distribution function $F_{\gamma_n}^{-1}\left(p^{\text{out}}\right)$, that is:

$$\gamma_n^{\text{tgt}} = F_{\gamma_n}^{-1}\left(p^{\text{out}}\right) \tag{4.28a}$$

$$= \inf\left\{y \in \mathbb{R}_+ \mid F_{\gamma_n}(y) \geq p^{\text{out}}\right\}. \tag{4.28b}$$

4.4 Numerical results

In this section, we compare the MILP method, proposed in Section 4.3.1, with the worst-case method, described in Section 4.3.2. We first present the test scenario and parameters. We then compare the bandwidth produced by the carrier plans, B^{milp} and B^{wc}, respectively computed using the MILP and the worst-case methods.

4.4.1 Test scenario

For our test scenario, we selected a Ka beam in Europe. We generated 489 rain maps of 200 by 200 km centered on (50.79°N, 7.87°E). In all scenarios, the value of $p^{\min}$ never fell below $3.5 \cdot 10^{-5}$. Thus, to satisfy the condition $T \geq 1/p^{\min}$, the 489 rain maps were circularly shifted

multiple times in all directions across the area to obtain $T = 30,000$ samples. Figs. 4.3a and 4.3b respectively show the rain rate and the rain attenuation CCDFs obtained, with solid lines representing averages and dotted lines representing minimums/maximums amongst terminals. On average, the synthetic curves are close to the ITU curves. The differences among the attenuation curves are due to the methods used to compute the attenuation from the rain rate. For the MultiEXCELL maps, we used the ATM PROP method [66], which differs slightly from the recommendation ITU-R P.618 [30].

In addition, $N = 500$ terrestrial terminals were generated in the rain map area based on the population density data of SEDAC [67] (see Fig. 4.4). The terminals' return link total CINR is computed following Eq. (4.3), of which the parameters are given in Table 4.1. The values of the CIMR and the downlink CNR were assumed constant and relatively high such that the uplink CNR is the lowest of the three link budget components.

We selected a maximum information rate of 1 Mbps and a 1:50 contention ratio as suggested in [68], giving us $R^{\text{ci}} = 20$ kbps. We used a FMT mode set with $K = 10$ modes based on the DVB-RCS2 standard [32]. The FMT mode SNR thresholds and spectral efficiencies, shown in Table 4.2, are extracted from [48, Table III].

One goal was to show the evolution of both methods' performances across a range of typical

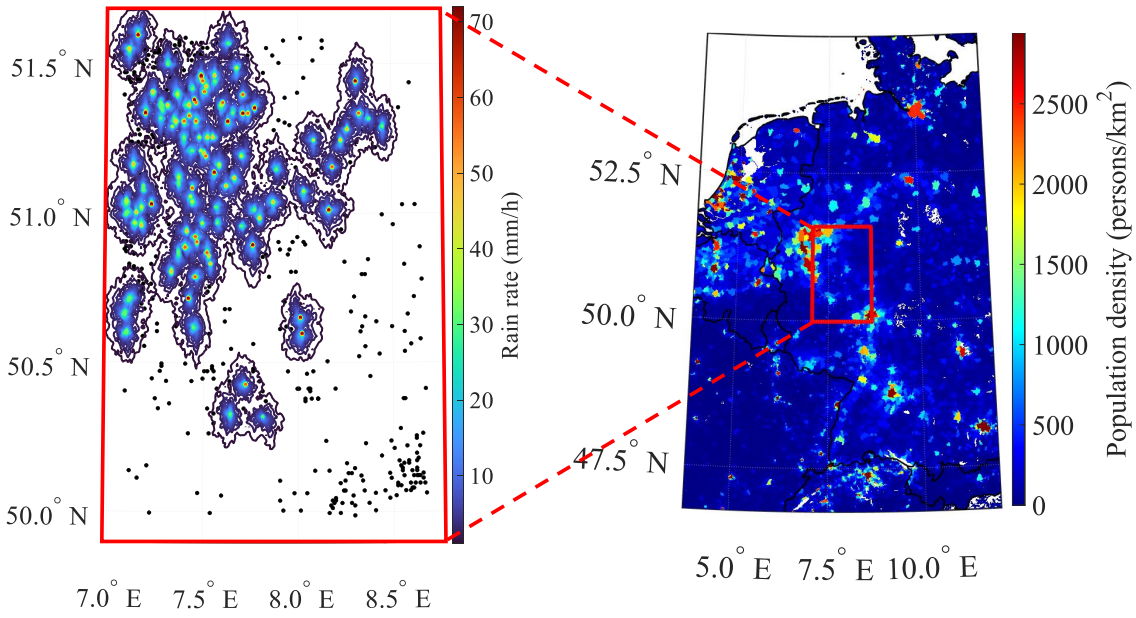

Figure 4.4: Population density used for the terminal generation (right, inside red rectangle) as well as rain map example (left) over generated terminals (black dots)

Table 4.1: Simulation link parameters

Name	**Value**	**Unit**
Frequency	29.75	GHz
Terminals antenna diameter	0.85	m
Terminals antenna gain	45.6	dBi
Satellite longitude	28.5	°East
Average satellite G/T	14.8	dB/K
CIMR	20	dB
CNR	30	dB

values of $p^{\text{out}} \in [p^{\text{lb}} = 0.1\%, p^{\text{ub}} = 5\%]$. However, the performances of the MILP solution also depend on the value of $p^{\min}$, as explained at the end of Section 4.3.1. For a given p^{out} value, and given the link budget parameters presented earlier in this section, the value of $p^{\min}$ can be controlled by changing the value of EIRP_0. However, the value of EIRP_0 is also influenced by other factors that are beyond the scope of this dissertation, such as the forward link design and the tradeoff between the bandwidth costs and the terminals' equipment costs [9, Section 9.2].

Table 4.2: DVB-RCS2 FMT mode parameters

Modulation	**Code rate**	**Spectral efficiency**	**Required** $\frac{E^{\text{s}}}{N_0}$
QPSK	1/3	0.54	0
QPSK	1/2	0.83	2.3
QPSK	2/3	1.16	3.9
QPSK	3/4	1.31	5
QPSK	5/6	1.47	6.1
8-PSK	2/3	1.57	8.2
8-PSK	3/4	1.76	9.3
8-PSK	5/6	1.96	11
16-QAM	3/4	2.31	11.6
16-QAM	5/6	2.57	13

Thus, two different approaches were followed for the computation of this parameter:

- One where EIRP_0 is computed for $p^{\text{out}} = p^{\text{lb}}$ to ensure the following:

$$\min_n \gamma_n \left(\bar{F}_{a_n}^{-1} \left(p^{\text{lb}} \right) \right) \geq \theta \left(1 \right) . \tag{4.29}$$

  Thus, the value of EIRP_0 is fixed for all p^{out} values, and the value of $p^{\min}$ increases with p^{out}. While this approach minimizes bandwidth costs, it maximizes terminals' equipment costs (amplifier and antenna). We will refer to this approach as *bandwidth over equipment* (BOE) scenario.

- A second one where EIRP_0 is computed for each value of p^{out} to ensure the following:

$$\min_n \gamma_n \left(\bar{F}_{a_n}^{-1} \left(p^{\text{out}} \right) \right) \geq \theta \left(1 \right) . \tag{4.30}$$

  Thus, the value of EIRP_0 varies with p^{out}, and the value of $p^{\min}$ remains relatively constant across p^{out} values. This approach minimizes terminals' equipment costs but maximizes bandwidth costs. We will refer to this approach as *equipment over bandwidth* (EOB) scenario.

Real-life satellite networks will neither completely favor equipment nor bandwidth, as both CAPEX and OPEX play a role in the total network price. Thus, we expect the bandwidth performances of our solution applied to such networks to fall in between those two scenarios, of which the results are shown in the following sections.

4.4.2 Bandwidth performance

As depicted by the red curves in Fig. 4.5, the relative bandwidth gain of B^{milp} w.r.t. B^{wc}, i.e., $(B^{\text{wc}} - B^{\text{milp}})/B^{\text{wc}}$, globally increases when p^{out} decreases, and becomes significant (greater than 10%) for $p^{\text{out}} \leq 1\%$ in both scenarios. In both figures, the gain is negative for high p^{out} values (not commonly seen in BSM networks). Then, it rapidly increases to positive values in the EOB scenario, while the increase is slower in the BOE scenario. We then conclude that higher EIRP_0 values will decrease the potential gain the MILP method offers over the worst-case method. The fact that the MILP solution underperforms the worst-case methods for high outage probability values can be explained by several factors:

- The average annual probability of rain in Europe is around 5%. Thus, the impact of rain fade becomes less and less significant for $p^{\text{out}} \geq 1\%$, and the worst-case solution gets closer and closer to optimality.
- The solution of the worst-case method does not necessarily satisfy the accommodation constraint (4.19b). Thus, when the worst-case solution gets close to optimal, the MILP solution is penalized by being more conservative.
- The solving time was limited. This aspect is discussed in further detail in Section 4.5.1.

The local variations in gain observed in Fig. 4.5 are mainly due to the variations of B^{wc}, represented by a black solid line in Figs. 4.6a and 4.6b.

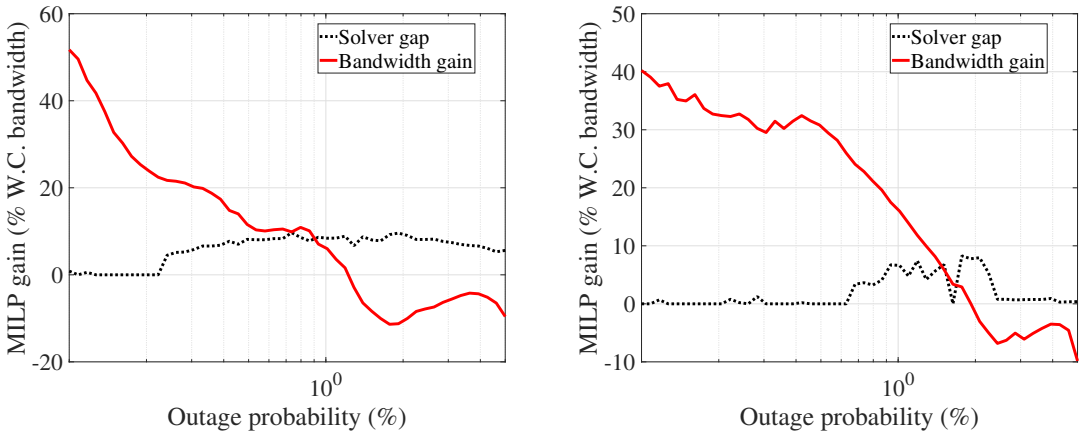

(a) Bandwidth gain and solver gap, BOE (b) Bandwidth gain and solver gap, EOB

Figure 4.5: Relative bandwidth gain $(B^{\text{wc}} - B^{\text{milp}})/B^{\text{wc}}$ and solver gap $(B^{\text{milp}} - B^{\text{lb}})/B^{\text{milp}}$ as a function of p^{out} with (a) BOE and (b) EOB scenarios.

4.4.3 Worst terminal outage

As many simulations had to be run, we imposed a time limit on the MILP solving. The consequence is that for some values of p^{out}, the solver was not able to find the optimal integer value. The black dotted curves in Fig. 4.5 represent the relative gap $(B^{\text{milp}} - B^{\text{lb}})/B^{\text{milp}}$, with the lower bound B^{lb} being the solution of problem (4.21) with relaxed constraints, i.e., $\boldsymbol{\alpha} \in [0, 1]^T$. We observe that the gap curve is overall higher for the BOE scenario than for the EOB scenario. Thus, finding an actual minimum is likely to take more time when the value of EIRP_0 is high. However, a positive gap value does not necessarily imply that a better point exists, but rather that not all options have been explored. Simulations for specific p^{out} values

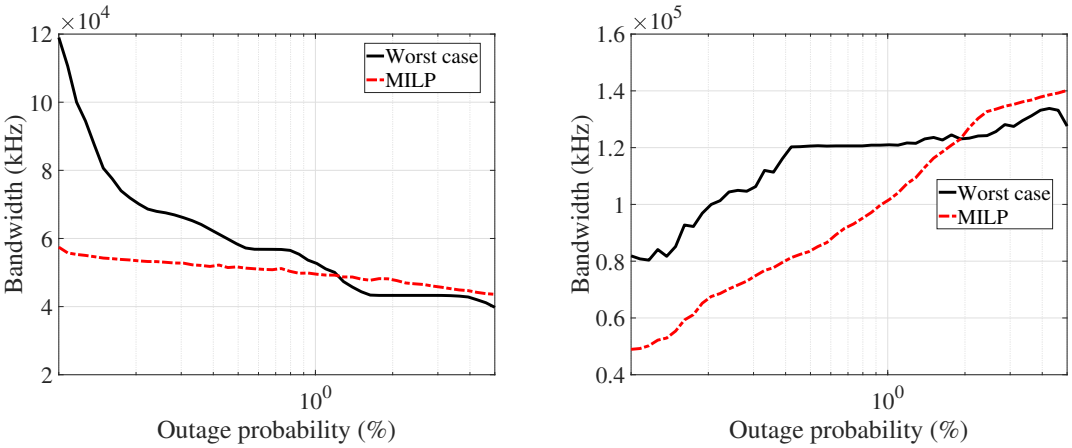

(a) B^{milp} and B^{wc}, BOE (b) B^{milp} and B^{wc}, EOB

Figure 4.6: Evolution of B^{milp} and B^{wc} as a function of p^{out} with (a) BOE and (b) EOB scenarios.

with longer time limits tend to show a reduction in the gap due to finding a higher B^{lb} rather than finding a more bandwidth-efficient solution.

While the MILP method showed overall promising bandwidth performances, it is also important to verify the satisfaction of the outage probability constraint. To this end, we created a test RRM algorithm that determines, for each sample $\hat{\mathbf{x}}(\mathbf{a}_t)$, which terminal will be denied service. For a given sample, the decision to deny service to terminal n is made by comparing $\gamma_n(a_{n,t})$ to γ_n^{wc} and the terminal's clear sky CINR. Terminals are removed from the demand $\hat{\mathbf{x}}(\mathbf{a}_t)$ until the inequality in (4.12) is satisfied. Once $\mathbf{x}^{\text{opt}}$ has been compared against all samples, the algorithm returns the highest outage proportion (link outage + congestion outage) amongst terminals. We name this value the worst terminal outage p^{wto}.

Fig. 4.7 shows the p^{wto} obtained when testing the carrier plans produced by both methods. We can see that both the MILP and the worst-case methods are able to satisfy $p^{\text{wto}} \leq p^{\text{out}}$. Moreover, our MILP method provides lower p^{wto} than the worst-case method. It is then apparent that increasing the bandwidth efficiency of the solution does not necessarily come at the expense of higher outage probability. The gap between the two methods is quite significant in the BOE scenario, while moderate in the EOB scenario. This difference could be explained by the value of EIRP_0, which is higher in the BOE scenario for high values of p^{out}.

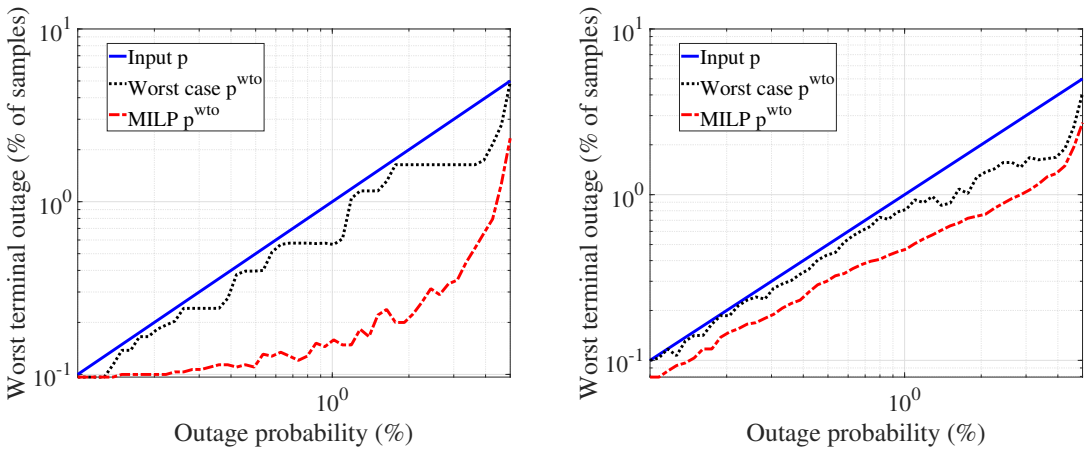

(a) Worst terminal outage p^{wto}, BOE (b) Worst terminal outage p^{wto}, EOB

Figure 4.7: Comparison of p^{wto} for the worst case and the MILP methods as a function of requested p^{out}, with (a) BOE and (b) EOB scenarios.

4.5 Discussions

4.5.1 MILP solver implementation

The convergence time of the MILP method depends on the solver's implementation and parameters. In our case, we used the integrated MATLAB integer linear programming solver *intlinprog*.[2] We limited the solver's execution in time to 6 hours per value of p^{out}, with simulations running in parallel on single core threads. We also instructed the solver to stop if it found an integer solution within 1% of the relaxed solution, as gains lower or equal to 1% will not be significant in the context of network cost optimization. Execution times of several hours are affordable in our problem as the carrier plan optimization is not a real-time problem in the context of SCP. We also tested other solvers in specific scenarios, most notably the SCIP [59] and CVX [69], [70] solvers. No notable differences in bandwidth gain or solver gap were observed with those parameters. However, we observed a quicker reduction in the solver's gap when running a specific simulation on multiple cores with CVX.

4.5.2 Variability of rain

In Fig. 4.5, we observed a crossing point at which the MILP bandwidth increased from negative values to positive ones. This crossing point depends on the average annual probability of rain p_0 across terminals. As p_0 depends on the terminals' geographical locations, the crossing point

[2] Available at https://www.mathworks.com/products/optimization.html (visited on 24/11/2023).

is expected to change for networks serving tropical or desertic regions, where p_0 is respectively higher and lower than in our European scenario.

The number of samples T also plays a role in the variability of rain amongst terminals. The lower the exceedance probability is, the lower the number of samples representing this probability. As shown in Fig. 4.3, this translates into a high variability among terminals' CCDFs at low exceedance probabilities. Higher T values would reduce this effect and bring the dotted curves in Fig. 4.3 closer to the average curves.

The variability of rain amongst terminals is also impacted by the geographical separation between terminals in the network. In our scenario, 200 by 200 km maps were used, as MultiEXCELL does not allow for the generation of much larger fields. The consequence is that the variability of rain is rather low, and mainly tied to T.

4.5.3 RRM policy

The curves shown in Fig. 4.7 depend on the RRM policy, of which an example was presented in Section 4.4.3. One important property of this policy is that it stops denying service to terminals when the accommodation property is satisfied. Thanks to the conservative nature of the accommodation property, the MILP method will guarantee $p^{\text{wto}} \leq p^{\text{out}}$ for any RRM policy that delivers service to all terminals if the accommodation property is satisfied, i.e., if there are enough satellite resources available to serve all terminals. On the other hand, the worst-case method does not come with such a guarantee; indeed, it can be straightforwardly verified by testing the resulting carrier plan on a drop policy which drops the terminals based on a predetermined order, regardless of their CINR.

4.5.4 Heterogeneity for QoS and number of terminals

In a real BSM network, it is common to have different QoS parameters (R^{ci} and p^{out}) among terminals. In this context, a way to use our technique would be to group terminals under QoS groups, run the optimization for each group separately, and then merge the resulting carrier plans. This approach, however, has no optimality guarantees. Heterogeneous QoS requirements are explored in Chapter 5.

Another concern is the disparity in the number of terminals between the design stage and deployment phase, as well as its increase during the network lifetime. If the number of terminals was overestimated during the design phase, then the carrier plan is still valid,

although not optimal. On the other hand, if the number of terminals was underestimated, there would be more congestion than anticipated, and the QoS might not be achieved. Therefore, real applications of our solution will likely have to anticipate a future rise in the number of terminals and take margins accordingly.

4.6 Conclusion

In this chapter, we presented the CPO problem for return links using ACM with SCP and proposed a more bandwidth-efficient solution compared to current dimensioning methods. We defined the return link carrier plan design problem as applicable to broadband networks with adaptive return links and proposed a MILP optimization formulation that explicitly accounts for the spatial correlation of the tropospheric fade, using time series generators. Finally, we introduced a dimensioning benchmark inspired by the academic literature and compared it to our MILP method in a European test scenario.

The numerical results illustrated how the proposed MILP method brings a bandwidth reduction between 10% and 50% w.r.t. benchmark for outage probabilities less than 1%, while also being able to provide lower outage statistics.

From those results, we concluded that the MILP method can improve the carrier plan of BSM return networks using ACM by reducing their cost and providing stronger QoS guarantees.

Chapter 5

Adaptive coding and modulation with adaptive carrier plan

This chapter focuses on solving the SRD problem in the context of ACM return links with ACP. It is divided into two major parts: the theoretical part and the application part, as illustrated in Fig. 5.1. Both parts are composed of several sections and are of relatively equal length.

The theoretical part regroups all the sections that focus on the theory behind the satellite

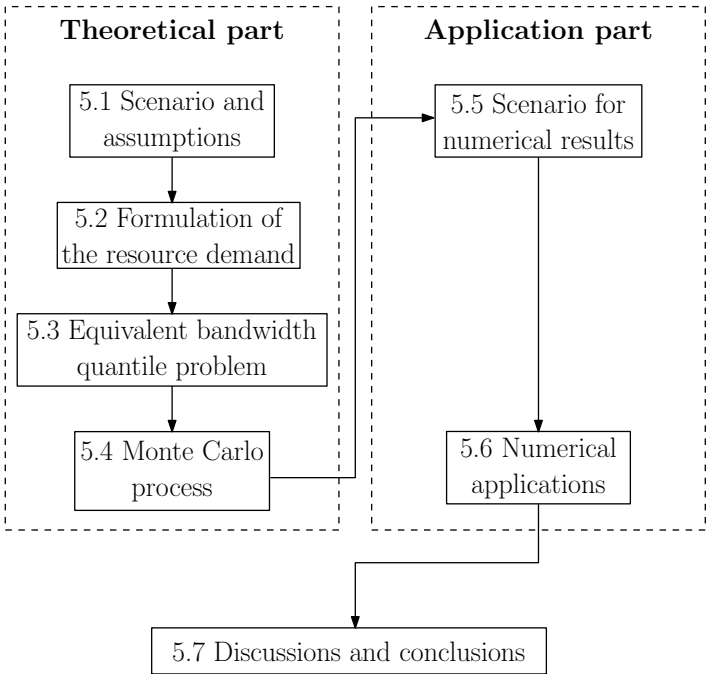

Figure 5.1: Illustration of the chapter's contents.

resource dimensioning problem and the use of rain sample generators to solve it. It is composed of four sections. Section 5.1 presents the definitions and assumptions related to our problem. Section 5.2 explains how to express the satellite resource demand at the system level for given rain attenuation. Section 5.3 presents the resource dimensioning problem formulated as a quantile estimation problem. Section 5.4 proposes a Monte Carlo method to approximate the solution.

Then, the application part focuses on applying the theory presented in the previous part to a realistic multibeam satellite scenario. It is composed of two sections. Section 5.5 provides a complete description of the models and data used for the numerical simulations. Note that this section is only a description of a scenario that fits the assumptions described in Section 5.1, and can be read independently of Sections 5.2 to 5.4. Section 5.6 presents the numerical results, providing a numerical verification of the Monte Carlo method and comparisons against independent (optimistic) and fully correlated (pessimistic) rain fade assumptions. Finally, Section 5.7 concludes the chapter.

5.1 Scenario and assumptions

In this section, we describe the scenario and the assumptions relevant to the resource-demand model presented later in Section 5.2. This section firstly introduces definitions related to the SLA, of which the traffic aspects are discussed in Section 5.1.2 and the availability aspects are discussed in Section 5.1.3. Then, assumptions for network, satellite payload, and link budget aspects are listed in Sections 5.1.4, 5.1.5, and 5.1.6, respectively.

We tackle the problem of dimensioning the satellite's bandwidth and power needed for the return path of a broadband multibeam GEO satellite network serving N source terminals, as illustrated in Fig. 5.2. The terminals are assumed to be earth stations with a fixed known location.

5.1.1 SLA and QoS definitions

In this section, we look at the most common services proposed in broadband return links, and how SLA are refined into key parameters for our design process. The requirements in the SLA usually take a similar form to what is described by the ETSI in [24], with application/service-specific QoS parameters. For the dimensioning process, it is necessary to extract and aggregate

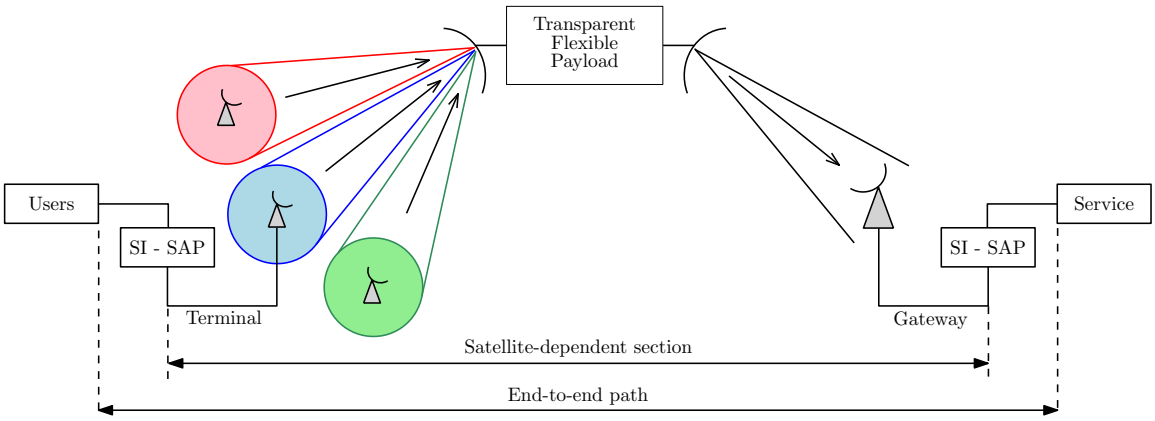

Figure 5.2: Illustration of the multibeam BSM return network scenario. The satellite-dependent path is delimited by the *satellite-independent service access point* (SI-SAP) interfaces.

the relevant information into key parameters, which are used as inputs to the dimensioning methodology. For the purpose of satellite resource dimensioning, we can identify two main SLA categories: traffic, discussed in Section 5.1.2, and availability, discussed in Section 5.1.3.

Throughout the rest of this chapter, we assume that the traffic demand is independent across terminals and from the link conditions.

5.1.2 Traffic SLA

Global standardizing institutions have investigated broadband networks and their compatibility with satellite networks. The ETSI presents in [21] an architecture where IP and higher layer traffic (satellite-independent layer) are converted into lower satellite-dependent layers through an SI-SAP interface. The SLAs are usually defined at an application/service level, i.e., at the satellite-independent layers. The ETSI [71, Section 4.1] and the ITU [72, Section 6] have defined several service categories for broadband networks (e.g., conversational, messaging, transactions, etc.).

It is also important to note that SLA requirements are usually not defined per terminal, but rather per "*service package*" (SP), corresponding to typical user profiles. The number and composition of the SPs are usually driven by pricing and network technologies. For the rest of this chapter, let us assume that S SPs are available. Each terminal n will subscribe to one and only one SP denoted as s_n, and the set of terminals subscribed to the s-th SP is denoted as $\mathcal{N}_s = \{n \in \mathcal{I}_N \mid s_n = s\}$.

Traffic characterization

Traffic characterization, done at the service level, consists of modeling the expected throughput requirements of each service. It also allows us to estimate the statistical multiplexing that can be used to save resources. The list of SLA requirements is heterogeneous and is very much dependent on the service category, as can be seen in [24, Section 5]. Factoring all those individual requirements inside the resource dimensioning process would unnecessarily complexify it, as not all of them are equally important. We propose to summarize the SLA of any service class into three parameters:

- The maximum information rate R^{mi}, in bps, which should be achievable under favorable network conditions, but with no availability guarantees.
- The minimum/committed rate of the service R^{ci}, in bps, which comes with a given availability target. This rate is the rate necessary for one terminal to get the service at a minimum acceptable quality.
- The expected proportion of active terminals p^{at}, i.e., the expected simultaneous demand for the service.

To illustrate these concepts, we present in Appendix A how to compute the three parameters R^{mi}, R^{ci}, and p^{at} for some popular traffic classes, based on some SLA inputs. We provide examples based on industry and academic literature [73, Section 4.3], [8, Section 6.2], however, note that the nature of SLA requirements is quite scenario-dependent. Therefore, the reader might have to adapt the computations when faced with SLA requirements of a different nature.

Mapping at SI-SAP interface

To ensure the satisfaction of SLAs, the traffic must be split into different classes, each class having its own QoS and priority. As service categories are defined at the application level, the QoS has to be translated to the different protocol layers in the network. The process of translating QoS/priority from one layer to another is called QoS/priority mapping. The mapping of IP QoS classes to satellite-dependent layer classes happens at the SI-SAP interface. The ITU proposes six different classes in [74] for IP-based services. The ETSI proposes eight different BSM traffic classes in [71, Section 5], allowing the mapping of higher level ITU

or *Diff Serv* traffic classes to satellite-dependent lower-layers traffic classes (e.g., ATM and DVB-RCS). These BSM traffic classes are identified by their *queue ID* (QID).

For our problem, we will assume that Q traffic classes are available at the SI-SAP interface, with $q = 1$ being the lowest priority class and $q = Q$ being the highest.[1] We assume that the service categories have been mapped to each traffic class $q \in \mathcal{I}_Q$, such that we can define $R_{s,q}^{\text{ci}}$ and $R_{s,q}^{\text{mi}}$ as the sum of the corresponding rates of the services mapped to traffic class q, and $p_{s,q}^{\text{at}}$ as the maximum among the services.

5.1.3 Availability SLA

The ETSI defines the IP service availability based on the *IP packet loss ratio* (IPLR) [25, Section 7.4]. The IP service is defined as available if the IPLR is below or equal to a pre-determined threshold, and unavailable (equivalently, in outage) otherwise. The same definition is found with the ITU [74, Section 7].

The potential causes of an increase in IPLR are several. To identify the ones related to the satellite-dependent part of the connection, the ITU-R S.521-4 defines an end-to-end satellite link as a hypothetical reference digital path. The ITU-R S.1806-0 uses this definition to introduce path availability (averaged over the measured time). It is defined as:

$$\text{Availability} = (100 - \text{Unavailability}) \qquad [\%]\,, \tag{5.1}$$

in which

$$\text{Unavailability} = \frac{\text{Unavailable time}}{\text{Measured time}} \cdot 100 \qquad [\%]\,. \tag{5.2}$$

The Measured time can be one day/month/year, with an hourly unit time. The Unavailable time is defined per terminal n as a period in time where the QoS is not met for a minimum consecutive duration of ΔT^{out} (recommend to be 10 s). The QoS at the path level is generally defined using the BER metric, which is directly related to the IPLR.

However, this definition of availability is only valid for transmission at a given rate. In the context of networks using ACM technologies and services that require a minimum throughput to be usable, we need to expand this definition. Indeed, ACM allows to trade BER with throughput when changing transmission mode. Thus, it is possible that an ACM transmission

[1] If needed, one can define $q = 0$ as the Best Effort class, which is rarely considered during the dimensioning process.

mode allows an acceptable IPLR but at the expense of lowering the connection throughput below the service minimum rate (i.e., the committed rate). In this case, the IP service is available, but not the application-level service. To measure the availability of an application-level service, we need to also look at the throughput achieved when the BER threshold is met. This characteristic of ACM-enabled networks is acknowledged in the ITU-R S.2131-1 [75, Section 2.4], which presents the notion of throughput degradation as a function of the SNR.

In our case, we will define the service availability as the time duration in which both the BER and the committed information rate necessary for the service are met. Furthermore, we define the SP availability as the time duration in which *all* included services are available. Let us assume the SPs come with an advertised outage probability p_s^{adv}, over a measurement period T^{tot}, in seconds, and a given outage duration threshold ΔT_s^{out}, in seconds, above which the outage time is effectively counted. Then, if we can predict the total outage time T_n^{out} of terminal n during T^{tot}, accounting for ΔT_s^{out}, we can compute the outage probability p_n^{out} of this terminal as:

$$p_n^{\text{out}} = \frac{T_n^{\text{out}}}{T^{\text{tot}}} \,. \tag{5.3}$$

The availability SLA is then translated into the satisfaction of the following constraint:

$$p_n^{\text{out}} \leq p_{s_n}^{\text{adv}} \qquad \forall n \in \mathcal{I}_N \,. \tag{5.4}$$

The computation of T_n^{out} is not trivial. For now, let us remark that we can divide this quantity into distinct components, each representing a different outage cause:

1. The outage time due to link unavailability, written T_n^{link}, in seconds, defined as the sum of durations greater than $\Delta T_{s_n}^{\text{out}}$ in which the link fade is too strong to allow transmitting at the committed rates and appropriate BER. This quantity solely depends on the terminal's link budget design.

2. The outage time due to congestion, written T_n^{con}, in seconds, defined as the sum of durations in which the link can sustain both committed rates and BER, but the satellite resources available for allocation are insufficient due to a number of concurrent terminals exceeding expectations. This quantity is affected by the amount of satellite resources available and the rain conditions on the satellite coverage.

3. The outage time due to other causes unrelated to rain conditions, such as equipment

failure or sun transit [10, p. 29].

In this chapter, we will focus on the outage cases affected by the satellite resource dimensioning process and by rain fade, i.e., cases 1) and 2). We will assume that $T_n^{\text{out}} = T_n^{\text{link}} + T_n^{\text{con}}$. Other sources of outage can be added to this definition by considering them uncorrelated to 1) and 2).

5.1.4 Network assumptions

We assume that the return link access uses an MF-TDMA scheme, capable of dynamically allocating bandwidth (examples are found in [32] and [36, Section 7.2]).[2] We assume that individual channel sizes are a multiple c of a minimum channel bandwidth $\Delta B^{\min}$, with $c \in \mathcal{I}_C$, and C being the maximum channel multiplier. We will refer to c as the channel/carrier size. We also assume that all terminals share the same MF-TDMA resources.[3]

The MF-TDMA resource allocation is handled by an RRM algorithm (e.g., [35]). However, there is no one standard RRM algorithm for all satellite return networks. To remain as general as possible, we will not make assumptions about the behavior of the RRM algorithm in this chapter.

In addition, we assume that ACM is enabled, thus terminals can adapt their FMT mode in real time. They can choose to emit from a pool of K FMT modes (e.g., [32, Annex A]) defined by the following characteristics:

- The SNR activation thresholds $\{\theta(1), \ldots, \theta(K)\}$, derived from the desired BER.[4]
- The spectral efficiencies $\{\eta^{\text{spe}}(1), \ldots, \eta^{\text{spe}}(K)\}$, in bps/Hz. We assume $\eta^{\text{spe}}(k)$ increases with $\theta(k)$.

Finally, we assume a star topology network. Each source terminal $n \in \mathcal{I}_N$ emits to its destination gateway $d_n \in \mathcal{I}_D$, with D being the number of destination gateways.

5.1.5 Satellite payload assumptions

We assume that the satellite uplink coverage is split into M beams, with each beam $m \in \mathcal{I}_M$ being assigned a pair $\left(\text{freq}_m^{\text{ul}}, \text{pol}_m^{\text{ul}}\right)$ denoting its frequency and polarization, respectively. The

[2] See also https://www.gilat.com/technologies/elastix-access-scheme/ for an example in the industry (visited on 04/12/2023).

[3] If not, the dimensioning problem should be split into several sub-problems for which this assumption holds.

[4] We assume the BER is identical for all SPs and services. If not, a conservative assumption is to take the lowest BER value to get the highest SNR thresholds.

frequency-polarization pair is commonly referred to as the "color" of the beam. We assume the downlink is composed of spot beams covering the gateways' locations.

In this chapter, we assume the payload is transparent and flexible in a similar way to the scenario described in [49, Section II.B]. It is assumed that the beams covering the terminals' locations are able to dynamically share satellite transponders' power.[5] We assume that V transponders are available for dynamic allocation.

5.1.6 Link budget assumptions

We assume knowledge of the link budget function $\gamma_{0,n}\left(\mathbf{a}_{n,t}^{\text{tot}}\right)$, in Hz, that computes the *carrier-to-interference-plus-noise-spectral-density ratio* (CINR_0)[6] of terminal n when transmitting under rain attenuation $\mathbf{a}_{n,t}^{\text{tot}} = (a_{n,t}, a_{d_n,t})$, where $a_{n,t}$ and $a_{d_n,t}$ are respectively the attenuation at terminal's n and at gateway's d_n locations at given time t. Typical link budget models are found in [8, Chapter 5], [73, Chapter 5]. We assume that $\gamma_{0,n}\left(\mathbf{a}_{n,t}^{\text{tot}}\right)$ does not depend on the channel size c,[7] and that it is a nonincreasing function of $a_{n,t}$ and $a_{d_n,t}$. We also assume given the *input back off* (IBO) function of terminal n, denoted as $\text{IBO}_n\left(a_{n,t}\right)$ and that it is a nonincreasing function of $a_{n,t}$. Note that examples of both $\gamma_{0,n}\left(\mathbf{a}_{n,t}^{\text{tot}}\right)$ and $\text{IBO}_n\left(a_{n,t}\right)$ functions are described in great details in Sections 5.5.2, 5.5.3, and 5.5.4, which can be read independently of the following sections.

5.2 Formulation of the resource demand

In this section, we present the satellite resource demand model given the assumptions made in the previous section. Firstly, Section 5.2.1 establishes the various relationships and notations between information rates, FMT modes, and attenuation conditions. Then, the satellite resource demand model is introduced from a terminal-level perspective, with Section 5.2.2 focusing on the bandwidth demand, Section 5.2.3 focusing on the power demand, and Section 5.2.4 presenting the bandwidth vs. power trade-off. From the expression of the resource demand, Section 5.2.5 deduces some requirements on the terminal's emission capabilities for clear sky and fade conditions. Finally, the system-level resource demand is expressed in

[5] If not, the dimensioning problem should be split into several sub-problems for which this assumption holds.

[6] In this chapter, it is important to distinguish between the carrier-to-noise ratio, which is a ratio between two powers, and the carrier-to-noise-spectral-density ratio, which is the ratio between a power and a power spectral density (see [8, Section 5.6.1]).

[7] We implicitly assume that the terminals are transmitting at full power under rain fade.

Section 5.2.6.

5.2.1 Transmission at a given rate

Let us assume that terminal n has to transmit an information rate R^{i} at time t. We want to know what channel size and FMT mode could support this transmission, if any.

For each FMT mode k, the minimum channel size required to transmit rate R^{i} is given by:

$$c^{\min}\left(R^{\mathrm{i}}, k\right) = \left\lceil \frac{R^{\mathrm{i}}}{\eta^{\mathrm{spe}}\left(k\right) \cdot \Delta B^{\min}} \right\rceil . \tag{5.5}$$

Let us remember that each FMT mode comes with SNR activation thresholds. Let us define the signal-to-noise-spectral-density activation threshold $\theta_0(k, c)$, in Hz, as a function of the channel size:

$$\theta_0(k, c) = \theta\left(k\right) \cdot c \cdot \Delta B^{\min} \qquad [\mathrm{Hz}] . \tag{5.6}$$

In order to transmit R^{i} on FMT mode k at time t, terminal n should therefore satisfy the following CINR_0 condition:

$$\gamma_{0,n}\left(\mathbf{a}_{n,t}^{\mathrm{tot}}\right) \geq \theta_0\left(k, c^{\min}\left(R^{\mathrm{i}}, k\right)\right) . \tag{5.7}$$

This condition is necessary, but not sufficient. Let us remember that the channel size is bounded by C. Therefore, the transmission is not possible if $c^{\min}\left(R^{\mathrm{i}}, k\right) > C$. As we assumed that $\eta^{\mathrm{spe}}\left(k\right)$ is an increasing function of k, $c^{\min}\left(R^{\mathrm{i}}, k\right)$ is a nonincreasing function of k. Thus, C imposes a lower bound on the FMT that can be used. The minimum channel size $c^{\min}\left(R^{\mathrm{i}}, k\right)$ is a non-increasing function of k for a given R^{i}, thus, such lower bound is found by counting the number of modes unable to support the transmission and adding one, that is:

$$k^{\min}\left(R^{\mathrm{i}}\right) = 1 + \sum_{k=1}^{K} \mathbb{1}_{c^{\min}(R^{\mathrm{i}},k)>C} . \tag{5.8}$$

Transmission at minimum bandwidth

Since $c^{\min}\left(R^{\mathrm{i}}, k\right)$ is a nonincreasing function of k, we know that the FMT mode minimizing the channel size required for transmission at a given rate R^{i} is the highest value k that satisfies

inequality (5.7). Such upper bound is given by:

$$k_n^{\max}\left(R^{\mathrm{i}}, \mathbf{a}_{n,t}^{\mathrm{tot}}\right) = \max\ \{0\} \cup \left\{k \in \mathcal{I}_K \mid \gamma_{0,n}\left(\mathbf{a}_{n,t}^{\mathrm{tot}}\right) \geq \theta_0\left(k, c^{\min}\left(R^{\mathrm{i}}, k\right)\right)\right\} . \tag{5.9}$$

Remark that this definition allows $k_n^{\max}$ to take a null value in the case no FMT mode satisfies (5.7). In order to generalize the equations that depend on the FMT mode, we need to define $\theta(0)$ and $\eta^{\mathrm{spe}}(0)$. A natural behavior for a terminal trying to transmit at rate R^{i} but not able to reach it would be to transmit at the highest achievable rate,[8] using the most robust FMT mode available, i.e., $k = 1$. Following this logic, we should define $\theta(0) = \theta(1)$ and $\eta^{\mathrm{spe}}(0) = \eta^{\mathrm{spe}}(1)$, with the implicit understanding that rate R^{i} is not achievable.

Finally, let us also remark that in the case $k_n^{\max}\left(R^{\mathrm{i}}, \mathbf{a}_{n,t}^{\mathrm{tot}}\right) < k^{\min}\left(R^{\mathrm{i}}\right)$, the transmission at information rate R^{i} is not possible at time t due to the constraint on the maximum channel size.

Transmission at highest achievable rate

Let us now assume terminal n wants to transmit at the highest achievable information rate $R_n^{\max}(k, \mathbf{a}_{n,t}^{\mathrm{tot}})$ using the FMT mode k at time t. To find such a rate, we first need to compute the largest channel size $c_n^{\max}\left(k, \mathbf{a}_{n,t}^{\mathrm{tot}}\right)$ available for transmission:

$$c_n^{\max}\left(k, \mathbf{a}_{n,t}^{\mathrm{tot}}\right) = \min\left(\left\lfloor \frac{\gamma_{0,n}\left(\mathbf{a}_{n,t}^{\mathrm{tot}}\right)}{\theta(k) \cdot \Delta B^{\min}} \right\rfloor, C\right) . \tag{5.10}$$

We deduce the expression of the maximum achievable rate:

$$R_n^{\max}(k, \mathbf{a}_{n,t}^{\mathrm{tot}}) = \eta^{\mathrm{spe}}(k) \cdot c_n^{\max}\left(k, \mathbf{a}_{n,t}^{\mathrm{tot}}\right) \cdot \Delta B^{\min} \qquad [\mathrm{bps}] . \tag{5.11}$$

[8] For a given $\gamma_{0,n}\left(\mathbf{a}_{n,t}^{\mathrm{tot}}\right)$, the highest rate is reached using the mode with the highest $\eta^{\mathrm{spe}}(k)/\theta(k)$ ratio (see Eq. (5.11) later on). This is usually mode 1, due to the greater variations in $\theta(k)$ values.

Transmission at SLA rates

In this chapter, we will often refer to the transmissions at the sum of the committed rates $\sum_{q=1}^{Q} R_{s_n,q}^{\mathrm{ci}}$. For the sake of simplicity, we define:

$$c_s^{\mathrm{ci}}(k) = c^{\min}\left(\sum_{q=1}^{Q} R_{s,q}^{\mathrm{ci}}, k\right) \tag{5.12a}$$

$$^{\downarrow}k_s^{\mathrm{ci}} = k^{\min}\left(\sum_{q=1}^{Q} R_{s,q}^{\mathrm{ci}}\right) \tag{5.12b}$$

$$^{\uparrow}k_n^{\mathrm{ci}}\left(\mathbf{a}_{n,t}^{\mathrm{tot}}\right) = k_n^{\max}\left(\sum_{q=1}^{Q} R_{s_n,q}^{\mathrm{ci}}, \mathbf{a}_{n,t}^{\mathrm{tot}}\right) , \tag{5.12c}$$

with $c^{\min}$ as defined in Eq. (5.5), $k^{\min}$ as defined in Eq. (5.8), and $k^{\max}$ as defined in Eq. (5.9).

5.2.2 Expression of the bandwidth demand

Assuming terminal n requests access to the satellite services at time t, its bandwidth demand $b_{n,q}^{\mathrm{D}}\left(\mathbf{a}_{n,t}^{\mathrm{tot}}, k\right)$ depends on the achievable rate of the link, and therefore on the FMT mode k used for transmission. The minimum channel size needed for transmission at committed rates is given by $c^{\mathrm{ci}}(s_n, k)$. Thus, the link's support of committed rates can be assessed via the fraction $c_n^{\max}\left(k, \mathbf{a}_{n,t}^{\mathrm{tot}}\right) / c^{\mathrm{ci}}(s_n, k)$, with $c_n^{\max}\left(k, \mathbf{a}_{n,t}^{\mathrm{tot}}\right)$ the largest channel size available for transmission defined in Eq. (5.10). If this fraction is strictly below 1, the rate supported by the link is below the committed rates, and the services are unavailable using FMT mode k. If this fraction is above or equal to 1, the committed rates are supported by FMT mode k. We can express the achievable committed rate of terminal n, for the traffic class q, at time t, and transmitting on the FMT mode k, as a function of the link's quality:

$$R_{n,q}^{\mathrm{ca}}\left(\mathbf{a}_{n,t}^{\mathrm{tot}}, k\right) = R_{s_n,q}^{\mathrm{ci}} \cdot \min\left(1, \frac{c_n^{\max}\left(k, \mathbf{a}_{n,t}^{\mathrm{tot}}\right)}{c^{\mathrm{ci}}(s_n, k)}\right) \qquad [\mathrm{bps}] . \tag{5.13}$$

Therefore, we propose to model the individual bandwidth demand $b_{n,q}^{\mathrm{D}}\left(\mathbf{a}_{n,t}^{\mathrm{tot}}, k\right)$ of terminal n, at time t, and using the FMT mode k, as the following:

$$b_{n,q}^{\mathrm{D}}\left(\mathbf{a}_{n,t}^{\mathrm{tot}}, k\right) = \frac{R_{n,q}^{\mathrm{ca}}\left(\mathbf{a}_{n,t}^{\mathrm{tot}}, k\right)}{\eta^{\mathrm{spe}}(k)} \qquad [\mathrm{Hz}] . \tag{5.14}$$

5.2.3 Expression of the power demand

As explained in the introduction of this chapter, the billing of the network is set on the resource that is proportionally utilized the most [9, Chapter 13], [10, p. 29]. Therefore, we also need to compute the power demand.

The fraction of available transponder power used by terminal n can be expressed as the ratio between the current IBO of the terminal's carrier, denoted $\mathrm{IBO}_n\left(a_{n,t}\right)$,[9] and the total IBO of the satellite transponder v_n, denoted as $\mathrm{IBO}_{v_n}^{\mathrm{tot}}$, to which the channel was affected. However, this power demand corresponds to a transmission at maximum power for the terminal. For the purpose of satellite resource dimensioning, we need to compute the committed power demand, i.e., the power demand corresponding to the committed bandwidth demand as expressed in Eq. (5.14). Let us remark that the maximum bandwidth sustainable for terminal n, at time t, and using the FMT mode k, is given by the fraction $\gamma_{0,n}\left(\mathbf{a}_{n,t}^{\mathrm{tot}}\right)/\theta\left(k\right)$. Thus, the committed bandwidth demand represents a proportion $b_{n,q}^{\mathrm{D}}\left(\mathbf{a}_{n,t}^{\mathrm{tot}},k\right)\cdot\theta\left(k\right)/\gamma_{0,n}\left(\mathbf{a}_{n,t}^{\mathrm{tot}}\right)$ of the maximum bandwidth achievable. Therefore, the committed fraction of power demanded relative to the total power available can be expressed as:

$$P_{n,q}^{\mathrm{D}}\left(\mathbf{a}_{n,t}^{\mathrm{tot}},k\right)=\frac{b_{n,q}^{\mathrm{D}}\left(\mathbf{a}_{n,t}^{\mathrm{tot}},k\right)\cdot\theta\left(k\right)}{\gamma_{0,n}\left(\mathbf{a}_{n,t}^{\mathrm{tot}}\right)}\cdot\frac{\mathrm{IBO}_n\left(a_{n,t}\right)}{\mathrm{IBO}_{v_n}^{\mathrm{tot}}}\,. \tag{5.15}$$

The comparison between the bandwidth and power utilization is usually done by converting the requested power to *power-equivalent bandwidth* (PEB), as follows:[10]

$$b_{n,q}^{\mathrm{pe,D}}\left(\mathbf{a}_{n,t}^{\mathrm{tot}},k\right)=B_{v_n}^{\mathrm{trans}}\cdot P_{n,q}^{\mathrm{D}}\left(\mathbf{a}_{n,t}^{\mathrm{tot}},k\right)\qquad[\mathrm{Hz}]\,. \tag{5.16}$$

with $B_{v_n}^{\mathrm{trans}}$ being the bandwidth of the transponder v_n. The PEB value corresponds to the transponder bandwidth that should be used to match the transponder power demand. If all transmissions amplified by this transponder have a bandwidth demand matching the PEB demand, then the transponder utilization is maximized in the sense that bandwidth and power are equally utilized.

[9] More details are given about the IBO later in Section 5.5.2.

[10] See https://www.satcom.guru/2015/02/link-budget-background-definitions-and.html for more details on the concept of PEB (visited on 04/12/2023).

5.2.4 Balanced FMT mode

We assume that the terminals, if possible, will transmit using the FMT mode that supports committed rates and minimizes the satellite resource demand. Denoting $k_n^{\mathrm{msr}}\left(\mathbf{a}_{n,t}^{\mathrm{tot}}\right)$ the FMT mode that minimizes the satellite resource demand for given attenuation conditions $\mathbf{a}_{n,t}^{\mathrm{tot}}$, it is given as:

$$k_n^{\mathrm{msr}}\left(\mathbf{a}_{n,t}^{\mathrm{tot}}\right) = \underset{k\in\mathcal{K}_n^{\mathrm{ci}}\left(\mathbf{a}_{n,t}^{\mathrm{tot}}\right)}{\arg\min} \max\left(\sum_{q=1}^{Q} b_{n,q}^{\mathrm{D}}\left(\mathbf{a}_{n,t}^{\mathrm{tot}},k\right), \sum_{q=1}^{Q} b_{n,q}^{\mathrm{pe,D}}\left(\mathbf{a}_{n,t}^{\mathrm{tot}},k\right)\right), \tag{5.17}$$

with $b_{n,q}^{\mathrm{D}}\left(\mathbf{a}_{n,t}^{\mathrm{tot}},k\right)$ being the bandwidth demand defined in Eq. (5.14), $b_{n,q}^{\mathrm{pe,D}}\left(\mathbf{a}_{n,t}^{\mathrm{tot}},k\right)$ being the PEB demand defined in Eq. (5.16), and $\mathcal{K}_n^{\mathrm{ci}}\left(\mathbf{a}_{n,t}^{\mathrm{tot}}\right)$ the set of FMT modes suitable for transmission at committed rates, expressed as:

$$\mathcal{K}_n^{\mathrm{ci}}\left(\mathbf{a}_{n,t}^{\mathrm{tot}}\right) = \left\{ {}^{\downarrow}k_{s_n}^{\mathrm{ci}} \leq k \leq {}^{\uparrow}k_n^{\mathrm{ci}}\left(\mathbf{a}_{n,t}^{\mathrm{tot}}\right) \mid (5.7) \right\}, \tag{5.18}$$

with ${}^{\downarrow}k_{s_n}^{\mathrm{ci}}$ and ${}^{\uparrow}k_n^{\mathrm{ci}}\left(\mathbf{a}_{n,t}^{\mathrm{tot}}\right)$ respectively the lowest and highest FMT modes supporting a transmission at committed rates given the attenuation conditions $\mathbf{a}_{n,t}^{\mathrm{tot}}$, as defined in Eq. (5.12).

As illustrated in Fig. 5.3, the bandwidth demand $b_{n,q}^{\mathrm{D}}\left(\mathbf{a}_{n,t}^{\mathrm{tot}},k\right)$ tends to decrease with k while the PEB demand $b_{n,q}^{\mathrm{pe,D}}\left(\mathbf{a}_{n,t}^{\mathrm{tot}},k\right)$ tends to decrease. Thus, the FMT mode $k_n^{\mathrm{msr}}\left(\mathbf{a}_{n,t}^{\mathrm{tot}}\right)$ will correspond to the mode that allows the values of the bandwidth and the PEB demands to be the closest to each other among all the FMT modes in $\mathcal{K}_n^{\mathrm{ci}}\left(\mathbf{a}_{n,t}^{\mathrm{tot}}\right)$. It is said that this mode "balances" the bandwidth and power demands, hence we call it the *balanced* FMT mode.

Note that $k_n^{\mathrm{msr}}\left(\mathbf{a}_{n,t}^{\mathrm{tot}}\right)$ is defined only when at least one FMT allows transmission at the committed rates, i.e., when ${}^{\uparrow}k_n^{\mathrm{ci}}\left(\mathbf{a}_{n,t}^{\mathrm{tot}}\right) \geq {}^{\downarrow}k_{s_n}^{\mathrm{ci}}$. Thus, the most suitable FMT mode for

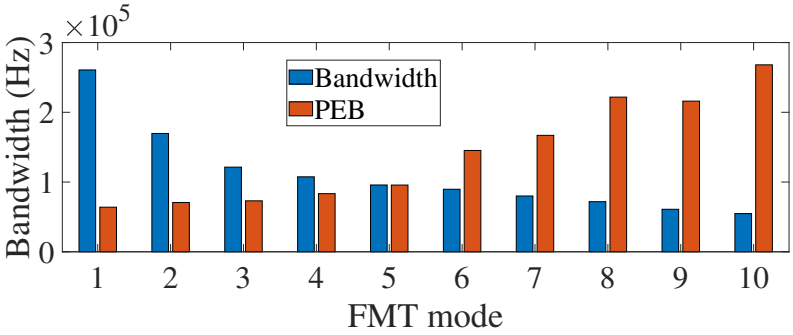

Figure 5.3: Illustration of the bandwidth vs. PEB (i.e., power) demand tradeoff for a transmission at committed rates. Here, $k_n^{\mathrm{msr}}\left(\mathbf{a}_{n,t}^{\mathrm{tot}}\right) = 5$.

transmission is:

$$\bar{k}_n^{\mathrm{ci}}\left(\mathbf{a}_{n,t}^{\mathrm{tot}}\right) = \begin{cases} {}^{\uparrow}k_n^{\mathrm{ci}}\left(\mathbf{a}_{n,t}^{\mathrm{tot}}\right) & \text{if } {}^{\uparrow}k_n^{\mathrm{ci}}\left(\mathbf{a}_{n,t}^{\mathrm{tot}}\right) < {}^{\downarrow}k_{s_n}^{\mathrm{ci}} \\ k_n^{\mathrm{msr}}\left(\mathbf{a}_{n,t}^{\mathrm{tot}}\right) & \text{otherwise.} \end{cases} \tag{5.19}$$

The resource demand model at the terminal level is summarized in Fig. 5.4.

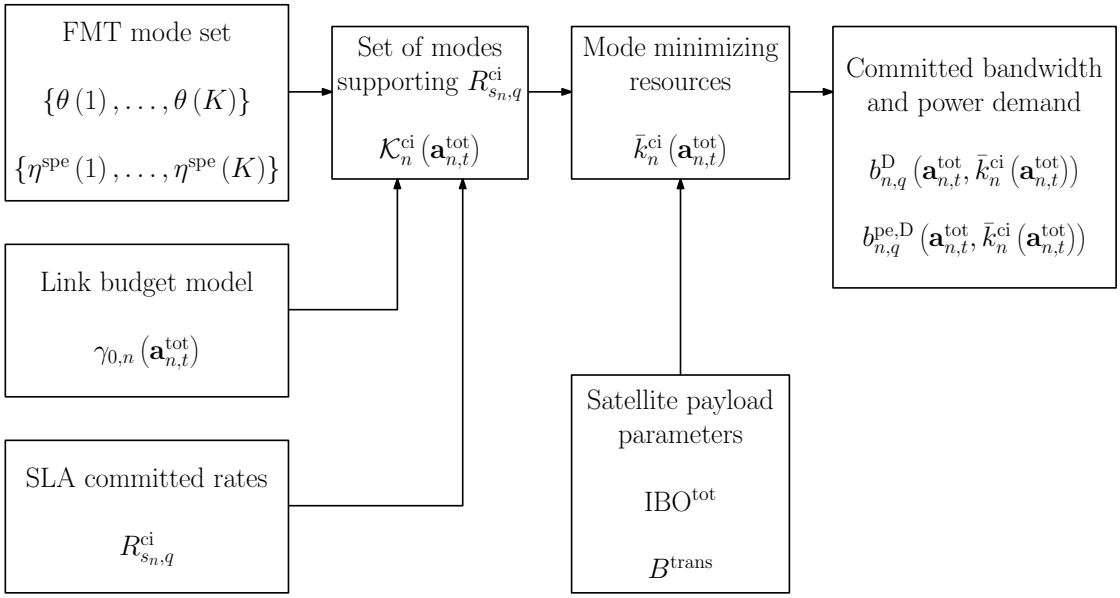

Figure 5.4: Illustration of the resource demand model at the terminal level

5.2.5 Ground station requirements

Knowing the FMT mode that terminal n will select under given fade $\mathbf{a}_{n,t}^{\mathrm{tot}}$, we can deduce some requirements that all terminals must satisfy to enable the dimensioning process. We will present those requirements in the following sections and assume those are met in the rest of the chapter. Let us remark that the design of ground stations can be affected by factors other than the ones we have presented so far (e.g., forward link design).

Clear sky requirement

As assumed in Section 5.1.1, the maximum rate $\max_{q\in I_Q} R_{s_n,q}^{\mathrm{mi}}$ must be achievable at least under the most favorable conditions, i.e., when the sky is clear and $\mathbf{a}_{n,t}^{\mathrm{tot}} = (1,1)$. Therefore, the clear sky requirement is:

$$k_n^{\max}\left(\max_{q\in I_Q} R_{s_n,q}^{\mathrm{mi}}, (1,1)\right) \geq k^{\min}\left(\max_{q\in I_Q} R_{s_n,q}^{\mathrm{mi}}\right), \tag{5.20}$$

with $k^{\min}$ as defined in Eq. (5.8) and $k^{\max}$ as defined in Eq. (5.9).

Fade requirement

As assumed in Section 5.1.1, the probability of terminal n not being able to transmit at committed rates $\sum_{q=1}^{Q} R_{s_n,q}^{\text{ci}}$ must not exceed $p_{s_n}^{\text{adv}}$.[11] Thus, the fade requirement is:

$$P\left(\bar{k}_n^{\text{ci}}\left((A_n, A_{d_n})\right) < {}^{\downarrow}k_{s_n}^{\text{ci}}\right) \leq p_{s_n}^{\text{adv}}\,, \tag{5.21}$$

with $\bar{k}_n^{\text{ci}}$ as defined in Eq. (5.19), ${}^{\downarrow}k_{s_n}^{\text{ci}}$ as defined in Eq. (5.12), and where A_n and A_{d_n} are the random variables of the rain attenuation at the respective locations of terminal n and gateway d_n. Such property can be verified by looking at [76], which allows to get a numerical estimate of $P\left(\bar{k}_n^{\text{ci}}\left((A_n, A_{d_n})\right) < k\right)$ for any k. We explain the method in more detail in Appendix B.

5.2.6 Resource demand at system level

So far, we have expressed the individual bandwidth demand $b_{n,q}^{\text{D}}\left(\mathbf{a}_{n,t}^{\text{tot}}, \bar{k}_n^{\text{ci}}\left(\mathbf{a}_{n,t}^{\text{tot}}\right)\right)$ assuming that terminal n is requesting access to the satellite services. However, terminals are not active all the time. When taking a system-level viewpoint, the total bandwidth demand should account for the statistical probability of terminals requesting the services. Thus, from the system point of view, the bandwidth demand of terminal n, for traffic class q, under the attenuation conditions $\mathbf{a}_{n,t}^{\text{tot}}$, can be modeled with the following random variable:

$$B_{n,q}^{\text{D}}\left(\mathbf{a}_{n,t}^{\text{tot}}\right) = b_{n,q}^{\text{D}}\left(\mathbf{a}_{n,t}^{\text{tot}}, \bar{k}_n^{\text{ci}}\left(\mathbf{a}_{n,t}^{\text{tot}}\right)\right) \cdot X_{n,q}\,, \tag{5.22}$$

with $X_{n,q}$ following a Bernoulli distribution with probability of success $p_{s_n,q}^{\text{at}}$. Note that $X_{n,q}$ is independent of the attenuation $\mathbf{a}_{n,t}^{\text{tot}}$ due to the assumption of independence between traffic demand and attenuation conditions made in Section 5.1.1.

Let $\mathbf{A}_t^{\text{tot}}$ be an $N \times 2$ matrix containing the uplink and downlink attenuation couples for each link at time t, i.e., $\mathbf{A}_t^{\text{tot}}(n,1) = a_{n,t}$ and $\mathbf{A}_t^{\text{tot}}(n,2) = a_{d_n,t}$. For a high number of terminals N and the attenuation conditions $\mathbf{A}_t^{\text{tot}}$, the total bandwidth demand will likely be

[11] In this case, we take a worst-case approach by assuming the terminal requests all services at the same time.

close to its expected value b^{TD},[12] which is expressed as:

$$b^{\mathrm{TD}}\left(\mathbf{A}_t^{\mathrm{tot}}\right) = \mathbb{E}_X\left(\sum_{n=1}^{N}\sum_{q=1}^{Q} B_{n,q}^{\mathrm{D}}\left(\mathbf{a}_{n,t}^{\mathrm{tot}}\right)\right) \tag{5.23a}$$

$$= \sum_{n=1}^{N}\sum_{q=1}^{Q} \mathbb{E}_X\left(B_{n,q}^{\mathrm{D}}\left(\mathbf{a}_{n,t}^{\mathrm{tot}}\right)\right) \tag{5.23b}$$

$$= \sum_{n=1}^{N}\sum_{q=1}^{Q} b_{n,q}^{\mathrm{D}}\left(\mathbf{a}_{n,t}^{\mathrm{tot}}, \bar{k}_n^{\mathrm{ci}}\left(\mathbf{a}_{n,t}^{\mathrm{tot}}\right)\right) \cdot \mathbb{E}_X\left(X_{n,q}\right) \tag{5.23c}$$

$$= \sum_{n=1}^{N}\sum_{q=1}^{Q} b_{n,q}^{\mathrm{D}}\left(\mathbf{a}_{n,t}^{\mathrm{tot}}, \bar{k}_n^{\mathrm{ci}}\left(\mathbf{a}_{n,t}^{\mathrm{tot}}\right)\right) \cdot p_{s_n,q}^{\mathrm{at}} \qquad [\mathrm{Hz}]\ , \tag{5.23d}$$

with $\mathbb{E}_X$ being the expectation operator on the random variables $X_{n,q}$. Similarly, the expected total PEB demand is expressed as:

$$b^{\mathrm{pe,TD}}\left(\mathbf{A}_t^{\mathrm{tot}}\right) = \sum_{n=1}^{N}\sum_{q=1}^{Q} b_{n,q}^{\mathrm{pe,D}}\left(\mathbf{a}_{n,t}^{\mathrm{tot}}, \bar{k}_n^{\mathrm{ci}}\left(\mathbf{a}_{n,t}^{\mathrm{tot}}\right)\right) \cdot p_{s_n,q}^{\mathrm{at}} \qquad [\mathrm{Hz}]\ . \tag{5.24}$$

Finally, the total equivalent bandwidth demand is:

$$b^{\mathrm{eq,TD}}\left(\mathbf{A}_t^{\mathrm{tot}}\right) = \max\left(b^{\mathrm{pe,TD}}\left(\mathbf{A}_t^{\mathrm{tot}}\right), b^{\mathrm{TD}}\left(\mathbf{A}_t^{\mathrm{tot}}\right)\right) \qquad [\mathrm{Hz}]\ . \tag{5.25}$$

5.3 Equivalent bandwidth quantile problem

The optimal network equivalent bandwidth b^{net} is the smallest one for which the outage probability p_n^{out} of all terminals, as defined in Eq. (5.3), is smaller than or equal to the advertised outage probability defined in the SLA, i.e., $p_n^{\mathrm{out}} \leq p_{s_n}^{\mathrm{adv}}$ for all n. We defined in Section 5.1.3 $p_n^{\mathrm{out}} = T_n^{\mathrm{out}}/T^{\mathrm{tot}}$ and $T_n^{\mathrm{out}} = T_n^{\mathrm{link}} + T_n^{\mathrm{con}}$. Thus, the condition on b^{net} can be formulated as:

$$\frac{T_n^{\mathrm{link}} + T_n^{\mathrm{con}}}{T^{\mathrm{tot}}} \leq p_{s_n}^{\mathrm{adv}} \qquad \forall n \in \mathcal{I}_n\,, \tag{5.26}$$

In the following sections, we will investigate how to express T_n^{link} and T_n^{con} given the bandwidth demand model presented in Section 5.2. Section 5.3.1 focuses on the expression of T_n^{link}, while Section 5.3.2 focuses on the expression of T_n^{con}. Finally, Section 5.3.3 injects both expressions

[12] Considering "close to" as a confidence interval of κ standard deviations and width $\alpha \cdot b^{\mathrm{TD}}$, one can estimate the minimum number of terminals needed using the binomial distribution, with a success probability p equal to the average $p_{s_n,q}^{\mathrm{at}}$, with $\sqrt{\kappa/\alpha} \cdot (p \cdot (1-p))^{-1}$.

into Eq. (5.26), and the optimal network equivalent bandwidth is expressed as the solution of a quantile estimation problem.

5.3.1 Computation of link outage time

The value T_n^{link} represents the duration in which terminal n is under outage due to link conditions, for consecutive periods greater than $\Delta T_{s_n}^{\text{out}}$. From the previous sections, we know the link might not allow the satisfaction of SLA rates when $\bar{k}_n^{\text{ci}}\left(\mathbf{a}_{n,t}^{\text{tot}}\right) < {}^{\downarrow}k_{s_n}^{\text{ci}}$.

At the time of writing this chapter, there is no method to compute T_n^{link}. The best approximation available is described in the ITU-R P.1623 [77, Annex 1]. It allows us to compute T_n^{link} for separate uplink and downlink with the following formula:

$$T_n^{\text{link}} = F(d > \Delta T_{s_n}^{\text{out}} \mid A_n > a) \cdot \bar{F}_{A_n}(a) \cdot T^{\text{tot}} \qquad [\text{s}] \ , \tag{5.27}$$

where $F(d > \Delta T_{s_n}^{\text{out}} \mid A_n > a)$, the conditioned CCDF of the outage duration, is computed following the recommendation, and a is a given attenuation value.[13]

Thus, we propose to approximate T_n^{link} via the following methodology. First, compute the probability p_n^* of using an FMT mode lower than ${}^{\downarrow}k_{s_n}^{\text{ci}}$:

$$p_n^* = P\left(\bar{k}_n^{\text{ci}}\left((A_n, A_{d_n})\right) < {}^{\downarrow}k_{s_n}^{\text{ci}}\right) \ , \tag{5.28}$$

using the method described in Appendix B. Then, compute the attenuation values $a_n^* = \bar{F}_{A_n}^{-1}(p_n^*)$ and $a_{d_n}^* = \bar{F}_{A_{d_n}}^{-1}(p_n^*)$. Then, compute the two values:

$$T_n^* = F(d > \Delta T_{s_n}^{\text{out}} \mid A_n > a_n^*) \cdot p_n^* \cdot T^{\text{tot}} \qquad [\text{s}] \tag{5.29a}$$

$$T_{d_n}^* = F(d > \Delta T_{s_n}^{\text{out}} \mid A_{d_n} > a_{d_n}^*) \cdot p_n^* \cdot T^{\text{tot}} \qquad [\text{s}] \ . \tag{5.29b}$$

Finally, define $T_n^{\text{link}} = \max\left(T_n^*, T_{d_n}^*\right)$.

Note that the rest of the problem formulation does not depend on the technique to compute the value of T_n^{link}, as long as $T_n^{\text{link}} < p_{s_n}^{\text{adv}} \cdot T^{\text{tot}}$ is satisfied. Thus, the computation method described in this section can be seamlessly changed to any other model satisfying such a condition.

[13] ITU-R P.1623 warns such method presents a high standard deviation w.r.t. collected data. Designers might want to add margins to increase the confidence interval.

5.3.2 Expression of congestion outage time

The value T_n^{con} represents the duration in which terminal n is under outage due to congestion, i.e., due to a lack of satellite resources. At a given time instance t, two necessary conditions have to be met for such a case to happen:

- The first condition is for terminal n to have a link in working conditions, i.e., $\bar{k}_n^{\text{ci}}\left(\mathbf{a}_{n,t}^{\text{tot}}\right) \geq {}^{\downarrow}k_{s_n}^{\text{ci}}$.
- The second condition is that the network equivalent bandwidth b^{net} is strictly lower than the total demand $b^{\text{eq,TD}}\left(\mathbf{A}_t^{\text{tot}}\right)$.

Determining if these two conditions are sufficient to cause terminal n to be denied service would require knowledge of the RRM algorithm. Without such information, we should take the worst-case assumption that those conditions are sufficient. Thus T_n^{con} can be expressed as:

$$T_n^{\text{con}} = T^{\text{tot}} \cdot P\left(\left\{\bar{k}_n^{\text{ci}}\left(\mathbf{a}_{n,t}^{\text{tot}}\right) \geq {}^{\downarrow}k_{s_n}^{\text{ci}}\right\} \bigcap \left\{B > b^{\text{net}}\right\}\right) . \tag{5.30}$$

with $\bar{K}_n^{\text{ci}}$ and B being the random variables associated with $\bar{k}_n^{\text{ci}}\left(\mathbf{a}_{n,t}^{\text{tot}}\right)$ and $b^{\text{eq,TD}}\left(\mathbf{A}_t^{\text{tot}}\right)$, respectively. The joint probability is not trivially expressed as the two events are not independent. However, the following inequality always holds:

$$T_n^{\text{con}} \leq T^{\text{tot}} \cdot P\left(B > b^{\text{net}}\right) . \tag{5.31}$$

5.3.3 Formulation of the quantile problem

The diagram in Fig. 5.5 summarizes the possible outage causes.

We therefore have the following inequality:

$$\frac{T_n^{\text{link}} + T_n^{\text{con}}}{T^{\text{tot}}} \leq \frac{T_n^{\text{link}}}{T^{\text{tot}}} + P\left(B > b^{\text{net}}\right) . \tag{5.32}$$

Thus, the inequality (5.26) is satisfied if b^{net} satisfies:

$$\frac{T_n^{\text{link}}}{T^{\text{tot}}} + P\left(B > b^{\text{net}}\right) \leq p_{s_n}^{\text{adv}} \qquad \forall n \in \mathcal{I}_n \tag{5.33a}$$

$$\iff P\left(B > b^{\text{net}}\right) \leq p_{s_n}^{\text{adv}} - \frac{T_n^{\text{link}}}{T^{\text{tot}}} \qquad \forall n \in \mathcal{I}_n \tag{5.33b}$$

$$\iff P\left(B > b^{\text{net}}\right) \leq \min_{n \in I_N}\left(p_{s_n}^{\text{adv}} - \frac{T_n^{\text{link}}}{T^{\text{tot}}}\right) . \tag{5.33c}$$

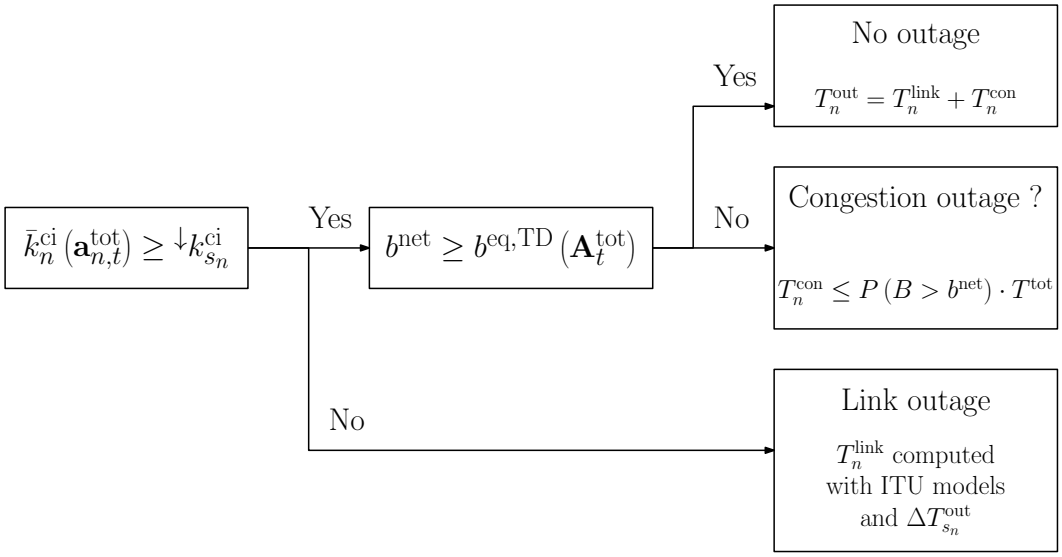

Figure 5.5: Tree of possible outage causes

The minimum value $b^{\min}$ satisfying the previous condition is solution of:

$$P\left(B > b^{\min}\right) = p^{\min}\,, \tag{5.34}$$

where:

$$p^{\min} = \min_{n \in I_N} \left(p_{s_n}^{\mathrm{adv}} - \frac{T_n^{\mathrm{link}}}{T^{\mathrm{tot}}} \right)\,. \tag{5.35}$$

the problem is equivalently formulated as:

$$b^{\min} = F_B^{-1}\left(1 - p^{\min}\right) \qquad [\mathrm{Hz}]\,, \tag{5.36}$$

with F_B being the CDF of the random variable B and F_B^{-1} its inverse function, generally defined as [78, Section 1.5]:

$$F_B^{-1}(p) = \inf\left\{b \mid F_B\left(b\right) \geq p\right\}\,. \tag{5.37}$$

The quantity $b^{\min}$ is commonly called the "$\left(1 - p^{\min}\right)$-th" quantile of F_B.

5.4 Monte Carlo process

In this section, we present a Monte Carlo method to estimate the value of $b^{\min}$ within a desired confidence interval. A quick review of the available techniques in the literature to estimate

the bandwidth CDF is presented in Section 5.4.1. Then, Section 5.4.2 introduces the basic concepts relative to the Monte-Carlo sampling technique, while Section 5.4.3 presents a specific type of confidence interval, called the binomial confidence interval. Finally, Section 5.4.4 proposes an algorithm that uses the binomial confidence interval to estimate $b^{\min}$ within a desired confidence interval.

5.4.1 Estimation of the bandwidth CDF

We presented the main methods for estimating F_B in Section 2.2.3. We pointed out that Monte Carlo sampling using spatially correlated rain fade time series generators is to this day the most viable and accurate way.

We also observed in the existing literature the lack of indications on how such a Monte Carlo process would be implemented in the context of satellite resource dimensioning. Since Monte Carlo relies on the generation of random samples, it is crucial that a confidence interval is given on the result. Due to asymptotic convergence properties, the width of the confidence interval for a given confidence level will tend to decrease when the number of generated samples T increases. Thus, there is a trade-off between the width of the confidence interval and the number of samples to generate. In other words, there is a trade-off between the precision of the simulation and its complexity.

Some indications regarding the number of samples to generate are found in [43, Section 4.4.2]. It suggested that a sampling period of one second is necessary to correctly represent the behavior of FMT techniques in individual terminal channels. This assumption is corroborated by other contributions investigating FMTs [79, Section 3], [37, Section 3.1]. As for the duration of the simulation, the authors recommend a total time duration of "several years" for the purpose of network simulation. This notion of several years is explained in better detail in another publication from the same authors [80]. It is found that empirical CDFs of rain fade generated at a one-second sampling period present large statistical variations over a single year duration, and generating samples over a duration of 5 to 10 years would greatly reduce this variation. A simulation spanning over one year at a one-second sampling period implies generating around 31 million samples. Thus, to correctly represent the behavior of individual terminal channels, we can estimate T to be 310 million samples per terminal.

This reasoning makes perfect sense in the context of designing and validating FMT techniques. However, we are interested in estimating the distribution of B, which is a sum of

arbitrarily correlated random variables. It is possible that the correct representation of all individual channels is not necessary to estimate the value of $b^{\min}$ within a given confidence interval. Thus, the number of samples we actually need to generate could be significantly lower.

5.4.2 Monte Carlo sampling

Let us assume we can generate a time series of T attenuation samples per terminal's location, $a_{n,t},\ t \in \mathcal{I}_T$, using one of the previously mentioned models. We assume those samples are spatially correlated, but not temporally correlated.[14] From this attenuation time series, we can compute the bandwidth time series $b^{\text{eq,TD}}\left(\mathbf{A}_t^{\text{tot}}\right)$ following the steps given in Section 5.2. By sorting this time series by increasing values of $b^{\text{eq,TD}}\left(\mathbf{A}_t^{\text{tot}}\right)$, we obtain an empirical cumulative distribution $\hat{F}_{B,T}$ of B, defined as [78, Section 1.5]:

$$\hat{F}_{B,T}(b) = \frac{1}{T}\sum_{t=1}^{T} \mathbb{1}_{b^{\text{eq,TD}}\left(\mathbf{A}_t^{\text{tot}}\right)<b}\,, \tag{5.38}$$

with $\mathbb{1}_{b^{\text{eq,TD}}\left(\mathbf{A}_t^{\text{tot}}\right)<b}$ equal to 1 if $b^{\text{eq,TD}}\left(\mathbf{A}_t^{\text{tot}}\right) < b$, and 0 otherwise.

We understand naturally that $\hat{F}_{B,T}$ is an approximation of F_B, of which the precision will depend on $T \in \mathbb{N}$ and the evaluation point $b \in \mathbb{R}$. Assuming we generated T samples, we have an empirical estimate $\hat{b}_T^{\min} = \hat{F}_{B,T}^{-1}(1-p^{\min})$ of $b^{\min}$, with $\hat{F}_{B,T}^{-1}$ the inverse empirical CDF, defined in a similar way as the inverse CDF:

$$\hat{F}_{B,T}^{-1}(p) = \inf\left\{b \mid \hat{F}_{B,T}(b) \geq p\right\} \qquad [\text{Hz}]\ . \tag{5.39}$$

Another equivalent but more practical definition of $\hat{b}_T^{\min}$ is found in [81, Section 3.1] with order statistics. Let $b^{\text{eq,TD}}\left(\mathbf{A}_{1:T}^{\text{tot}}\right) \leq b^{\text{eq,TD}}\left(\mathbf{A}_{2:T}^{\text{tot}}\right) \leq \ldots \leq b^{\text{eq,TD}}\left(\mathbf{A}_{T:T}^{\text{tot}}\right)$ be the sorted values of the samples $b^{\text{eq,TD}}\left(\mathbf{A}_1^{\text{tot}}\right), b^{\text{eq,TD}}\left(\mathbf{A}_2^{\text{tot}}\right), \ldots, b^{\text{eq,TD}}\left(\mathbf{A}_T^{\text{tot}}\right)$ in increasing order, with $b^{\text{eq,TD}}\left(\mathbf{A}_{1:T}^{\text{tot}}\right)$ being the smallest value and $b^{\text{eq,TD}}\left(\mathbf{A}_{T:T}^{\text{tot}}\right)$ the largest. In this case, we have:

$$\hat{b}_T^{\min} = b^{\text{eq,TD}}\left(\mathbf{A}_{\lceil T\cdot(1-p^{\min})\rceil:T}^{\text{tot}}\right) \qquad [\text{Hz}]\ . \tag{5.40}$$

We see that, in general, $\hat{F}_{B,T}^{-1}(1-p^{\min}) \geq b^{\min}$. It is possible to minimize the gap

[14] As our objective is to build the CDF of B over a quite long period of time, its temporal correlation has little relevance.

$\hat{F}^{-1}_{B,T}(1-p^{\min}) - b^{\min}$ by choosing T such that $\left\lceil T\cdot(1-p^{\min})\right\rceil - T\cdot(1-p^{\min})$ is minimal. It is obtained if $T = \left\lceil N^{\min}/p^{\min}\right\rceil$, with $N^{\min}\in\mathbb{N}$. The difference is expressed as:

$$\left\lceil N^{\min}/p^{\min}\right\rceil = N^{\min}/p^{\min} + \delta^{\min}\,, \tag{5.41}$$

with $\delta^{\min}\in[0,1)$. For any value $N^{\min}\in\mathbb{N}$, we deduce the following:

$$\begin{aligned} & T\cdot p^{\min} = N^{\min} + \delta^{\min}\cdot p^{\min} && \text{(5.42a)}\\ \iff & -T\cdot p^{\min} = -N^{\min} - \delta^{\min}\cdot p^{\min} && \text{(5.42b)}\\ \implies & \left\lceil -T\cdot p^{\min}\right\rceil = -N^{\min}\,. && \text{(5.42c)} \end{aligned}$$

We deduce the expression of the difference $\left\lceil T\cdot(1-p^{\min})\right\rceil - T\cdot(1-p^{\min})$ with the following:

$$\begin{aligned} & \left\lceil T\cdot(1-p^{\min})\right\rceil - T\cdot(1-p^{\min}) && \text{(5.43a)}\\ =& T + \left\lceil -T\cdot p^{\min}\right\rceil - T + T\cdot p^{\min} && \text{(5.43b)}\\ =& -N^{\min} + N^{\min} + \delta^{\min}\cdot p^{\min} && \text{(5.43c)}\\ =& \delta^{\min}\cdot p^{\min} && \text{(5.43d)} \end{aligned}$$

since $\delta^{\min}\in[0,1)$, we know the error is less than $p^{\min}$, which is negligible compared to $T\cdot(1-p^{\min})$.

5.4.3 Binomial confidence interval

Let us remark that $\hat{b}^{\min}_T$ is a random variable, i.e., its value changes for every new time series of length T. As described in [81, Section 6.1], it is possible, for a given sequence of T samples, to find a confidence interval $\mathcal{C}_T = \left[b^{\text{eq,TD}}\left(\mathbf{A}^{\text{tot}}_{t^{\inf}:T}\right), b^{\text{eq,TD}}\left(\mathbf{A}^{\text{tot}}_{t^{\sup}:T}\right)\right)$ with confidence level $1-\alpha^{\text{conf}}$ that verifies the following:

$$P\left(b^{\min}\in\mathcal{C}_T\right)\geq 1-\alpha^{\text{conf}}. \tag{5.44}$$

The indexes $t^{\inf}$ and $t^{\sup}$ are found by looking at the nature of the random variable $\Omega_T = T \cdot \hat{F}_{B,T}(b^{\min})$, given by:

$$\Omega_T = \sum_{t=1}^{T} \mathbb{1}_{b^{\text{eq,TD}}\left(\mathbf{A}_t^{\text{tot}}\right) < b^{\min}} \,. \tag{5.45}$$

It is apparent that Ω_T follows a binomial distribution $\mathcal{B}\left(T, 1 - p^{\min}\right)$.

The probability of $b^{\min}$ being inside an interval $\left[b^{\text{eq,TD}}\left(\mathbf{A}_{t_1:T}^{\text{tot}}\right), b^{\text{eq,TD}}\left(\mathbf{A}_{t_2:T}^{\text{tot}}\right)\right)$ is linked to Ω_T with the following:

$$P\left(b^{\text{eq,TD}}\left(\mathbf{A}_{t_1:T}^{\text{tot}}\right) \leq b^{\min} < b^{\text{eq,TD}}\left(\mathbf{A}_{t_2:T}^{\text{tot}}\right)\right) = P\left(t_1 \leq \Omega_T < t_2\right) \tag{5.46a}$$

$$= 1 - P\left(\Omega_T < t_1\right) - P\left(\Omega_T \geq t_2\right) \,. \tag{5.46b}$$

Thus, $\mathcal{C}_T$ has a confidence level $1 - \alpha^{\text{conf}}$ if $t^{\inf}$ and $t^{\sup}$ satisfy the following:

$$P\Big(\Omega_T < t^{\inf}\Big) + P\Big(\Omega_T \geq t^{\sup}\Big) \leq \alpha^{\text{conf}} \tag{5.47}$$

One solution is to look for $t^{\inf}$ and $t^{\sup}$ satisfying:

$$t^{\inf} = \max\left\{t \mid P\left(\Omega_T < t\right) \leq \frac{\alpha^{\text{conf}}}{2}\right\} \,, \tag{5.48a}$$

$$t^{\sup} = \min\left\{t \mid P\left(\Omega_T \geq t\right) \leq \frac{\alpha^{\text{conf}}}{2}\right\} \,. \tag{5.48b}$$

Please note that the choice of using $\alpha^{\text{conf}}/2$ in both expressions is arbitrary. Any couple $\lambda \cdot \alpha^{\text{conf}}, (1-\lambda) \cdot \alpha^{\text{conf}}$, with $\lambda \in (0,1)$ would also lead to correct values of $t^{\inf}$ and $t^{\sup}$.[15]

Now, let us remember that $\Omega_T \sim \mathcal{B}\left(T, 1 - p^{\min}\right)$. Thus, for any $t \in \mathcal{I}_T$, we can compute the probability $P\left(\Omega_T < t\right) = P\left(\Omega_T \leq t - 1\right)$ using the regularized incomplete beta function:

$$P\left(\Omega_T \leq t - 1\right) = \frac{\text{iBeta}\left(p^{\min}, T - t + 1, t\right)}{\text{Beta}\left(T - t + 1, t\right)} \,. \tag{5.49}$$

with Beta being the well-known beta function and iBeta the incomplete beta function.[16] We deduce the expression of $P\left(\Omega_T \geq t\right)$, which is equal to $1 - P\left(\Omega_T < t\right)$. Since $P\left(\Omega_T < t\right)$ is a monotonic function of t, any root finding algorithm, such as bisection, will quickly find the

[15] An interesting problem, not addressed in this chapter, would be to find λ for which the width of the confidence interval is minimal.

[16] The regularized incomplete beta function is implemented in Matlab with the function betainc.

values of t^{inf} and t^{sup}.

5.4.4 Confidence interval with given relative precision

Let us assume now that we want, for a given confidence level $1-\alpha^{\text{conf}}$, that our estimate $\hat{b}_T^{\min}$ lies within a certain relative confidence interval $\mathcal{C}_{\delta^{\text{B}}} = \left[(1-\delta^{\text{B}})\cdot b^{\min}, (1+\delta^{\text{B}})\cdot b^{\min}\right]$ of the theoretical value $b^{\min}$, with $\delta^{\text{B}} \in (0,1)$, i.e.:

$$P\left(\hat{b}_T^{\min} \in \mathcal{C}_{\delta^{\text{B}}}\right) \geq 1-\alpha^{\text{conf}}\,. \tag{5.50}$$

Note the difference with the definition of the binomial confidence interval. In this section, we want to have the probability of a random variable to be within a pre-determined interval, while in the binomial case, we have the probability of a fixed quantity to be within a random interval.

The value of $\delta^{\text{B}}\cdot b^{\min}$ is unknown at the start of the process. However, we know that $b^{\text{eq,cs}} \leq b^{\min}$, with $b^{\text{eq,cs}}$ the clear sky equivalent bandwidth demand. It is computed as:

$$b^{\text{eq,cs}} = \max\left(b^{\text{pe,cs}}, b^{\text{cs}}\right) \qquad [\text{Hz}]\,. \tag{5.51}$$

with b^{cs} being the clear sky bandwidth demand:

$$b^{\text{cs}} = \sum_{n=1}^{N} b_{n,q}^{\text{D}}\left((1,1), \bar{k}_n^{\text{ci}}\left((1,1)\right)\right)\cdot p_{s_n,q}^{\text{at}} \qquad [\text{Hz}]\,, \tag{5.52}$$

and $b^{\text{pe,cs}}$ being the clear sky PEB demand:

$$b^{\text{pe,cs}} = \sum_{n=1}^{N} b_{n}^{\text{pe,D}}\left((1,1), \bar{k}_n^{\text{ci}}\left((1,1)\right)\right)\cdot p_{s_n,q}^{\text{at}} \qquad [\text{Hz}]\,. \tag{5.53}$$

Thus, if the width of the confidence interval is less or equal to $\delta^{\text{B}}\cdot b^{\text{eq,cs}}$, it is also less or equal to $\delta^{\text{B}}\cdot b^{\min}$.

The remaining question is then to build confidence intervals of width $\delta^{\text{B}}\cdot b^{\text{eq,cs}}$ or less that would satisfy (5.50). To this end, we propose the method described in Algorithm 2, with $\lambda^{\text{inc}} \in \mathbb{R}_+$ being a desired increase rate.

Let us remark that the confidence level of the interval given by Algorithm 2 is not equal to $P\left(b^{\min} \in \mathcal{C}_T\right)$, but to $P\left(b^{\min} \in \mathcal{C}_T \mid b^{\text{eq,TD}}\left(\mathbf{A}_{t^{\text{sup}}:T}^{\text{tot}}\right) - b^{\text{eq,TD}}\left(\mathbf{A}_{t^{\text{inf}}:T}^{\text{tot}}\right) \leq \delta^{\text{B}}\cdot b^{\text{eq,cs}}\right)$.

Algorithm 2 Monte Carlo process

$N^{\min} \leftarrow 0$
$T \leftarrow 0$
sample sequence $\leftarrow$ *empty*
iterate $\leftarrow$ *true*
while *iterate* **do**
  $N^{\min} \leftarrow \max\left(1, \lambda^{\text{inc}} \cdot N^{\min}\right)$
  Generate $\left\lceil N^{\min}/p^{\min} \right\rceil - T$ new samples.
  Add new samples to *sample sequence*.
  if $P\left(\Omega_T \geq T\right) \leq \alpha^{\text{conf}}/2$ **then**
    Compute t^{inf} and t^{sup}.
    Sort *sample sequence*.
    $width \leftarrow b^{\text{eq,TD}}\left(\mathbf{A}^{\text{tot}}_{t^{\text{sup}}:T}\right) - b^{\text{eq,TD}}\left(\mathbf{A}^{\text{tot}}_{t^{\text{inf}}:T}\right)$
    $iterate \leftarrow width > \delta^{\text{B}} \cdot b^{\text{eq,cs}}$.
  end if
end while
$\hat{b}^{\min}_T \leftarrow b^{\text{eq,TD}}\left(\mathbf{A}^{\text{tot}}_{\lceil T\cdot(1-p^{\min})\rceil:T}\right)$

If T is such that $P\left(b^{\text{eq,TD}}\left(\mathbf{A}^{\text{tot}}_{t^{\text{sup}}:T}\right) - b^{\text{eq,TD}}\left(\mathbf{A}^{\text{tot}}_{t^{\text{inf}}:T}\right) \leq \delta^{\text{B}} \cdot b^{\text{eq,cs}}\right) \approx 1$, then the conditional probability is similar to $P\left(b^{\min} \in \mathcal{C}_T\right)$. This is the case when T is large. However, if $P\left(b^{\text{eq,TD}}\left(\mathbf{A}^{\text{tot}}_{t^{\text{sup}}:T}\right) - b^{\text{eq,TD}}\left(\mathbf{A}^{\text{tot}}_{t^{\text{inf}}:T}\right) \leq \delta^{\text{B}} \cdot b^{\text{eq,cs}}\right) \ll 1$, the conditional probability may be different, potentially lower, than $P\left(b^{\min} \in \mathcal{C}_T\right)$. This is possible for small values of T. Fig. 5.6 illustrates both cases, with f_B being the probability density function of the random variable B (please note that those functions are not necessarily symmetric).

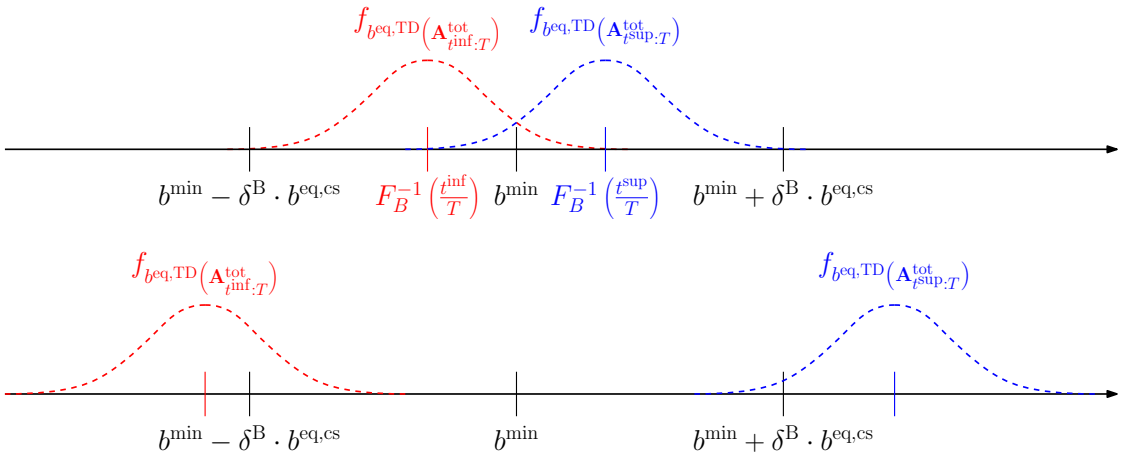

Figure 5.6: Illustration of cases where $P\left(b^{\text{eq,TD}}\left(\mathbf{A}^{\text{tot}}_{t^{\text{sup}}:T}\right) - b^{\text{eq,TD}}\left(\mathbf{A}^{\text{tot}}_{t^{\text{inf}}:T}\right) \leq \delta^{\text{B}} \cdot b^{\text{eq,cs}}\right) \approx 1$ (up) and $P\left(b^{\text{eq,TD}}\left(\mathbf{A}^{\text{tot}}_{t^{\text{sup}}:T}\right) - b^{\text{eq,TD}}\left(\mathbf{A}^{\text{tot}}_{t^{\text{inf}}:T}\right) \leq \delta^{\text{B}} \cdot b^{\text{eq,cs}}\right) \ll 1$ (down).

On the other hand, we have the following implication:

$$\left(b^{\min} \in \mathcal{C}_T \mid b^{\mathrm{eq,TD}}\left(\mathbf{A}^{\mathrm{tot}}_{t^{\mathrm{sup}}:T}\right) - b^{\mathrm{eq,TD}}\left(\mathbf{A}^{\mathrm{tot}}_{t^{\mathrm{inf}}:T}\right) \leq \delta^{\mathrm{B}} \cdot b^{\mathrm{eq,cs}}\right) \implies \hat{b}^{\min}_T \in \mathcal{C}_{\delta^{\mathrm{B}}}\,. \tag{5.54}$$

Thus, we know that:

$$P\left(\hat{b}^{\min}_T \in \mathcal{C}_{\delta^{\mathrm{B}}}\right) \geq P\left(b^{\min} \in \mathcal{C}_T \mid b^{\mathrm{eq,TD}}\left(\mathbf{A}^{\mathrm{tot}}_{t^{\mathrm{sup}}:T}\right) - b^{\mathrm{eq,TD}}\left(\mathbf{A}^{\mathrm{tot}}_{t^{\mathrm{inf}}:T}\right) \leq \delta^{\mathrm{B}} \cdot b^{\mathrm{eq,cs}}\right) \tag{5.55}$$

Whether this inequality is large enough to compensate for the reduction in the confidence level for lower values of T is unknown and requires validation via numerical application, as shown in Section 5.6.1.

5.5 Scenario for numerical results

This section describes the models and parameters used to compute the numerical results presented in Section 5.6. The main goal was to build typical residential and enterprise BSM scenarios over regions of different areas in order to study the impact of rain fade correlation. Firstly, Section 5.5.1 describes all parameters related to SLA and the network configuration, in compliance with the concepts and assumptions described in Sections 5.1.2, 5.1.3, and 5.1.4. Then, Section 5.5.2, 5.5.3, and 5.5.4 present respectively the thermal link budget, interference, and composite link budget models used for the IBO and the CINR_0, in accordance with Section 5.1.6. Section 5.5.5 presents all the parameters related to the satellite and its payload, in accordance with Section 5.1.5. Section 5.5.6 presents the generation method for the terminal and the gateway, as well as a dimensioning method for the terminals' antenna diameter and power that complies with the requirements expressed in Section 5.2.5. Finally, Section 5.5.7 explains how the rain attenuation samples were generated. Note that the entire simulation was coded in Matlab.

5.5.1 Network parameters

This section describes all parameters related to the SLAs and the modem configuration.

SLA for residential BSM

The UK government defines a broadband universal service as a connection with at least 1 Mbps of upload rate and a contention ratio that does not exceed 1:50 [68]. Table 5.1 allows to compare this statement with existing private satellite broadband offers. Telephony services can be included or optional.

	skyDSL[a]	**NordNet**[b]	**FreedomSat**[c]	**OuiSat**[d]
Peak upload rate (Mbps)	1–6	5	6	6
Availability (%)	97	N/S[e]	99.5	N/S
Contention ratio	1:50	N/S	N/S	N/S

[a] http://www.skydsl.eu/en-FR/Personal/Internet-via-satellite
[b] https://www.nordnet.com/connexion-internet/internet-satellite
[c] https://www.freedomsat.com
[d] https://www.ouisat.fr
[e] N/S = not specified

Table 5.1: List of private satellite broadband offers in France on 04/09/2023

From these figures, we established three subscription archetypes:

- SP 1 (60% of terminals): 1 Mbps upload, 1:50 contention ratio. No telephony service.
- SP 2 (30% of terminals): 2 Mbps upload, 1:30 contention ratio. One voice line.
- SP 3 (10% of terminals): 6 Mbps upload, 1:30 contention ratio. Three voice lines.

To convert the IP rates into layer 2 rates, we assumed the ATM protocol was used [82]. An ATM cell is composed of a 5-byte header and a 48-byte payload, thus we assumed a 10% overhead from layer 2 conversion. Assuming all non-telephony traffic is sent in bulk, we have two traffic classes for any SP $s \in \{1, 2, 3\}$.

The first traffic class $q = 1$ corresponds to bulk traffic. R_s^{mi} is the advertised peak rate and ρ^{OB} is the contention ratio. The expected proportion of active terminals p_s^{at} is set to 1.

The second class $q = 2$ corresponds to the real-time voice traffic. The number of lines per terminal N_s^{lines} is directly given as advertised. We take the values $\bar{R}_s^{\mathrm{call}} = 1$ call/hour and $\bar{T}_s^{\mathrm{call}} = 3$ minutes from [73, Table 4.1]. The maximum rate $R_s^{\mathrm{mi,call}}$ is set to the standard 64 kbps, and the committed rate $R_s^{\mathrm{ci,call}}$ is set to 16 kbps. Finally, the call blocking probability p_s^{call} is set to a typical value of 2%.

The different SLA rates are obtained with the methodology described in Appendix A. It is assumed all SPs come with an advertised availability of 99.5%, thus an outage probability of $p^{\text{adv}} = 0.5\%$.

SLA for enterprise BSM

Typical enterprise BSM offers do not exist, as each network is designed for a specific client running a specific business (see [9, Section 8.2.1]). However, online sources from satellite service providers[17] indicate that contention ratios for enterprise satellite networks are typically lower than residential networks, ranging from 1:10 to 1:4. Therefore, we propose to take the same SPs as for the residential scenario, with the exception of the contention ratio. The list of SPs for the enterprise BSM scenario is:

- SP 1 (60% of terminals): 1 Mbps upload, 1:10 contention ratio. No telephony service.
- SP 2 (30% of terminals): 2 Mbps upload, 1:4 contention ratio. One voice line.
- SP 3 (10% of terminals): 6 Mbps upload, 1:4 contention ratio. Three voice lines.

The different SLA rates are obtained with the same methodology as for the residential SLAs. We used the same outage probability.

Modem parameters

The minimum channel bandwidth $\Delta B^{\min}$ is set to 64 kHz. The maximum channel multiplier C is set to 256, thus allowing a maximum channel bandwidth of 16.384 MHz. Table 5.2 shows the selected FMT mode parameters ($K = 10$), taken from [48, Table III] in compliance with the ETSI DVB-RCS2 standard [32].

5.5.2 Basic link budget model

In this section, we present the link budget model for a transparent payload, mainly inspired from [8, Chapter 5] and [73, Chapter 5].

[17] See https://www.bcsatellite.net/blog/residential-vs-enterprise-class-services/ and https://www.satmarin.com/which-contention-ratio-is-good-for-you/ (visited on 27/11/2023).

Table 5.2: DVB-RCS2 ModCod parameters

Modulation	**Code rate**	**Spectral efficiency (bps/Hz)**	**Required E_s/N_0 (dB)**
QPSK	1/3	0.54	0
QPSK	1/2	0.83	2.3
QPSK	2/3	1.16	3.9
QPSK	3/4	1.31	5
QPSK	5/6	1.47	6.1
8-PSK	2/3	1.57	8.2
8-PSK	3/4	1.76	9.3
8-PSK	5/6	1.96	11
16-QAM	3/4	2.31	11.6
16-QAM	5/6	2.57	13

Uplink

The uplink received power at the satellite antenna level is expressed as:

$$P_n^{\mathrm{Rx,ul}}\left(a_{n,t}\right) = \frac{P_n^{\mathrm{Tx,ul}} \cdot G_n^{\mathrm{Tx,ul}}\left(0\right)}{L_n^{\mathrm{Tx,ul}}} \cdot \frac{G_{m_n}^{\mathrm{Rx,ul}}\left(\psi_n^{\mathrm{ul}}\right)}{L_n^{\mathrm{fs}}\left(\lambda_{m_n}^{\mathrm{ul}}\right) \cdot a_{n,t}} \qquad [\mathrm{W}]\ , \tag{5.56}$$

where:

- $P_n^{\mathrm{Rx,ul}}$, in W, is the received power at the satellite antenna level.
- $P_n^{\mathrm{Tx,ul}}$, in W, and $G_n^{\mathrm{Tx,ul}}\left(0\right)$ are respectively the maximum power and antenna gain of terminal n in the direction of the main lobe axis.
- $L_n^{\mathrm{Tx,ul}}$ is the feeder losses.
- $L_n^{\mathrm{fs}}\left(\lambda_{m_n}^{\mathrm{ul}}\right)$ is the free space loss between terminal n and the satellite, and $\lambda_{m_n}^{\mathrm{ul}}$ is the uplink wavelength associated with beam m_n, in m.
- $G_{m_n}^{\mathrm{Rx,ul}}\left(\psi_n^{\mathrm{ul}}\right)$ is the receiving gain of the satellite beam m_n in the direction of terminal n, and ψ_n^{ul} is the angle between terminal n and the center of beam m_n.

The quantity $P_n^{\mathrm{Tx,ul}} \cdot G_n^{\mathrm{Tx,ul}}(0) / L_n^{\mathrm{Tx,ul}}$ is commonly referred to as the *equivalent isotropic radiated power* (EIRP).

The thermal-noise-power-spectral-density at the satellite antenna level is expressed as:

$$N_{0,n}^{\mathrm{ul}} = T_{m_n}^{\mathrm{ul}} \cdot k^{\mathrm{B}} \qquad [\mathrm{W/Hz}] \ . \tag{5.57}$$

with $T_{m_n}^{\mathrm{ul}}$, in K, being the noise temperature at the satellite antenna level, and k^{B} being the Boltzmann constant.

Finally, the uplink CNR_0 is defined as the ratio between the received power and the noise power density $P_n^{\mathrm{Rx,ul}}(a_{n,t}) / N_{0,n}^{\mathrm{ul}}$.

Amplification

The power flux density $\Phi_n^{\mathrm{ul}}(a_{n,t})$ received by the satellite antenna is given by:

$$\Phi_n^{\mathrm{ul}}(a_{n,t}) = \frac{P_n^{\mathrm{Rx,ul}}(a_{n,t})}{G_{m_n}^{\mathrm{Rx,ul}}(\psi_n^{\mathrm{ul}})} \cdot \left(\frac{4 \cdot \pi}{\lambda_{m_n}^{\mathrm{ul}}}\right)^2 \qquad [\mathrm{W/m^2}] \ . \tag{5.58}$$

This value is usually compared against the *saturation power flux density* (SFD) $\Phi_{m_n,v_n}^{\mathrm{ul,sat}}\left(\psi_n^{\mathrm{ul}}\right)$ of the transponder v_n in the direction of the terminal, given by:

$$\Phi_{m_n,v_n}^{\mathrm{ul,sat}}\left(\psi_n^{\mathrm{ul}}\right) = \Phi_{m_n,v_n}^{\mathrm{ul,nom}} \cdot \frac{G_{m_n}^{\mathrm{Rx,ul}}(0)}{G_{m_n}^{\mathrm{Rx,ul}}(\psi_n^{\mathrm{ul}})} \qquad [\mathrm{W/m^2}] \ , \tag{5.59}$$

with $\Phi_{m_n,v_n}^{\mathrm{ul,nom}}$ being the nominal SFD of the transponder v_n on the main lobe axis of beam m_n (assumed given). The amplifier IBO is given by the ratio:

$$\mathrm{IBO}_n(a_{n,t}) = \frac{\Phi_n^{\mathrm{ul}}(a_{n,t})}{\Phi_{m_n,v_n}^{\mathrm{ul,sat}}(\psi_n^{\mathrm{ul}})} = \frac{P_n^{\mathrm{Rx,ul}}(a_{n,t}) \cdot (4 \cdot \pi)^2}{\left(\lambda_{m_n}^{\mathrm{ul}}\right)^2 \cdot G_{m_n}^{\mathrm{Rx,ul}}(0) \cdot \Phi_{m_n,v_n}^{\mathrm{ul,nom}}} \ . \tag{5.60}$$

The output power of the amplifier is:

$$P_n^{\mathrm{Tx,dl}}(a_{n,t}) = \mathrm{OBO}_n(a_{n,t}) \cdot P_{v_n}^{\mathrm{out,sat}} \qquad [\mathrm{W}] \ , \tag{5.61}$$

where $P_{v_n}^{\mathrm{out,sat}}$ is the saturation output power of the amplifier v_n and OBO_n is the IBO vs *output back-off* (OBO) function of this amplifier. Given that multiple terminals share the same transponder, it is reasonable to assume that the amplifier will be set to operate at a

significant total input back off $\mathrm{IBO}_{v_n}^{\mathrm{tot}}$ to avoid high intermodulation interference [83, Appendix 5.2]. Thus, we can expect the amplifier to operate in its linear region. Thus, OBO_n is:

$$\mathrm{OBO}_n\left(a_{n,t}\right) = 10^{\beta_{v_n}^{\mathrm{I/O}}/10} \cdot \left(\mathrm{IBO}_n\left(a_{n,t}\right)\right)^{\alpha_{v_n}^{\mathrm{I/O}}} , \tag{5.62}$$

where $\alpha_{v_n}^{\mathrm{I/O}}$ and $\beta_{v_n}^{\mathrm{I/O}}$ are two constants obtained by performing a linear regression on the OBO function in the linear region [73, Appendix 6].

Downlink

The expression of the downlink power-to-noise-spectral-density ratio at the gateway's receiver is given as:

$$\frac{P_{d_n}^{\mathrm{Rx,dl}}\left(\mathbf{a}_{n,t}^{\mathrm{tot}}\right)}{N_{0,d_n}^{\mathrm{dl}}\left(a_{d_n,t}\right)} = \frac{P_n^{\mathrm{Tx,dl}}\left(a_{n,t}\right) \cdot G_{m_{d_n}}^{\mathrm{Tx,dl}}\left(\psi_{d_n}^{\mathrm{dl}}\right)}{L_{m_{d_n}}^{\mathrm{Tx,dl}}} \cdot \frac{1}{L_{d_n}^{\mathrm{fs}}\left(\lambda_{m_{d_n}}^{\mathrm{dl}}\right) \cdot a_{d_n,t}} \cdot \frac{G_{d_n}^{\mathrm{Rx,dl}}\left(0\right)}{T_{d_n}^{\mathrm{dl}}\left(a_{d_n,t}\right)} \cdot \frac{1}{k^{\mathrm{B}}} \quad [\mathrm{Hz}] , \tag{5.63}$$

where:

- $G_{m_{d_n}}^{\mathrm{Tx,dl}}\left(\psi_{d_n}^{\mathrm{dl}}\right)$ is the antenna gain of beam m_{d_n} toward the destination gateway d_n, and $\psi_{d_n}^{\mathrm{dl}}$ is the angle between the gateway d_n and the center of beam m_{d_n}.
- $L_{m_{d_n}}^{\mathrm{Tx,dl}}$ is the satellite feeder losses.
- $L_{d_n}^{\mathrm{fs}}\left(\lambda_{m_{d_n}}^{\mathrm{dl}}\right)$ is the free space loss between the satellite and the destination gateway d_n, and $\lambda_{m_{d_n}}^{\mathrm{dl}}$ is the downlink wavelength associated with beam m_{d_n}, in m.
- $G_{d_n}^{\mathrm{Rx,dl}}\left(0\right)$ is the antenna gain of destination gateway d_n toward the satellite.
- $T_{d_n}^{\mathrm{dl}}\left(a_{d_n,t}\right)$, in K, is the noise temperature at the destination receiver level.

5.5.3 Interference model

This section presents the models for the different types of interference that we considered in our scenario, mostly inspired from [8, Chapter 5] and [73, Chapter 5].

Intermodulation ratio

For amplifiers operating in multicarrier mode, the *noise power ratio* (NPR) method is commonly used to compute the interference noise density [84]. It consists in loading the

amplifier with white noise on the whole amplifier bandwidth, with a power equal to input saturation power of the amplifier. Then, a notch filter is used to create the equivalent of an empty channel in the middle of interfering channels. The NPR is read as the ratio between the noise output power density of the notch filter's passband and the noise output power density of the notch filter's stopband.

Let us assume the NPR value is known for the number of channels supported by the transponder $\left\lfloor B_{v_n}^{\text{trans}} / \Delta B^{\min} \right\rfloor$ and the desired $\text{IBO}_{v_n}^{\text{tot}}$ value. Then, the intermodulation noise power density $I_{0,n}^{\text{im}}$ is obtained by dividing the output power density at the $\text{IBO}_{v_n}^{\text{tot}}$ value by the NPR:

$$I_{0,n}^{\text{im}} = \frac{\text{OBO}_{v_n}^{\text{tot}} \cdot P_{v_n}^{\text{out,sat}}}{\text{NPR}_{v_n} \cdot B_{v_n}^{\text{trans}}} \qquad [\text{W/Hz}] \ . \tag{5.64}$$

The *carrier-to-intermodulation-noise-spectral-density ratio* (CIMR_0) is obtained by comparing $I_{0,n}^{\text{im}}$ to the carrier power at the amplifier's output $P_n^{\text{Tx,dl}}(a_{n,t})$.

Co-channel interference from frequency reuse

The *co-channel interference* (CCI) is caused by emissions in other beams using the same color, i.e., the same frequency and polarization. This type of interference is typical of multibeam satellite systems using frequency reuse.

For a given beam m, we define the set of interfering beams $\mathcal{M}_m^{\text{i,ul}}$ as any $m^{\text{i}} \neq m$ such that $\left(\text{freq}_{m^{\text{i}}}^{\text{ul}}, \text{pol}_{m^{\text{i}}}^{\text{ul}}\right) = \left(\text{freq}_m^{\text{ul}}, \text{pol}_m^{\text{ul}}\right)$. The co-channel uplink interfering power is given by the sum of interfering power coming from each interfering beam $m^{\text{i}} \in \mathcal{M}_{m_n}^{\text{i,ul}}$. In the absence of knowledge on interfering signals, it is reasonable to assume that interferers will emit with a *power spectral density* (PSD) matching what is required to bring the amplifier of the receiver to its nominal IBO. Assuming that the interference comes from the closest edge of beam m^{i}, which is separated by an angle $\psi_{m_n,m^{\text{i}}}^{\text{cci}}$ from the center of beam m_n, the uplink PSD of the interfering beams is given by:

$$I_{0,n}^{\text{ul,cci}} = \sum_{m^{\text{i}} \in \mathcal{M}_{m_n}^{\text{i,ul}}} \frac{P_{0,n}^{\text{i,ul}}\left(m^{\text{i}}\right) \cdot G_{m_n}^{\text{Rx,ul}}\left(\psi_{m_n,m^{\text{i}}}^{\text{cci}}\right)}{G_{m^{\text{i}}}^{\text{Rx,ul}}\left(\psi_{m^{\text{i}}}^{\text{edge}}\right)} \qquad [\text{W/Hz}] \ , \tag{5.65}$$

where:

$$P_{0,n}^{\text{i,ul}}(m) = \frac{\text{IBO}_{v_n}^{\text{tot}} \cdot \Phi_{m,v_n}^{\text{ul,nom}} \cdot \left(\lambda_m^{\text{ul}}\right)^2 \cdot G_m^{\text{Rx,ul}}(0)}{B_{v_n}^{\text{trans}} \cdot (4 \cdot \pi)^2} \qquad [\text{W/Hz}] \ , \tag{5.66}$$

and:

- $G_{m}^{\mathrm{Rx,ul}}(0)$ is the antenna gain of the satellite at the center beam m.
- $G_{m^{\mathrm{i}}}^{\mathrm{Rx,ul}}\left(\psi_{m^{\mathrm{i}}}^{\mathrm{edge}}\right)$ is the antenna gain of beam m_i at the edge of its coverage, and $\psi_{m^{\mathrm{i}}}^{\mathrm{edge}}$ is the angle between the center and the edge of beam m^{i}.
- $G_{m_n}^{\mathrm{Rx,ul}}\left(\psi_{m_n,m^{\mathrm{i}}}^{\mathrm{cci}}\right)$ is the satellite antenna gain of beam m_n in the direction of the edge of beam m^{i}.

Equivalently, we define the set of interfering beams $\mathcal{M}_{m}^{\mathrm{i,dl}}$ as any $m^{\mathrm{i}} \neq m$ such that $\left(\mathrm{freq}_{m^{\mathrm{i}}}^{\mathrm{dl}}, \mathrm{pol}_{m^{\mathrm{i}}}^{\mathrm{dl}}\right) = \left(\mathrm{freq}_{m}^{\mathrm{dl}}, \mathrm{pol}_{m}^{\mathrm{dl}}\right)$. Let us denote $\psi_{m^{\mathrm{i}},d_n}^{\mathrm{cci}}$ the separation angle between the center of beam m^{i} and the destination station d_n, from the satellite point of view. The downlink PSD of the interfering beams is given by:

$$I_{0,n}^{\mathrm{dl,cci}}\left(a_{d_n,t}\right) = \sum_{m^{\mathrm{i}} \in \mathcal{M}_{m_{d_n}}^{\mathrm{i,dl}}} \frac{P_{0,n}^{\mathrm{i,dl}}\left(m^{\mathrm{i}}, \psi_{m^{\mathrm{i}},d_n}^{\mathrm{cci}}\right) \cdot G_{d_n}^{\mathrm{Rx,dl}}\left(0\right)}{L_{d_n}^{\mathrm{fs}}\left(\lambda_{m_{d_n}}^{\mathrm{dl}}\right) \cdot a_{d_n,t}} \qquad [\mathrm{W/Hz}]\ . \tag{5.67}$$

where:

$$P_{0,n}^{\mathrm{i,dl}}\left(m, \psi\right) = \frac{\mathrm{OBO}_{v_n}^{\mathrm{tot}} \cdot P_{v_n}^{\mathrm{out,sat}} \cdot G_{m}^{\mathrm{Tx,dl}}\left(\psi\right)}{B_{v_n}^{\mathrm{trans}} \cdot L_{m}^{\mathrm{Tx,dl}}} \qquad [\mathrm{W/Hz}]\ , \tag{5.68}$$

and $G_{m^{\mathrm{i}}}^{\mathrm{Tx,dl}}\left(\psi_{m^{\mathrm{i}},d_n}^{\mathrm{cci}}\right)$ is the satellite antenna gain of beam m^{i} in the direction of the destination d_n.

Cross-polarization interference

The *cross-polarization interference* (XPI) comes from carriers being transmitted at the same frequency on an orthogonal polarization. This interference is mitigated by the cross-polarization isolation of the receiver. The XPI is also impacted by the depolarization effect of rain and ice, called *cross-polarization discrimination* (XPD).

For the uplink, the XPI comes from cross-polarization emissions being received by the satellite receiver. The XPI uplink PSD is given by [73, Section 5.5.3]:

$$I_{0,n}^{\mathrm{ul,xpi}}\left(a_{n,t}\right) = \frac{P_{0,n}^{\mathrm{i,ul}}\left(m_n\right)}{L_{m_n}^{\mathrm{ul,xpi}}} + \frac{P_{0,n}^{\mathrm{i,ul}}\left(m_n\right)}{L^{\mathrm{ul,xpd}}(a_{n,t})} \qquad [\mathrm{W/Hz}]\ , \tag{5.69}$$

where $L_{m_n}^{\mathrm{ul,xpi}}$ are the losses due to the cross-polarization isolation of the satellite receiver, and $L^{\mathrm{ul,xpd}}(a_{n,t})$ the depolarization due to rain effects. The expression of $L^{\mathrm{ul,xpd}}(a_{n,t})$ as a function of $a_{n,t}$ is found in [30, Section 4.1].

For the downlink, the XPI comes from cross-polarization emissions being received by the destination d_n receiver. The XPI downlink PSD is given by:

$$I_{0,n}^{\mathrm{dl,xpi}}\left(a_{d_n,t}\right) = P_{0,n}^{\mathrm{i,dl}}\left(m_{d_n}, \psi_{d_n}^{\mathrm{dl}}\right) \cdot \left(\frac{1}{L_{d_n}^{\mathrm{dl,xpi}}} + \frac{1}{L^{\mathrm{dl,xpd}}(a_{d_n,t})}\right) \cdot \frac{G_{d_n}^{\mathrm{Rx,dl}}(0)}{L_{d_n}^{\mathrm{fs}}\left(\lambda_{m_{d_n}}^{\mathrm{dl}}\right) \cdot a_{d_n,t}} \qquad [\mathrm{W/Hz}]\ , \tag{5.70}$$

where $L_{d_n}^{\mathrm{dl,xpi}}$ are the losses due to the cross-polarization isolation of the satellite receiver, and $L^{\mathrm{dl,xpd}}(a_{d_n,t})$ the depolarization due to rain effects. The expression of $L^{\mathrm{dl,xpd}}(a_{d_n,t})$ is the same as $L^{\mathrm{ul,xpd}}(a_{n,t})$.

Adjacent channel interference

The *adjacent channel interference* (ACI) is caused by adjacent carrier off-band emissions inside the emission band used by terminal n. It is a function of the carrier spacing and the pulse shaping. Let us denote L^{acs} the loss corresponding to the adjacent channel isolation factor. The ACI uplink PSD is given by:

$$I_{0,n}^{\mathrm{ul,aci}} = \frac{P_{0,n}^{\mathrm{i,ul}}(m_n)}{L^{\mathrm{acs}}} \qquad [\mathrm{W/Hz}]\ . \tag{5.71}$$

Similarly, the ACI downlink PSD is given by:

$$I_{0,n}^{\mathrm{dl,aci}}\left(a_{d_n,t}\right) = \frac{P_{0,n}^{\mathrm{i,dl}}\left(m_{d_n}, \psi_{d_n}^{\mathrm{dl}}\right) \cdot G_{d_n}^{\mathrm{Rx,dl}}(0)}{L^{\mathrm{acs}} \cdot L_{d_n}^{\mathrm{fs}}\left(\lambda_{m_{d_n}}^{\mathrm{dl}}\right) \cdot a_{d_n,t}} \qquad [\mathrm{W/Hz}]\ . \tag{5.72}$$

Adjacent satellite interference

The adjacent satellite systems in the GEO arc can produce interference with our network, on the uplink and the downlink. This is called *adjacent satellite interference* (ASI).

The uplink ASI is caused by terminals from another satellite system emitting in the same frequency band. Let us assume the adjacent satellite is at a relative orbital position $\Delta\psi^{\mathrm{orb}}$ w.r.t. our satellite's orbital position. From the perspective of a ground station the angle between those two satellites ψ^{asi} can be approximated by [73, Section 5.5.4]:

$$\psi^{\mathrm{asi}} = 1.15 \cdot \Delta\psi^{\mathrm{orb}}\ . \tag{5.73}$$

Let us assume that the interfering station is located at the center of our beam, and is emitting

with a PSD corresponding to the maximum allowed by the ITU regulations (e.g., [52]). The uplink PSD of the interfering station is therefore given by:

$$I_{0,n}^{\text{ul,asi}} = \frac{P_0^{\text{i,lim}}\left(\psi^{\text{asi}}\right) \cdot G_{m_n}^{\text{Rx,ul}}(0)}{L^{\text{fs,center}}\left(\lambda_{m_n}^{\text{ul}}\right)} \qquad [\text{W/Hz}] \ , \tag{5.74}$$

where $P_0^{\text{i,lim}}\left(\psi^{\text{asi}}\right)$ is the PSD limitation at the output of the station antenna, and $L^{\text{fs,center}}\left(\lambda_{m_n}^{\text{ul}}\right)$ is the free space loss for a terminal located at the center of the beam m_n.

The downlink ASI is caused by an adjacent satellite emitting in the same frequency band in the direction of d_n. In the absence of knowledge about the adjacent satellite emissions, it is reasonable to assume that the maximum adjacent satellite EIRP density is the same as the one of our satellite. The downlink PSD of the interfering satellite is given by:

$$I_{0,n}^{\text{dl,asi}}\left(a_{d_n,t}\right) = \frac{P_{0,n}^{\text{i,dl}}\left(m_{d_n},0\right) \cdot G_{d_n}^{\text{Rx,dl}}(\psi^{\text{asi}})}{L_{d_n}^{\text{fs}} \cdot a_{d_n,t}} \qquad [\text{W/Hz}] \ . \tag{5.75}$$

5.5.4 Composite link budget model

The total uplink interference PSD is given by:

$$I_{0,n}^{\text{ul,tot}}\left(a_{n,t}\right) = I_{0,n}^{\text{ul,aci}} + I_{0,n}^{\text{ul,asi}} + I_{0,n}^{\text{ul,cci}} + I_{0,n}^{\text{ul,xpi}}\left(a_{n,t}\right) \qquad [\text{W/Hz}] \ . \tag{5.76}$$

Similarly, the total downlink interference PSD is given by:

$$I_{0,n}^{\text{dl,tot}}\left(a_{d_n,t}\right) = I_{0,n}^{\text{dl,aci}}\left(a_{d_n,t}\right) + I_{0,n}^{\text{dl,asi}}\left(a_{d_n,t}\right) + I_{0,n}^{\text{dl,cci}}\left(a_{d_n,t}\right) + I_{0,n}^{\text{dl,xpi}}\left(a_{d_n,t}\right) \qquad [\text{W/Hz}] \ . \tag{5.77}$$

For a non-regenerative payload, the total CINR_0, $\gamma_{0,n}\left(\mathbf{a}_{n,t}^{\text{tot}}\right)$, is expressed with the composite formula [8, Section 5.9.2.2]:

$$\begin{aligned}\left(\gamma_{0,n}\left(\mathbf{a}_{n,t}^{\text{tot}}\right)\right)^{-1} = &\left(\frac{P_n^{\text{Rx,ul}}\left(a_{n,t}\right)}{N_{0,n}^{\text{ul}}}\right)^{-1} + \left(\frac{P_n^{\text{Rx,ul}}\left(a_{n,t}\right)}{I_{0,n}^{\text{ul,tot}}\left(a_{n,t}\right)}\right)^{-1} + \left(\frac{P_n^{\text{Tx,dl}}\left(a_{n,t}\right)}{I_{0,n}^{\text{im}}}\right)^{-1} \\ &+ \left(\frac{P_{d_n}^{\text{Rx,dl}}\left(\mathbf{a}_{n,t}^{\text{tot}}\right)}{N_{0,d_n}^{\text{dl}}\left(a_{d_n,t}\right)}\right)^{-1} + \left(\frac{P_{d_n}^{\text{Rx,dl}}\left(\mathbf{a}_{n,t}^{\text{tot}}\right)}{I_{0,n}^{\text{dl,tot}}\left(a_{d_n,t}\right)}\right)^{-1} \qquad [\text{Hz}] \ . \end{aligned} \tag{5.78}$$

5.5.5 Satellite parameters

This section presents the parameters and model relevant to the satellite payload.

Spectrum considerations

Focusing on the Ka-band fixed-satellite service spectrum allocations [85, Article 5], the minimum and maximum frequencies are set on 29.5-30 GHz for the uplink and 19.7-20.2 GHz for the downlink. Thus, the total spectrum available to the satellite is 500 MHz.

Let us denote $N^{\text{freq,ul}} = 2$ the number of frequencies available for beam coloring. Each beam has attributed a bandwidth of $500/N^{\text{freq,ul}}$ MHz, with $\text{freq}_m^{\text{ul}}$ being the uplink center frequency of beam m. The same is done for the downlink, although only one spot beam is present, and thus $N^{\text{freq,dl}} = 1$.

Coverage model

The satellite coverage is composed of multiple beams for the uplink and a single gateway spot beam for the downlink.

Uplink beams are generated with a given inter-beam angle separation $\Delta\psi^{\text{ib}}$, in degrees, following the method described in [86, Appendix A]. The color pair $\left(\text{freq}_m^{\text{ul}}, \text{pol}_m^{\text{ul}}\right)$ are attributed in a 4-color pattern with 2 frequencies and 2 linear polarizations, $\text{pol}_m^{\text{ul}} \in \{0°, 90°\}$ [87, Section 1.5]. The reflector diameter D^{sat} is computed such that the average beam gain at the tripoint intersection, denoted $G_m^{\text{Rx,ul}}\left(\Delta\psi^{\text{ib}}\right)$, matches the 4.3-dB contour [86, Section 6.2.2]. Thus, D^{sat} is computed to satisfy the following:

$$\frac{1}{M} \cdot \sum_{m=1}^{M} G_m^{\text{Rx,ul}}\left(\Delta\psi^{\text{ib}}\right) = \frac{1}{M} \cdot \sum_{m=1}^{M} \frac{G_m^{\text{Rx,ul}}(0)}{10^{0.43}}, \tag{5.79}$$

where the maximum antenna gain $G_m^{\text{Rx,ul}}(0)$ of the satellite is given as [8, Section 5.2]:

$$G_m^{\text{Rx,ul}}(0) = \eta^{\text{sat}} \cdot \left(\frac{\pi \cdot D^{\text{sat}} \cdot \text{freq}_m^{\text{ul}}}{c^{\text{light}}}\right)^2, \tag{5.80}$$

with η^{sat} the satellite antenna efficiency, and $G_m^{\text{Rx,ul}}\left(\Delta\psi^{\text{ib}}\right)$ is computed with the following Bessel functions to model the radiating pattern of the beams [42], [86], [88]:

$$G_m^{\text{Rx,ul}}(\psi) = G_m^{\text{Rx,ul}}(0) \cdot \left(\frac{J_1(u)}{2 \cdot u} + 36 \cdot \frac{J_3(u)}{u^3}\right)^2. \tag{5.81}$$

with $u = 2.07123 \cdot \sin(\psi)/\sin(\psi_m^{\text{3dB}}/2)$, and J_1 and J_3 being the Bessel functions of the first kind and order 1 and 3, respectively. Finally, the 3-dB beamwidth ψ_m^{3dB} of each beam is

obtained as [73, Appendix 4]:

$$\psi_m^{\text{3dB}} = \frac{70 \cdot c^{\text{light}}}{\text{freq}_m^{\text{ul}} \cdot D^{\text{sat}}} \qquad [\text{m}] \ , \tag{5.82}$$

with c^{light} being the speed of light. An example of beam footprint over France is shown in Fig. 5.7.

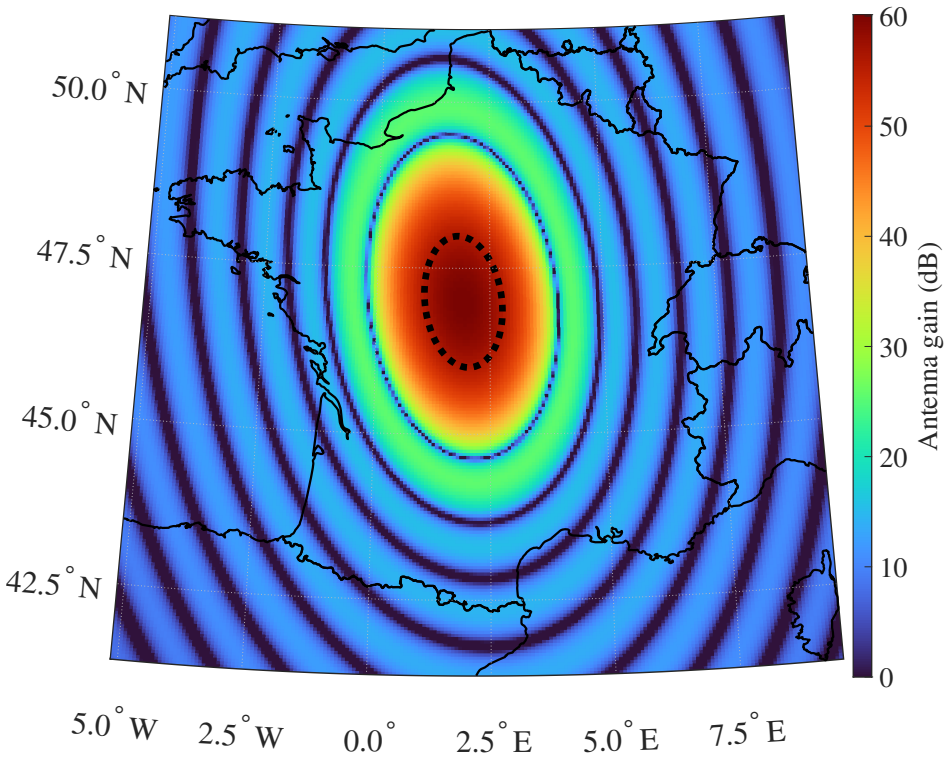

Figure 5.7: Example of beam footprint over France. The dotted black ellipse shows the 4.3-dB contour.

The downlink spot beam is centered at the gateway location (see Section 5.5.6). It is assumed that the antenna diameter and radiation pattern model are the same as the uplink. The values of $\Delta\psi^{\text{ib}}$, η^{sat} and other coverage parameters are available in the Payload section of Table 5.3.

Uplink noise temperature

We compute the uplink noise temperature T^{ul} following the model described in [8, Section 5.6.2]:

$$T^{\text{ul}} = \frac{T^{\text{ant,ul}}}{L^{\text{Rx,ul}}} + T^{\text{feeder}} \left(1 - \frac{1}{L^{\text{Rx,ul}}}\right) + T^{\text{eRx,ul}} \qquad [\text{K}] \ , \tag{5.83}$$

Symbol	**Value**	**Unit**	**Reference**
		Terminal	
η_n^{ant}	0.6	N/A[a]	[8, Section 5.6.2]
$L_n^{\text{Tx,ul}}$	0.2	dB	[73, Table 5.16]
		Payload	
$\Delta\psi^{\text{ib}}$	0.2	degrees	[87, Section 3]
η^{sat}	0.6	N/A	[8, Section 5.6.2]
$L^{\text{Rx,ul}}$	1	dB	[8, Section 5.6.2]
$T^{\text{ant,ul}}$	290	K	[8, Section 5.6.2]
T^{feeder}	290	K	[8, Section 5.6.2]
$T^{\text{eRx,ul}}$	290	K	[8, Section 5.6.2]
$P_v^{\text{out,sat}}$	100	W	[89, Table 1]
$\Phi_{m,v}^{\text{ul,nom}}$	-90	dB	[90]
$\alpha_v^{\text{I/O}}$	0.9	N/A	[73, Appendix 6]
$\beta_v^{\text{I/O}}$	4.5	N/A	[73, Appendix 6]
$\text{IBO}_v^{\text{tot}}$	$10^{-\beta_v^{\text{I/O}}/10}$	N/A	N/A
$L_m^{\text{Tx,dl}}$	1	dB	[73, Section 5.9]
		Interference	
NPR_v	17	dB	[87, Section 3.2]
L^{acs}	30	dB	[9, Table 3.2]
L^{xpi}	30	dB	[9, Table 3.2]
ψ^{orb}	4	degrees	[73, Section 5.5.4.1]
		Gateway	
$D_{d_n}^{\text{ant}}$	5	m	—-
$\eta_{d_n}^{\text{ant}}$	0.6	N/A	[8, Section 5.6.2]
$L_{d_n}^{\text{Rx,dl}}$	0.5	dB	[9, Table 3.2]
$T_{d_n}^{\text{F}}$	290	K	[8, Section 5.6.3]
$T_{d_n}^{\text{eRx,dl}}$	75	K	[8, Section 5.6.3]
T^{ground}	45	K	[8, Section 5.6.3]
T^{mr}	275	K	[30, Annex 1.3]

[a] N/A = non applicable.

Table 5.3: Parameters for results scenario

with $L^{\text{Rx,ul}}$ being the satellite feeder losses, $T^{\text{ant,ul}}$ being the satellite antenna temperature, T^{feeder} being the satellite feeder temperature, and $T^{\text{eRx,ul}}$ being the satellite receiving equipment temperature, of which the values are available in the Payload section of Table 5.3.

Transponder parameters

We assumed the payload is equipped with 30 amplifiers, each with an amplification power $P_v^{\text{out,sat}} = 100$ W [89, Table 1]. Thus, the payload total RF power pool is 3 kW, which is in line with current technologies [87, Table 9], [49, Section V]. The rest of the transponder parameters are available in the Payload section of Table 5.3.

Interference parameters

The interference noise density coming from various sources is computed according to the model described in Section 5.5.3. The interference EIRP mask of the ITU-R S.524 [52] is used to compute the PSD for the uplink ASI, to which a 3-dB loss as a result of coordination between satellite operators is applied. The cross-polarization degradation due to tropospheric effects is modeled following [30, Section 4.1]. Other interference parameters are given in the Interference section of Table 5.3.

5.5.6 Ground segment parameters

This section describes the parameters and methods used to generate the terminals and the gateway.

Terminals' location generation

For the purpose of studying the impact of fade correlation on the system, which is dependent on the inter-terminal distance, we propose to look at different coverages over Europe, ranging from global European coverage ($5.76 \cdot 10^6$ km^2, excluding Russia) down to Luxembourg ($2.59 \cdot 10^3$ km^2). As explained in Section 1.1, satellite services are more likely to be required in rural areas than in urban areas. Therefore, the terminals' locations are drawn inside the lands of the country/continent considered[18] following the inverse of the distribution of the population density, which is obtained from SEDAC's gridded world population dataset [67].

[18] Countries' borders are obtained from the "map unit" dataset at https://www.naturalearthdata.com/ (visited on 24/11/2023).

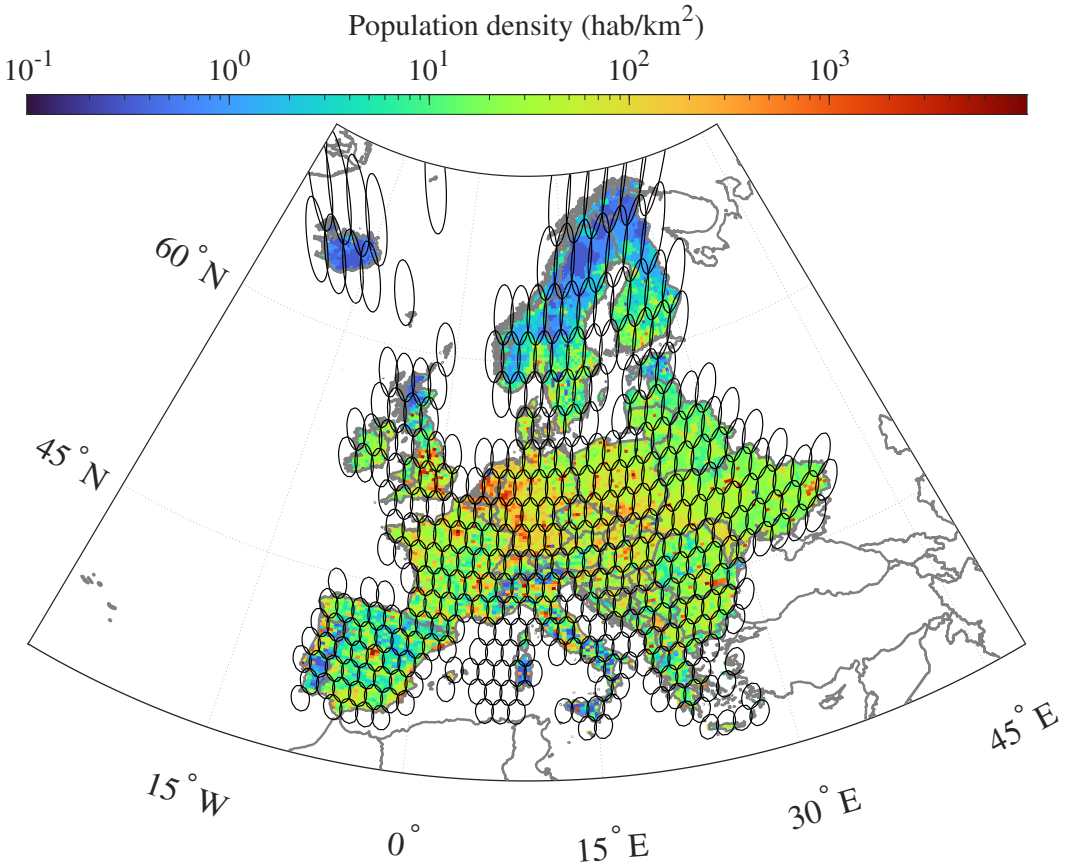

Figure 5.8: Example of population coverage over Europe. Black ellipses represent the 4.3-dB contour.

The gateway, on the other hand, is placed in a densely populated area (at least half of the maximum population density on the coverage). Each terminal is allocated to the beam that provides the highest receive antenna gain at its location.

Attenuation model

The annual probability of rain P_n^{rain} at the terminal's location is obtained by following the recommendation ITU-R P.618-13 [30, Section 2.2.1.2]. From the same model, the rain distribution log-normal parameters μ_n^{C} and σ_n^{C} are derived with the method described in ITU-R P.1057-6 [91, Annex 2]. The other tropospheric attenuation sources (clouds, gases, scintillation) are assumed to have a combined fixed value L^{trop} corresponding to the attenuation exceeded for a fraction of time equal to $p_{m_n}^{\text{adv}}$. The value of L^{trop} is obtained with the ITU model [30], excluding the rain component.

Antenna dimensioning

We assumed a given set of antenna diameters $\mathcal{D}^{\text{ant}} = \{0.6, 0.7, 0.8, 0.9\}$, in meters, available to the terminals. The antenna diameters are allocated to terminals with the goal of balancing link budget disparities. First, we compute the link imbalance caused by the geographical location ΔG^{geo} as:

$$\Delta G_n^{\text{geo}} = \frac{G_{m_n}^{\text{Rx,ul}}\left(\psi_n^{\text{ul}}\right)}{L_n^{\text{fs}}\left(\lambda_{m_n}^{\text{ul}}\right) \cdot \bar{F}_{A_n}^{-1}(p_{s_n}^{\text{adv}})} \,. \tag{5.84}$$

Then, we add the imbalance caused by SLA rate requirements as:

$$\Delta G_n^{\text{link}} = \frac{\Delta G^{\text{geo}}}{c_{s_n}^{\text{ci}}\left(1\right) \cdot \Delta B^{\min}} \,. \tag{5.85}$$

Finally, the imbalance range between the maximum and minimum ΔG_n^{link} can be divided into $|\mathcal{D}^{\text{ant}}|$ tiers of equal value range. The smallest antenna diameter is allocated to the tier with the highest ΔG_n^{geo} values, while the largest antenna diameter is allocated to the tier with the lowest ΔG_n^{geo} values. Once the antenna diameter D_n^{ant} is found, the maximum antenna gain $G_n^{\text{Tx,ul}}\left(0\right)$ is given by [8, Section 5.2]:

$$G_n^{\text{Tx,ul}}\left(0\right) = \eta_n^{\text{ant}} \cdot \left(\frac{\pi \cdot D_n^{\text{ant}} \cdot \text{freq}_{m_n}^{\text{ul}}}{c^{\text{light}}} \right)^2 \,. \tag{5.86}$$

The values of η_n^{ant} and $L_n^{\text{Tx,ul}}$ are found in Table 5.3. We deduce the 3-dB beamwidth ψ_n^{3dB} with the following [8, Section 5.2.2]:

$$\psi_n^{\text{3dB}} = 70 \cdot \pi \cdot \sqrt{\frac{\eta_n^{\text{ant}}}{G_n^{\text{Tx,ul}}\left(0\right)}} \,. \tag{5.87}$$

The expression of $G_n^{\text{Tx,ul}}(\psi)$ follows the Bessel model presented in Eq. (5.81).

Power dimensioning

The maximum emission power $P_n^{\text{Tx,ul}}$ is computed to satisfy the ground station requirements presented in Section 5.2.5. The first step consists of computing the minimum power $P_n^{\text{Tx,cs}}$ needed to achieve the clear sky requirement with the help of a root-finding algorithm. Then, another root finding computes the minimum power $P_n^{\text{Tx,fade}}$ needed to achieve the fade requirement, using the method described in Appendix B. Finally, the maximum emission

power $P_n^{\mathrm{Tx,ul}}$ is set to the maximum value between $P_n^{\mathrm{Tx,cs}}$ and $P_n^{\mathrm{Tx,fade}}$.

Gateway characteristics

The downlink noise temperature function $T^{\mathrm{dl}}\left(a_{d_n,t}\right)$ is given by the following model [8, Section 5.5.4]:

$$T_{d_n}^{\mathrm{dl}}\left(a_{d_n,t}\right) = \frac{T_{d_n}^{\mathrm{ant}}\left(a_{d_n,t}\right)}{L_{d_n}^{\mathrm{Rx,dl}}} + T_{d_n}^{\mathrm{eRx,dl}} + T_{d_n}^{\mathrm{F}} \cdot \left(1 - \frac{1}{L_{d_n}^{\mathrm{Rx,dl}}}\right) \qquad [\mathrm{K}]\ , \tag{5.88}$$

where $L_{d_n}^{\mathrm{Rx,dl}}$ is the receive feeder losses, $T_{d_n}^{\mathrm{F}}$ is the receive feeder temperature, and $T_{d_n}^{\mathrm{eRx,dl}}$ is the receive equipment temperature, assumed to be equal to the low noise amplifier temperature. The antenna temperature function is given by [8, Section 5.5.3]:

$$T_{d_n}^{\mathrm{ant}}\left(a_{d_n,t}\right) = \frac{T_{d_n}^{\mathrm{sky}}}{a_{d_n,t}} + T^{\mathrm{mr}}\left(1 - \frac{1}{a_{d_n,t}}\right) + T^{\mathrm{ground}} \qquad [\mathrm{K}]\ , \tag{5.89}$$

with T^{ground} being the ground noise temperature, T^{mr} the atmospheric mean radiating temperature, and $T_{d_n}^{\mathrm{sky}}$ the sky noise temperature in clear sky. We approximate the sky noise temperature with the background brightness temperature, given by [92, Section II.A]:

$$T_{d_n}^{\mathrm{sky}} = 2.725 + 20 \cdot \left(\frac{408 \cdot 10^6}{\mathrm{freq}_{m_{d_n}}^{\mathrm{dl}}}\right)^{2.75} \qquad [\mathrm{K}]\ . \tag{5.90}$$

The rest of the noise components values are given in the Gateway section of Table 5.3.

5.5.7 Generation of rain samples

For our simulations, we selected the ITU-R P.1853-2 model [93, Annex 1.5.2], although the temporal correlation is removed by bypassing the low-pass filtering step. Spatial correlation between sample sequences is introduced by performing a matrix multiplication with the Cholesky decomposition of an $(N + D) \times (N + D)$ covariance matrix, of which the coefficients are expressed as follows:

$$\rho_{n_1,n_2}^{\mathrm{G}} = 0.59 \cdot e^{-D_{n_1,n_2}/31} + 0.41 \cdot e^{-D_{n_1,n_2}/800}\ , \tag{5.91}$$

where D_{n_1,n_2} is the distance between terminal n_1 and n_2, in km. The complexity of this method is discussed in Section 5.7.1.

5.6 Numerical applications

This section shows the application of the Monte Carlo process presented in Section 5.4 to the specific BSM scenarios presented in Section 5.5. It is divided into two parts. The first one consists of Section 5.6.1 and provides a numerical validation of the Monte Carlo process. The second part uses $b^{\min}$ to provide a performance comparison between the several benchmarks inspired by the existing literature. Firstly, the benchmarks are introduced Section 5.6.2, based on the literature review presented in Section 2.2.3. Then, Section 5.6.3 presents and analyses the numerical results obtained across different coverages and SLA scenarios, as described in Section 5.5.

5.6.1 Validation of Monte Carlo method

This section provides numerical validation results for the Monte Carlo process we proposed in Section 5.4.4. The aim of the validation method is to assess the impact of the Monte Carlo bias by comparing $P\left(b^{\min} \in \mathcal{C}_T\right)$ and $P\left(\hat{b}_T^{\min} \in \mathcal{C}_{\delta^{\mathrm{B}}}\right)$ to a pre-determined confidence level $1-\alpha^{\mathrm{conf}}$.

Description of the validation method

The validation method consists of the following steps:

1. Generation of a specified scenario as per Section 5.5.
2. Repeat the iterative Monte Carlo process described in Section 5.4 N^{test} times.
3. Extract relevant outputs and build statistics.

For each Monte Carlo process $i \in \mathcal{I}_{N^{\mathrm{test}}}$, we extract the following outputs:

- The number of samples T_i.
- The estimate $\hat{b}_{T_i}^{\min}$.
- The lower bound $b^{\mathrm{eq,TD}}\left(\mathbf{A}^{\mathrm{tot}}_{t_i^{\mathrm{inf}}:T_i}\right)$ and the upper bound $b^{\mathrm{eq,TD}}\left(\mathbf{A}^{\mathrm{tot}}_{t_i^{\mathrm{sup}}:T_i}\right)$ of the confidence interval.

- The sample sequence.

Once all N^{test} processes are completed, we can build a larger empirical CDF of $T^{\text{test}} = \sum_{i=1}^{N^{\text{test}}} T_i$ samples, which allows us to compute a precise estimate $\hat{b}^{\min}_{T^{\text{test}}}$. We can then estimate the probabilities of $b^{\min}$ falling outside of the binomial confidence interval $P\left(b^{\min} \in \mathcal{C}_T\right)$ with the following:

$$P\left(b^{\min} \in \mathcal{C}_T\right) \approx 1 - \frac{\sum_{i=1}^{N^{\text{test}}} \mathbb{1}_{\hat{b}^{\min}_{T^{\text{test}}} < b^{\text{eq,TD}}\left(\mathbf{A}^{\text{tot}}_{i_i^{\text{inf}}:T_i}\right)}}{N^{\text{test}}} - \frac{\sum_{i=1}^{N^{\text{test}}} \mathbb{1}_{\hat{b}^{\min}_{T^{\text{test}}} \geq b^{\text{eq,TD}}\left(\mathbf{A}^{\text{tot}}_{i_i^{\text{sup}}:T_i}\right)}}{N^{\text{test}}}. \quad (5.92)$$

We can also estimate the probability $P\left(\hat{b}^{\min}_T \in \mathcal{C}_{\delta^{\text{B}}}\right)$ that the Monte Carlo estimate falls within the relative confidence interval $\mathcal{C}_{\delta^{\text{B}}} = \left((1-\delta^{\text{B}}) \cdot b^{\min}, (1+\delta^{\text{B}}) \cdot b^{\min}\right)$ with :

$$P\left(\hat{b}^{\min}_T \in \mathcal{C}_{\delta^{\text{B}}}\right) \approx 1 - \frac{\sum_{i=1}^{N^{\text{test}}} \mathbb{1}_{\hat{b}^{\min}_{T_i} < \hat{b}^{\min}_{T^{\text{test}}} \cdot (1-\delta^{\text{B}})}}{N^{\text{test}}} - \frac{\sum_{i=1}^{N^{\text{test}}} \mathbb{1}_{\hat{b}^{\min}_{T_i} \geq \hat{b}^{\min}_{T^{\text{test}}} \cdot (1+\delta^{\text{B}})}}{N^{\text{test}}}. \quad (5.93)$$

Finally, we compute the average number of samples $\bar{T} = T^{\text{test}}/N^{\text{test}}$.

Validation results

Table 5.4 shows results obtained for European coverage and $N = 100$ terminals with enterprise SLAs. This scenario was selected due to computational constraints, as $N^{\text{test}} = 10^4$ Monte Carlo simulations were computed, with a desired confidence level $1 - \alpha^{\text{conf}} = 0.95$ and rate of increase $\lambda^{\text{inc}} = 0.1$, for different values of δ^{B}.

As expected, the bias introduced by our Monte Carlo method lowers the confidence level of the binomial interval. However, it appears that the implication presented in Eq. (5.54) compensates for this reduction.

We also observe a sharp decrease in the average number of samples generated when increasing δ^{B}. The consequences of this behavior are further discussed in Section 5.7.1

	$\delta^{\text{B}} = 1\%$	2%	3%	5%
$\bar{T}$	324,888	66,127	56,214	16,799
$P\left(b^{\min} \in \mathcal{C}_T\right)$	0.9449	0.9308	0.9310	0.9350
$P\left(\hat{b}^{\min}_T \in \mathcal{C}_{\delta^{\text{B}}}\right)$	0.9993	0.9966	0.9969	0.9981

Table 5.4: Statistics obtained with the validation method.

5.6.2 Benchmarks

In this section, we present benchmarks based on the academic and industry literature we reviewed in Section 2.2.3. The first one makes the optimistic assumption of independent rain fade and leads to underestimating the amount of satellite resources. The second makes the pessimistic assumptions of fully correlated rain fade and leads to overestimating the amount of satellite resources. Comparing those two approaches to $b^{\min}$ will allow us to quantify the amount of under/overestimation, which as explained in Section 2.2.3 was unknown until now.

Independent rain fade

To evaluate the impact of rain fade correlation on the satellite resources, it is interesting to also compute $b^{\min}$ assuming independent rain fade. Computing such value is possible by using the same Monte Carlo method, to the exception that the covariance matrix coefficients introduced in Eq. (5.91) should be changed to $\rho^{\mathrm{G}}_{n_1,n_2} = \mathbb{1}_{n_1=n_2}$. We denote b^{id} the bandwidth resulting from the dimensioning process assuming independent rain fade.

Worst-case

The *worst-case* approach assumes full correlation of rain fade between terminals. We define for all terminal n the target FMT mode k_n^{tgt} such that:

$$\begin{aligned} &P\left(\bar{k}_n^{\mathrm{ci}}\left((A_n, A_{d_n})\right) < k_n^{\mathrm{tgt}} + 1\right) > p_{s_n}^{\mathrm{adv}} \\ &\text{and} \\ &P\left(\bar{k}_n^{\mathrm{ci}}\left((A_n, A_{d_n})\right) < k_n^{\mathrm{tgt}}\right) \leq p_{s_n}^{\mathrm{adv}} \end{aligned} \tag{5.94}$$

Assuming full correlation of fade between terminals, the worst-case bandwidth demand b^{wc} is given by:

$$b^{\mathrm{wc}} = \sum_{n=1}^{N}\sum_{q=1}^{Q} \frac{R_{s_n,q}^{\mathrm{ci}}}{\eta^{\mathrm{spe}}\left(k_n^{\mathrm{tgt}}\right)} \cdot p_{s_n,q}^{\mathrm{at}} \qquad [\mathrm{Hz}]\ . \tag{5.95}$$

The worst-case PEB demand $b^{\mathrm{pe,wc}}$ is computed by determining the worst-case total power demand. Let us remark that, knowing terminal n is transmitting using FMT mode $\bar{k}_n^{\mathrm{ci}}\left(\mathbf{a}_{n,t}^{\mathrm{tot}}\right) = k_n^{\mathrm{tgt}} > {}^{\downarrow}k_{s_n}^{\mathrm{ci}}$, the bandwidth demand is fixed. Thus, the power demand is maximized when $\mathrm{IBO}_n\left(a_{n,t}\right)$ is maximal and $\gamma_{0,n}\left(\mathbf{a}_{n,t}^{\mathrm{tot}}\right)$ is minimal.

On the one hand, the highest value of $\mathrm{IBO}_n\left(a_{n,t}\right)$ is reached when the uplink attenuation

is minimal, i.e., $a_{n,t} = 1$. On the other hand, the minimal value of $\gamma_{0,n}\left(\mathbf{a}_{n,t}^{\text{tot}}\right)$ for which $\bar{k}_n^{\text{ci}}\left(\mathbf{a}_{n,t}^{\text{tot}}\right) = k_n^{\text{tgt}}$ is $\gamma_{0,n}\left(\mathbf{a}_{n,t}^{\text{tot}}\right) = \theta_0\left(k_n^{\text{tgt}}, c^{\text{ci}}\left(s_n, k_n^{\text{tgt}}\right)\right)$. For a given value of uplink attenuation $a_{n,t}$, the corresponding downlink attenuation that satisfies the previous condition is the highest downlink attenuation $a_{d_n,t}$ that satisfies $\bar{k}_n^{\text{ci}}\left(\mathbf{a}_{n,t}^{\text{tot}}\right) = k_n^{\text{tgt}}$.

Thus, the worst-case power demand is found in two steps. The first step is to find, for each terminal n, the highest downlink attenuation value $a_{d_n,t}$ that satisfies the following:

$$\bar{k}_n^{\text{ci}}\left((1, a_{d_n,t})\right) = k_n^{\text{tgt}}\,. \tag{5.96}$$

The second step is to compute the worst-case power demand as follows:

$$b^{\text{pe,wc}} = B_{v_n}^{\text{trans}} \cdot \sum_{n=1}^{N}\sum_{q=1}^{Q} P_{n,q}^{\text{D}}\left((1, a_{d_n,t})\right) \cdot p_{s_n,q}^{\text{at}} \qquad [\text{Hz}]\,. \tag{5.97}$$

Finally, the worst-case equivalent bandwidth $b^{\text{eq,wc}}$ is given as the maximum between the power and bandwidth demands:

$$b^{\text{eq,wc}} = \max\left(b^{\text{wc}}, b^{\text{pe,wc}}\right) \qquad [\text{Hz}]\,. \tag{5.98}$$

5.6.3 Satellite resource comparison

Table 5.5 offers a comparison between b^{min} (introduced in Section 5.3.3) and $b^{\text{eq,cs}}$, b^{id}, and $b^{\text{eq,wc}}$, respectively the clear sky (introduced in Section 5.4.4), independent fade (introduced in Section 5.6.2) and worst-case (introduced in Section 5.6.2) benchmarks. These results were obtained for different coverages, characterized by the average correlation value $\bar{\rho}^{\text{G}}$, and for different numbers of terminals. The confidence level was set on $1-\alpha^{\text{conf}} = 0.95$ and the desired relative precision was set on $\delta^{\text{B}} = 1\%$. We provide the bandwidth results in absolute (MHz) and relative (%) values w.r.t. b^{min}, with $\Delta^{\text{min,cs}} = \left(b^{\text{eq,cs}}/b^{\text{min}} - 1\right)$, $\Delta^{\text{min,id}} = \left(b^{\text{id}}/b^{\text{min}} - 1\right)$, and $\Delta^{\text{min,wc}} = \left(b^{\text{eq,wc}}/b^{\text{min}} - 1\right)$.

General observations

We observe different behaviors of b^{min} for the residential and enterprise scenarios. However, we can make the general observation that the value of b^{min} is closer to the value of b^{id} than $b^{\text{eq,wc}}$ for Europe, France, and Germany coverages, regardless of the scenario. These results

Residential – $N = 100$								
Coverage	$\bar{\rho}^{\mathrm{G}}$	$b^{\mathrm{eq,cs}}$	$\Delta^{\mathrm{min,cs}}$	b^{id}	$\Delta^{\mathrm{min,id}}$	b^{min}	$b^{\mathrm{eq,wc}}$	$\Delta^{\mathrm{min,wc}}$
Europe	0.0901	2.55	-4%	2.65	0%	2.65	3.45	30%
France	0.2679	2.55	-4%	2.62	-2%	2.67	3.45	29%
Germany	0.2876	2.55	-4%	2.62	-2%	2.67	3.45	29%
Ireland	0.3796	2.53	-2%	2.58	0%	2.58	3.42	32%
Netherlands	0.4122	2.50	-4%	2.56	-2%	2.61	3.44	32%
Walloon Region	0.4712	2.49	-4%	2.55	-2%	2.61	3.44	32%
Luxembourg	0.6679	2.49	-5%	2.56	-3%	2.63	3.44	31%
Residential – $N = 10,000$								
Coverage	$\bar{\rho}^{\mathrm{G}}$	$b^{\mathrm{eq,cs}}$	$\Delta^{\mathrm{min,cs}}$	b^{id}	$\Delta^{\mathrm{min,id}}$	b^{min}	$b^{\mathrm{eq,wc}}$	$\Delta^{\mathrm{min,wc}}$
Europe	0.0877	250	-2%	251	-1%	254	338	33%
France	0.2612	250	-3%	251	-2%	257	338	31%
Germany	0.2880	250	-3%	251	-3%	258	338	31%
Ireland	0.3765	248	-2%	248	-1%	252	335	33%
Netherlands	0.4147	245	-4%	246	-4%	256	337	32%
Walloon Region	0.4700	244	-5%	246	-4%	256	337	32%
Luxembourg	0.6555	244	-5%	245	-5%	257	337	31%
Enterprise – $N = 100$								
Coverage	$\bar{\rho}^{\mathrm{G}}$	$b^{\mathrm{eq,cs}}$	$\Delta^{\mathrm{min,cs}}$	b^{id}	$\Delta^{\mathrm{min,id}}$	b^{min}	$b^{\mathrm{eq,wc}}$	$\Delta^{\mathrm{min,wc}}$
Europe	0.0901	17.2	-22%	20.7	-6%	22.0	34.9	59%
France	0.2587	17.2	-29%	20.7	-15%	24.2	34.2	41%
Germany	0.2872	17.2	-32%	20.7	-18%	25.3	34.7	37%
Ireland	0.3726	17.1	-31%	20.3	-19%	25.0	28.8	15%
Netherlands	0.4126	16.9	-37%	20.3	-24%	26.9	31.0	15%
Walloon Region	0.4689	16.9	-38%	20.1	-26%	27.2	30.3	11%
Luxembourg	0.6619	16.9	-46%	20.1	-35%	31.2	31.4	0%
Enterprise – $N = 10,000$								
Coverage	$\bar{\rho}^{\mathrm{G}}$	$b^{\mathrm{eq,cs}}$	$\Delta^{\mathrm{min,cs}}$	b^{id}	$\Delta^{\mathrm{min,id}}$	b^{min}	$b^{\mathrm{eq,wc}}$	$\Delta^{\mathrm{min,wc}}$
Europe	0.0884	1720	-15%	1780	-12%	2030	3520	74%
France	0.2615	1720	-29%	1790	-26%	2430	3490	44%
Germany	0.2881	1720	-30%	1790	-28%	2470	3490	41%
Ireland	0.3769	1700	-31%	1780	-28%	2460	2880	17%
Netherlands	0.4139	1690	-36%	1760	-33%	2640	3130	19%
Walloon Region	0.4713	1690	-37%	1770	-34%	2670	3030	13%
Luxembourg	0.6569	1690	-45%	1760	-43%	3090	3110	1%

Table 5.5: Comparison of bandwidth, absolute values in MHz, Δ^{min} in % of b^{min}.

would explain the empirical preference in the industry for assuming independence of rain fade rather than total correlation. The low amount of undersizing for coverages wider than Europe can probably be compensated by the typical safety margins found in real-life satellite network designs.

We also observe that the results for the Ireland scenario tend not to follow the general trend observed in other scenarios. Our explanation for this behavior is that Ireland has a different climate than the other coverages. Table 5.6 compares for different coverages the annual probability of rain P_n^{rain} and the uplink attenuation $\bar{F}_{A_n}^{-1}(p_{s_n}^{\text{adv}})$ exceeded with probability $p_{s_n}^{\text{adv}} = 0.5\%$ averaged across terminals. We observe that Ireland has the highest average annual probability value and the lowest average uplink attenuation value. More generally, we observe that the differences in P_n^{rain} and $\bar{F}_{A_n}^{-1}(p_{s_n}^{\text{adv}})$ are reflected in the differences in $b^{\text{eq,cs}}$ and $b^{\text{eq,wc}}$ between coverages in Table 5.5.

Coverage	Average P_n^{rain}	Average $\bar{F}_{A_n}^{-1}(p_{s_n}^{\text{adv}})$
Europe	6.18%	3.64
France	6.99%	3.58
Germany	6.65%	3.60
Ireland	10.3%	2.87
Netherlands	6.80%	3.17
Walloon Region	8.56%	3.09
Luxembourg	8.38%	3.09

Table 5.6: Comparison of average annual rain probability P_n^{rain} and average uplink attenuation $\bar{F}_{A_n}^{-1}(p_{s_n}^{\text{adv}})$ for an exceedance probability $p_{s_n}^{\text{adv}} = 0.5\%$.

Residential scenario

In the residential BSM scenario, the influence of rain fade, including its spatial correlation, on the satellite resource consumption is barely significant. The values of $b^{\text{eq,cs}}$ and b^{id} are within 5% of $b^{\min}$ regardless of the coverage and the number of terminals.

The low sensitivity of $b^{\min}$ to rain fade can be explained by the significant gap in the power required to satisfy the clear sky and fade requirements presented in Section 5.2.5. Fig. 5.9 illustrates the average power required among terminals to satisfy the clear sky requirement

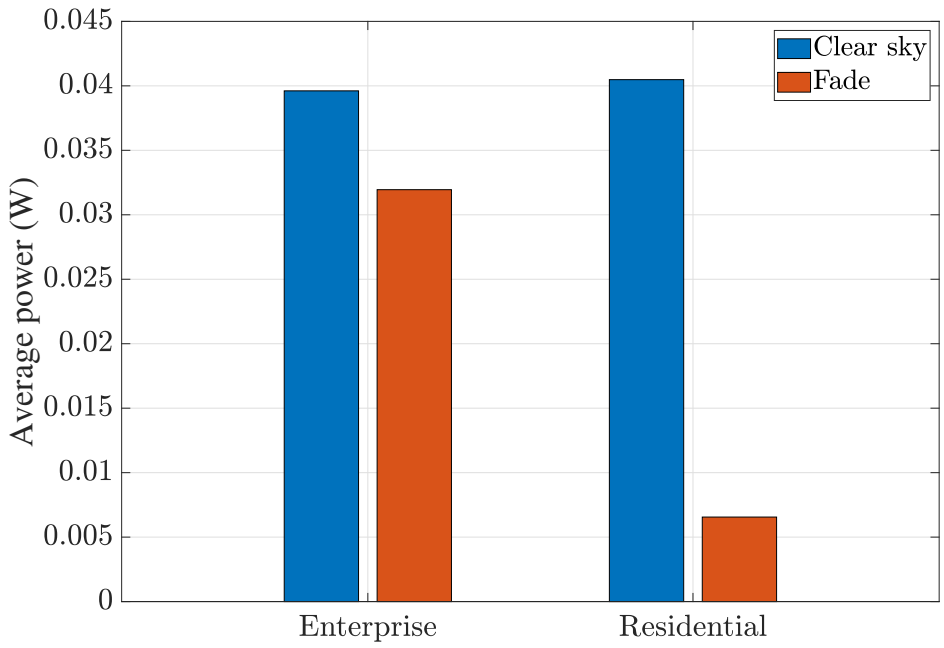

Figure 5.9: Comparison of the average power needed among terminals to satisfy the clear sky (blue) and fade (red) requirements, for residential and enterprise scenarios.

(red bars) and the fade requirement (blue bar). For the residential scenario, the fade power requirement is almost eight times lower than the clear sky power requirement.

This difference in power requirements can be explained by (i) the large contention ratio for the residential scenario, which results in maximum rates orders of magnitude above the committed rates; (ii) the comparatively weak average uplink attenuation that needs to be compensated for the fade requirement, which is around 3.76 for the Europe scenario for an exceedance probability of 0.5%; (iii) the dynamic range, i.e., the ratio between the lowest and the highest SNR threshold, of the FMT mode set, which is around 20. The combination of these three factors results in terminals using FMT modes in fade conditions that are close to the ones used in clear sky.

On the other hand, the relative gap of $b^{\min}$ to $b^{\text{eq,wc}}$ is systematically around 30%, which represents a significant amount of oversizing for the worst-case method. Thus, it is preferable to assume independent than fully correlated rain fade for the residential scenario. Finally, let us remark that $1.1 \cdot b^{\text{eq,cs}}$ is a relatively good approximation of $b^{\min}$ in all residential scenarios, and could be used as a quick thumb rule for networks where the clear sky requirements drive the dimensioning of the terminal's emission capabilities.

Enterprise scenario

In the enterprise BSM scenario, the influence of rain fade is significant. The values of $b^{\text{eq,cs}}$ and b^{id} are significantly lower than $b^{\min}$ regardless of the coverage and the number of terminals.

The high sensitivity of $b^{\min}$ to rain fade can be explained by the fact that the clear sky and fade power requirements are rather balanced, as illustrated in Fig. 5.9. These power requirements are more balanced than for the residential scenarios due to lower contention ratios in the enterprise scenarios. Thus, the FMT modes used by terminals in fade conditions are significantly different than the ones used in clear sky.

Moreover, we observe that the spatial correlation of rain fade has a significant influence. The relative gap between b^{id} and $b^{\min}$ increases with the average spatial correlation $\bar{\rho}^{\text{G}}$ while the relative gap between $b^{\min}$ and $b^{\text{eq,wc}}$ reduces. In total, $\Delta^{\min,\text{id}}$ increases by around 30%, while $\Delta^{\min,\text{wc}}$ decreases by 59% for $N = 100$ and 73% for $N = 10,000$.

Therefore, neither the independent nor the fully correlated rain fade assumptions can predict the consumption of satellite resources satisfactorily for all scenarios. The independent assumption could be used for the Europe coverage, and the worst-case method could be used for the Walloon region and Luxembourg coverage. However, any coverage size in between will require the computation of $b^{\min}$. Finally, let us remark that the thumb rule presented for the residential scenarios does not work when the clear sky requirements are not the main driver of the dimensioning of the terminal's emission capabilities.

5.7 Discussions and conclusions

5.7.1 Discussion on complexity

Complexity inherent to the Monte Carlo method

The Monte Carlo method presented in Section 5.4.4 necessitates the computation of T total bandwidth samples $b^{\text{eq,TD}}\left(\mathbf{A}_t^{\text{tot}}\right)$. Each total bandwidth sample requires computing $N \times K$ individual bandwidth samples $b_{n,q}^{\text{D}}\left(\mathbf{a}_{n,t}^{\text{tot}}, k\right)$ and individual power samples $b_{n,q}^{\text{pe,D}}\left(\mathbf{a}_{n,t}^{\text{tot}}, k\right)$. All K individual bandwidth and power samples are computed from the same link budget sample $\gamma_{0,n}\left(\mathbf{a}_{n,t}^{\text{tot}}\right)$. Thus, the Monte Carlo method requires $O\left(N \times T\right)$ calls to the link budget function, and $O\left(N \times T \times K\right)$ bandwidth computations.

Such complexity may be an issue considering our method cannot predict the number of

samples T needed for convergence. Given the strong dependency between T and δ^{B} illustrated in Section 5.6.1, a sound approach when computing resources are limited would be to run several Monte Carlo processes with decreasing δ^{B} values, until either the precision is deemed good enough or the computing limitations are reached.

Complexity inherent to the ITU-R P.1853-2 method

The matrix multiplication of the covariance matrix of size $(N+D)\times(N+D)$ by the random sample sequence of size $(N+D)\times T$ is a potential complexity issue for N larger than 10^4. It is likely that a high value of N coincides with a large coverage scenario. In such a case, it is possible to make the correlation sparse by setting $\rho^{\mathrm{G}}_{n_1,n_2}=0$ if the distance between n_1 and n_2 is above a predetermined distance threshold, say 1,000 km. Then, one needs to perform an incomplete Cholesky decomposition [94].[19] The rest of the generation process remains unchanged.

5.7.2 Conclusions

In this chapter, we presented a BSM scenario where return link satellite resources have to be dimensioned based on subscriber's SLAs. We showed how to convert SLAs into bandwidth and power demands, and then into a quantile estimation problem. We presented a Monte Carlo method to estimate such quantile. Finally, we provided numerical applications of our Monte Carlo method in enterprise and residential types of BSM networks.

Results showed that our Monte Carlo method is able to reach a predetermined relative confidence interval. They also showed that the spatial correlation of fade can significantly influence the consumption of satellite resources, and consequently the SRD process, for networks constrained by strong fade requirements. A dependency between the clear sky/fade power requirements balance and the sensitivity of the network to rain fade was observed.

[19] The incomplete Cholesky decomposition is implemented in Matlab with the ichol function.

Chapter 6

Conclusion and further work

This chapter provides a global conclusion to this dissertation and presents future research directions.

6.1 Conclusions

The principal objective of this Ph.D. was to investigate the SRD problem in the context of GEO broadband satellite networks affected by rain fade. The work focused on formulating resource-demand models depending on the network's adaptability to rain fade, and finding resource-optimal solutions while ensuring the satisfaction of the SLA.

In Chapter 3, we focused on the CCM scenario, i.e., the least adaptable. The CPO problem was presented, and several methods of varying complexity were proposed to solve it. Numerical results were presented for a European scenario, and small gains in resource consumption were observed overall compared to existing methods.

Nonetheless, the proper definition of the CPO problem allowed us to translate our solutions in the context of ACM with SCP, considering spatially correlated rain attenuation. The numerical results, presented in Chapter 4, showed a significant improvement over worst-case assumptions. Thus, the first proof of the importance of the spatial correlation of rain in the SRD problem was given.

The final work, presented in Chapter 5, aimed at addressing the main knowledge gaps left by the second work. The scenario was complexified to account for more modern technologies, and the statistical aspect of the problem was investigated to ensure the reliability of the solution. Finally, the numerical results allowed us to compare our solution against best-case

assumptions (no rain or independent rain), and a significant gap in resource consumption was observed in scenarios where fade requirements are comparable to clear sky requirements.

Conclusively, this dissertation proves that the spatial correlation of rain must be accounted for in order to properly solve the SRD problem in the context of BSM return networks constrained by significant fade requirements. In such scenarios, worst-case assumptions can lead to a significant overestimation of resource consumption, while best-case assumptions can lead to significant underestimation. Multiple methods were provided to solve the SRD problem accounting for the spatial correlation of rain fade using synthetic rain fade simulators, thus demonstrating their applicability to system-scale dimensioning. However, it should be acknowledged that the application of the solutions proposed in Chapter 3 and Chapter 4 to the scenario presented in Chapter 5 would require significant effort, mainly due to the incompatibility in the terminals' emission assumption and the nature of the satellite resources considered.

6.2 Unsuccessful attempts

So far, all the work that was presented in this dissertation led to interesting results. However, it is in the nature of the research process itself to investigate problems that sometimes lead to inconclusive results. Having knowledge of such unsuccessful attempts could save the time of any future researcher interested in the topic of this dissertation. Thus, let us take a moment to summarize what did *not* work.

6.2.1 Dirichlet distribution

In the early stages of the work presented in Chapter 4, the Dirichlet distribution [95, Chapter 49] was considered to model the FMT modes demand. This distribution models a multivariate random variable $\mathbf{X} = (X_1, X_2, \ldots, X_K)$ with the special property that $\sum_{k=1}^{K} X_k = 1$, thus very similar to the carrier plan constraints. This approach required estimating a "concentration" parameter for each X_k. No reliable estimation technique for this parameter was found due to the complex nature of the FMT mode requests and the inability to express their correlation.

6.2.2 Machine learning

The use of machine learning to accelerate the MILP problem-solving in Chapter 4 was considered, and more specifically *support-vector machine* (SVM) [96]. The idea was to use an SVM to learn an equation that would separate the carrier plans that satisfy the accommodation constraint from those that do not. A successful predictor would in theory accelerate the convergence time of the MILP problem presented in Section 4.3.1, as it removes the need to find the vector $\boldsymbol{\alpha}$. The main problem faced with this approach was the lack of reliability of the SVM predictor compared to what is typically expected in our dimensioning problem (e.g., 99.5%).

6.3 Future work

The work carried out in this project can be extended in multiple directions:

- **Accounting for the RRM algorithm policy**: The solutions to the SRD problem proposed in this dissertation are agnostic to the behavior of the RRM algorithm. However, the results presented in Chapter 4 hinted that significant gains could be obtained by accounting for the RRM algorithm in the satellite resource demand model. Examples of RRM algorithm policy are found in [36, Chapter 7]. The main challenge resides in abstracting the behavior of the RRM algorithm and integrating its impact into the resource demand model and the computation of the congestion outage time.

- **Accounting for the RRM algorithm update period**: The solutions to the SRD problem proposed in this dissertation assume either adaptive or static carrier plans. The notion of adaptability depends on the time variations of the rain fade. It is found in the literature instances of DVB-RCS implementations where the carrier plan is neither adaptive nor static [35], [37]. In such a case, the carrier is updated at regular time intervals that are significantly larger than the changes in FMT modes. The solution proposed in Chapter 5 covers such cases by making the worst-case assumption that the carrier plan is never updated, however, more resource-efficient solutions could potentially be reached by considering the RRM algorithm update period in the SRD problem.

- **Considering the forward link**: The work in this dissertation exclusively focused on the return link, however, an interactive satellite service needs both forward and return

links. In this context, the two-way service availability is defined as the joint availability of the forward and return links. The resource-demand model and the SRD problem have to be reformulated accordingly. Assuming the SRD problem also needs to be solved on the forward link, the forward link resource-demand needs to be expressed and evaluated together with the return link resource-demand to compute the two-way service availability. This direction would be particularly relevant in the context of meshed satellite networks.

- **Finding cost-optimal network design**: The SRD problem presented in this dissertation takes the ground segment design (mainly antenna gain and power of terminals and gateways) as an input. By minimizing the satellite resource consumption for a given ground segment design, we are able to provide the solution that minimizes the OPEX. However, the total cost of the satellite network also includes the CAPEX, which is greatly affected by the ground segment design. Hence, the problem of minimizing the total network cost needs to explore different ground segment designs, compute the CAPEX and OPEX for each design, and select the design that minimizes the sum. The challenge resides in exploring efficiently the space of possible ground segment designs, as exploring every single possibility would be extremely computationally expensive. One possibility that has been investigated in the literature is to use genetic algorithms [97].

- **Accounting for terminal and satellite mobility**: The work in this dissertation focused on scenarios where the terminals, the gateways, and the satellite have a fixed latitude-longitude location. However, broadband satellite services also include scenarios with mobile terminals and non-geostationary satellites. Any modification of the locations changes the distribution of rain attenuation of the uplink and the downlink and impacts the satellite resource demand. The main challenge is to model the impact of the satellite and terminals' mobility on the satellite resource demand CDF. Some aspects of this problem have been investigated in [98].

Appendix A

Examples of traffic characterization

A.1 Conversational audio/video

Let us define the following SLA parameters:

- N_s^{lines} is the number of call lines (video or audio) offered to each subscriber of SP s.
- $\bar{R}_s^{\text{call}}$ is the average number of calls per line and per unit of time (seconds, minutes, hours).
- $\bar{T}_s^{\text{call}}$ is the average duration of a call, in the same unit of time as $\bar{N}_s^{\text{call}}$.
- $R_s^{\text{ci,call}}$ is the information rate needed during a call connection at committed/acceptable quality (e.g., 12 kbps for audio, 480p for video).
- $R_s^{\text{mi,call}}$ is the information rate needed during a call connection at best quality (e.g., 64 kbps for audio, up to 1080p for video).
- p_s^{call} is the call blocking probability.

We assume that the N_s^{lines} lines are committed, therefore we deduce that $R_s^{\text{mi}} = N_s^{\text{lines}} \cdot R_s^{\text{mi,call}}$ and $R_s^{\text{ci}} = N_s^{\text{lines}} \cdot R_s^{\text{ci,call}}$.

The computation of p_s^{at} is achieved by the mean of an Erlang B formula. The traffic intensity E_s, in Erlang, is given by:

$$E_s = N_s^{\text{lines}} \cdot |\mathcal{N}_s| \cdot \bar{R}_s^{\text{call}} \cdot \bar{T}_s^{\text{call}} . \tag{A.1}$$

From this quantity, the Erlang B model allows to compute the maximum number of lines $N_s^{\text{lines,max}}$ that the network should support to ensure a call blocking probability p_s^{call} with the following formula:

$$p_s^{\text{call}} = \frac{\frac{E_s^{N_s^{\text{lines,max}}}}{N_s^{\text{lines,max}}!}}{\sum_{n=1}^{N_s^{\text{lines,max}}} \frac{E_s^n}{n!}} \,. \tag{A.2}$$

Finally, we can compute the expected proportion of active terminals as:

$$p_s^{\text{at}} = \frac{N_s^{\text{lines,max}}}{N_s^{\text{lines}} \cdot |\mathcal{N}_s|} \,. \tag{A.3}$$

Please note that voice only and video traffic have to be differentiated for the Erlang computations, therefore this process has to be potentially repeated twice, and the resulting rates should be summed.

A.2 Transactions

Let us define the following SLA parameters:

- R_s^{mi} is directly given as the maximum burst rate offered to each subscriber of SP s.
- λ_s^{abg} is the average burst generation rate per subscriber, in s^{-1}.
- l_s is the average length of a message, in bits.
- ΔT_s^{TTS} is the maximum acceptable time to send the message, in seconds. It represents the total emission time of the message but excludes propagation time and processing at the other end.
- p_s^{call} is the call blocking probability.

We deduce $R_s^{\text{ci}} = l_s / \Delta T_s^{\text{TTS}}$, and $p_s^{\text{at}} = \lambda_s^{\text{abg}}$.

A.3 Bulk

Bulk internet traffic differs from transactions, as acceptable delays are higher and sometimes undefined. Commonly found SLA requirements for this service type are:

- R_s^{mi} is the maximum burst rate offered to each subscriber of SP s.

- ρ^{OB} is the contention/overbooking ratio.

We deduce $R_s^{\mathrm{ci}} = R_s^{\mathrm{mi}}/\rho^{\mathrm{OB}}$. If p_s^{at} is not explicitly specified, a default value of $p_s^{\mathrm{at}} = 1$ should be assumed.

Appendix B

Computation of mode probability

This appendix focuses on computing $P\left(\bar{k}_n^{\mathrm{ci}}\left((A_n, A_{d_n})\right) < k\right)$ for a given value of k.

B.1 Monotonicity of $\bar{k}_n^{\mathrm{ci}}$

Let us first investigate the monotonic behavior of $\bar{k}_n^{\mathrm{ci}}$ with respect to a_n and a_{d_n}.

For any value of $\mathbf{a}_{n,t}^{\mathrm{tot}}$ such that $k \leq {}^{\uparrow}k_n^{\mathrm{ci}}\left(\mathbf{a}_{n,t}^{\mathrm{tot}}\right)$ (necessary condition for $\bar{k}_n^{\mathrm{ci}}\left(\mathbf{a}_{n,t}^{\mathrm{tot}}\right) = k$), the bandwidth demand $b_{n,q}^{\mathrm{D}}\left(\mathbf{a}_{n,t}^{\mathrm{tot}}, k\right)$ is unchanged. However, the same is not necessarily true for the power demand $P_{n,q}^{\mathrm{D}}\left(\mathbf{a}_{n,t}^{\mathrm{tot}}, k\right)$. Let us remember its expression:

$$P_{n,q}^{\mathrm{D}}\left(\mathbf{a}_{n,t}^{\mathrm{tot}}, k\right) = \frac{b_{n,q}^{\mathrm{D}}\left(\mathbf{a}_{n,t}^{\mathrm{tot}}, k\right) \cdot \theta\left(k\right)}{\gamma_{0,n}\left(\mathbf{a}_{n,t}^{\mathrm{tot}}\right)} \cdot \frac{\mathrm{IBO}_n\left(a_{n,t}\right)}{\mathrm{IBO}_{v_n}^{\mathrm{tot}}}. \tag{B.1}$$

Assuming $\mathbf{a}_{n,t}^{\mathrm{tot}}$ such that $k \leq {}^{\uparrow}k_n^{\mathrm{ci}}\left(\mathbf{a}_{n,t}^{\mathrm{tot}}\right)$, the only terms affected by rain are the CINR_0 $\gamma_{0,n}\left(\mathbf{a}_{n,t}^{\mathrm{tot}}\right)$ and the $\mathrm{IBO}_n\left(a_{n,t}\right)$. Given our link budget model, both functions are decreasing with respect to a_n, and $\gamma_{0,n}\left(\mathbf{a}_{n,t}^{\mathrm{tot}}\right)$ is also decreasing with respect to a_{d_n}. Thus, $P_{n,q}^{\mathrm{D}}\left(\mathbf{a}_{n,t}^{\mathrm{tot}}, k\right)$ is increasing when a_n is fixed and a_{d_n} increases.

Let us define $\mathbf{a}_{n,1}^{\mathrm{tot}}$ and $\mathbf{a}_{n,2}^{\mathrm{tot}}$ such that $a_{n,1} = a_{n,2}$ and $a_{d_n,1} \leq a_{d_n,2}$. If ${}^{\uparrow}k_n^{\mathrm{ci}}\left(\mathbf{a}_{n,2}^{\mathrm{tot}}\right) \leq {}^{\downarrow}k_{s_n}^{\mathrm{ci}}$, then $\bar{k}_n^{\mathrm{ci}}\left(\mathbf{a}_{n,2}^{\mathrm{tot}}\right) \leq \bar{k}_n^{\mathrm{ci}}\left(\mathbf{a}_{n,1}^{\mathrm{tot}}\right)$. If ${}^{\uparrow}k_n^{\mathrm{ci}}\left(\mathbf{a}_{n,2}^{\mathrm{tot}}\right) > {}^{\downarrow}k_{s_n}^{\mathrm{ci}}$, then ${}^{\uparrow}k_n^{\mathrm{ci}}\left(\mathbf{a}_{n,1}^{\mathrm{tot}}\right) > {}^{\downarrow}k_{s_n}^{\mathrm{ci}}$ and $\bar{k}_n^{\mathrm{ci}}\left(\mathbf{a}_{n,1}^{\mathrm{tot}}\right)$ satisfies by definition:

$$\underset{k \in K_n^{ci}\left(a_{n,1}^{tot}\right)}{\arg\min} \max\left(\sum_{q=1}^{Q} b_{n,q}^{\mathrm{D}}\left(\mathbf{a}_{n,1}^{\mathrm{tot}}, k\right), \sum_{q=1}^{Q} b_{n,q}^{\mathrm{pe,D}}\left(\mathbf{a}_{n,1}^{\mathrm{tot}}, k\right)\right) \tag{B.2}$$

For all $k' \in \mathcal{K}_n^{\mathrm{ci}}\left(\mathbf{a}_{n,1}^{\mathrm{tot}}\right)$ such that $k' > \bar{k}_n^{\mathrm{ci}}\left(\mathbf{a}_{n,1}^{\mathrm{tot}}\right)$, we have:

$$\max\left(\sum_{q=1}^{Q} b_{n,q}^{\mathrm{D}}\left(\mathbf{a}_{n,1}^{\mathrm{tot}}, k'\right), \sum_{q=1}^{Q} b_{n,q}^{\mathrm{pe,D}}\left(\mathbf{a}_{n,1}^{\mathrm{tot}}, k'\right)\right) > \max\left(\sum_{q=1}^{Q} b_{n,q}^{\mathrm{D}}\left(\mathbf{a}_{n,1}^{\mathrm{tot}}, \bar{k}_n^{\mathrm{ci}}\left(\mathbf{a}_{n,1}^{\mathrm{tot}}\right)\right), \sum_{q=1}^{Q} b_{n,q}^{\mathrm{pe,D}}\left(\mathbf{a}_{n,1}^{\mathrm{tot}}, \bar{k}_n^{\mathrm{ci}}\left(\mathbf{a}_{n,1}^{\mathrm{tot}}\right)\right)\right) . \quad \text{(B.3)}$$

However, we made the hypothesis in Section 5.1.4 that $\eta^{\mathrm{spe}}\left(k'\right) \leq \eta^{\mathrm{spe}}\left(\bar{k}_n^{\mathrm{ci}}\left(\mathbf{a}_{n,1}^{\mathrm{tot}}\right)\right)$, thus $b_{n,q}^{\mathrm{D}}\left(\mathbf{a}_{n,1}^{\mathrm{tot}}, k'\right) \leq b_{n,q}^{\mathrm{D}}\left(\mathbf{a}_{n,1}^{\mathrm{tot}}, \bar{k}_n^{\mathrm{ci}}\left(\mathbf{a}_{n,1}^{\mathrm{tot}}\right)\right)$ for all q. Therefore we have:

$$\sum_{q=1}^{Q} b_{n,q}^{\mathrm{pe,D}}\left(\mathbf{a}_{n,1}^{\mathrm{tot}}, k'\right) > \max\left(\sum_{q=1}^{Q} b_{n,q}^{\mathrm{D}}\left(\mathbf{a}_{n,1}^{\mathrm{tot}}, \bar{k}_n^{\mathrm{ci}}\left(\mathbf{a}_{n,1}^{\mathrm{tot}}\right)\right), \sum_{q=1}^{Q} b_{n,q}^{\mathrm{pe,D}}\left(\mathbf{a}_{n,1}^{\mathrm{tot}}, \bar{k}_n^{\mathrm{ci}}\left(\mathbf{a}_{n,1}^{\mathrm{tot}}\right)\right)\right) . \quad \text{(B.4)}$$

For any $k \in \mathcal{K}_n^{\mathrm{ci}}\left(\mathbf{a}_{n,2}^{\mathrm{tot}}\right) \subseteq \mathcal{K}_n^{\mathrm{ci}}\left(\mathbf{a}_{n,1}^{\mathrm{tot}}\right)$, let us remark the following:

$$b_{n,q}^{\mathrm{pe,D}}\left(\mathbf{a}_{n,2}^{\mathrm{tot}}, k\right) = \frac{\gamma_{0,n}\left(\mathbf{a}_{n,1}^{\mathrm{tot}}\right)}{\gamma_{0,n}\left(\mathbf{a}_{n,2}^{\mathrm{tot}}\right)} \cdot b_{n,q}^{\mathrm{pe,D}}\left(\mathbf{a}_{n,1}^{\mathrm{tot}}, k\right) . \quad \text{(B.5)}$$

Thus, we have:

$$\frac{\gamma_{0,n}\left(\mathbf{a}_{n,1}^{\mathrm{tot}}\right)}{\gamma_{0,n}\left(\mathbf{a}_{n,2}^{\mathrm{tot}}\right)} \cdot \sum_{q=1}^{Q} b_{n,q}^{\mathrm{pe,D}}\left(\mathbf{a}_{n,1}^{\mathrm{tot}}, k'\right) > \max\left(\sum_{q=1}^{Q} b_{n,q}^{\mathrm{D}}\left(\mathbf{a}_{n,1}^{\mathrm{tot}}, \bar{k}_n^{\mathrm{ci}}\left(\mathbf{a}_{n,1}^{\mathrm{tot}}\right)\right), \frac{\gamma_{0,n}\left(\mathbf{a}_{n,1}^{\mathrm{tot}}\right)}{\gamma_{0,n}\left(\mathbf{a}_{n,2}^{\mathrm{tot}}\right)} \cdot \sum_{q=1}^{Q} b_{n,q}^{\mathrm{pe,D}}\left(\mathbf{a}_{n,1}^{\mathrm{tot}}, \bar{k}_n^{\mathrm{ci}}\left(\mathbf{a}_{n,1}^{\mathrm{tot}}\right)\right)\right) , \quad \text{(B.6)}$$

which, if $k' \in \mathcal{K}_n^{\mathrm{ci}}\left(\mathbf{a}_{n,2}^{\mathrm{tot}}\right)$, implies the following:

$$\implies \sum_{q=1}^{Q} b_{n,q}^{\mathrm{pe,D}}\left(\mathbf{a}_{n,2}^{\mathrm{tot}}, k'\right) > \max\left(\sum_{q=1}^{Q} b_{n,q}^{\mathrm{D}}\left(\mathbf{a}_{n,2}^{\mathrm{tot}}, \bar{k}_n^{\mathrm{ci}}\left(\mathbf{a}_{n,2}^{\mathrm{tot}}\right)\right), \sum_{q=1}^{Q} b_{n,q}^{\mathrm{pe,D}}\left(\mathbf{a}_{n,2}^{\mathrm{tot}}, \bar{k}_n^{\mathrm{ci}}\left(\mathbf{a}_{n,2}^{\mathrm{tot}}\right)\right)\right) \quad \text{(B.7a)}$$

$$\implies k' > \bar{k}_n^{\mathrm{ci}}\left(\mathbf{a}_{n,2}^{\mathrm{tot}}\right) \quad \text{(B.7b)}$$

$$\implies \bar{k}_n^{\mathrm{ci}}\left(\mathbf{a}_{n,1}^{\mathrm{tot}}\right) \geq \bar{k}_n^{\mathrm{ci}}\left(\mathbf{a}_{n,2}^{\mathrm{tot}}\right) . \quad \text{(B.7c)}$$

In all cases, $\bar{k}_n^{\mathrm{ci}}\left(\mathbf{a}_{n,t}^{\mathrm{tot}}\right)$ cannot increase when a_n is fixed and a_{d_n} increases. However, it is not

necessarily true when a_n increases and a_{d_n} is fixed.

B.2 Detailed procedure

We will now exploit the monotonic property of $\bar{k}_n^{\mathrm{ci}}\left(\mathbf{a}_{n,t}^{\mathrm{tot}}\right)$ to solve our problem.

The first step is to find the lowest uplink attenuation $a_n^{\max}$ such that ${}^{\uparrow}k_n^{\mathrm{ci}}\left(\left(a_n^{\max}, 1\right)\right) < k$. The value of $a_n^{\max}$ is quickly found by using a bisection algorithm, such as presented in Algorithm 3.

Algorithm 3 Find maximum uplink attenuation

Require: k
Require: a_{d_n}
Require: ${}^{\uparrow}k_n^{\mathrm{ci}}$ ▷ The function ${}^{\uparrow}k_n^{\mathrm{ci}}$ is an input.
Require: precision ▷ Desired output relative precision.
  $a_n^{\mathrm{lb}} \leftarrow 1$
  $a_n^{\mathrm{ub}} \leftarrow 1$
  if ${}^{\uparrow}k_n^{\mathrm{ci}}\left(\left(a_n^{\mathrm{lb}}, a_{d_n}\right)\right) \geq k$ **then**
    $a_n^{\mathrm{ub}} \leftarrow 10^{10}$ ▷ Arbitrarily high value.
    while $|a_n^{\mathrm{ub}}/a_n^{\mathrm{lb}}| \geq 1 + \text{precision}$ **do**
      $a_n^{\mathrm{mid}} \leftarrow \left(a_n^{\mathrm{ub}} + a^{\mathrm{lb}}\right)/2$
      if ${}^{\uparrow}k_n^{\mathrm{ci}}\left(\left(a_n^{\mathrm{mid}}, a_{d_n}\right)\right) \geq k$ **then**
        $a_n^{\mathrm{lb}} \leftarrow a_n^{\mathrm{mid}}$
      else
        $a_n^{\mathrm{ub}} \leftarrow a_n^{\mathrm{mid}}$
      end if
    end while
  end if
  $a_n \leftarrow a_n^{\mathrm{ub}}$

We therefore know that for any $a_n \geq a_n^{\max}$ and $a_{d_n} \geq 1$, $k > {}^{\uparrow}k_n^{\mathrm{ci}}\left(\left(a_n, a_{d_n}\right)\right) \geq \bar{k}_n^{\mathrm{ci}}\left(\left(a_n, a_{d_n}\right)\right)$. Thus, the event $\bar{k}_n^{\mathrm{ci}}\left(\left(A_n, A_{d_n}\right)\right) \geq k$ is only possible if $A_n \in [1, a_n^{\max}]$. Now, let us divide the segment $[1, a_n^{\max}]$ into $I \geq 2$ values $a_{n,i}$, ordered increasingly, with $a_{n,1} = 1$ and $a_{n,I} = a_n^{\max}$. We know that for each $a_{n,i}$ value, $\bar{k}_n^{\mathrm{ci}}\left(\left(a_{n,i}, a_{d_n}\right)\right)$ is non-increasing when a_{d_n} increases. Thus, it exists the lowest downlink attenuation $a_{d_n,i}$ such that $\bar{k}_n^{\mathrm{ci}}\left(\left(a_{n,i}, a_{d_n,i}\right)\right) < k$. The value $a_{d_n,i}$ can be obtained by using Algorithm 3 and swapping the roles of uplink and downlink attenuations, and ${}^{\uparrow}k_n^{\mathrm{ci}}$ with $\bar{k}_n^{\mathrm{ci}}$.

We can then compute a numerical estimate of $P\left(\bar{k}_n^{\mathrm{ci}}\left(\left(A_n, A_{d_n}\right)\right) \geq k\right)$ with the following

sum of probabilities of disjoint events [76]:

$$P\left(\bar{k}_n^{\mathrm{ci}}\left((A_n, A_{d_n})\right) \geq k\right) \approx \sum_{i=2}^{I} P\left(a_{n,i-1} \leq A_n < a_{n,i}, 1 \leq A_{d_n} < a_{d_n,i}\right) \tag{B.8a}$$

$$\approx \sum_{i=2}^{I} P\left(a_{n,i-1} \leq A_n < a_{n,i}, A_{d_n} < a_{d_n,i}\right) . \tag{B.8b}$$

Figure B.1 illustrates the approximation for $I = 5$. For a given index $i \geq 2$, we decompose the terms inside the sum:

$$P\left(a_{n,i-1} \leq A_n < a_{n,i}, A_{d_n} < a_{d_n,i}\right) = P\left(A_n < a_{n,i}, A_{d_n} < a_{d_n,i}\right) - P\left(A_n < a_{n,i-1}, A_{d_n} < a_{d_n,i}\right) . \tag{B.9}$$

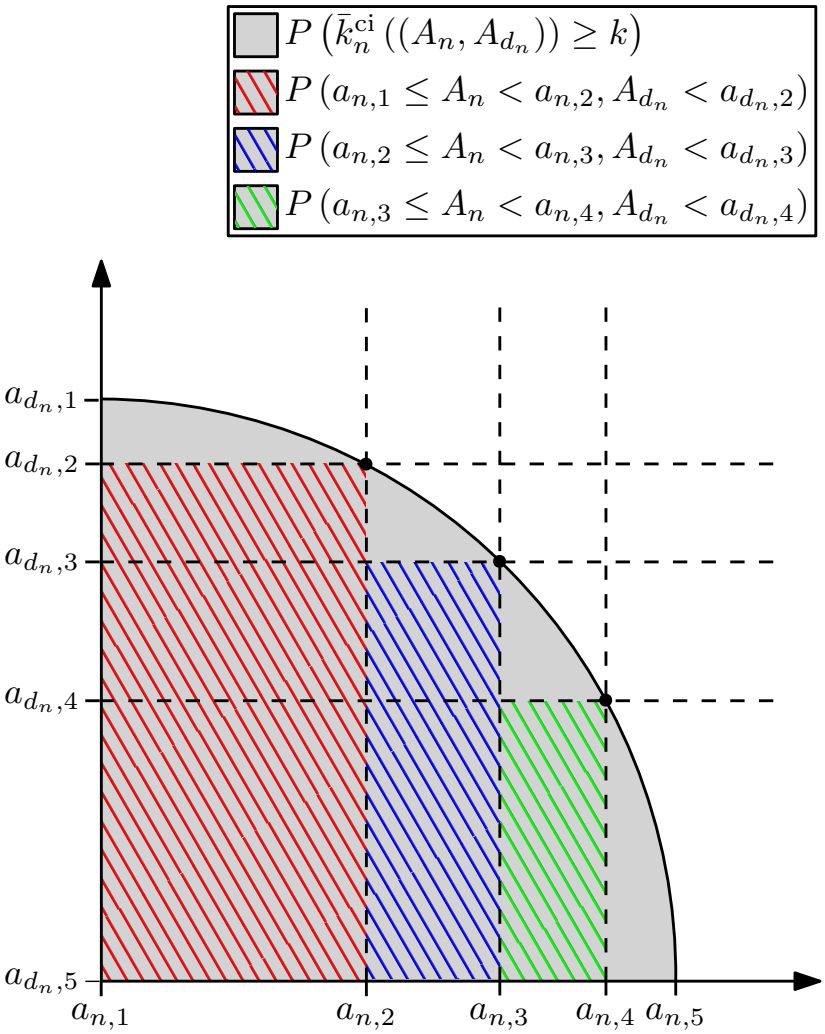

Figure B.1: Illustration of the joint probability space

Finally, let us remark that $P\left(A_n < a_n, A_{d_n} < a_{d_n}\right)$, for any value of a_n and a_{d_n}, is also expressed as:

$$P\left(A_n < a_n, A_{d_n} < a_{d_n}\right) = 1 - P\left(A_n \geq a_n\right) - P\left(A_{d_n} \geq a_{d_n}\right) + P\left(A_n \geq a_n, A_{d_n} \geq a_{d_n}\right) . \tag{B.10}$$

The probabilities $P\left(A_n \geq a_n\right)$ and $P\left(A_{d_n} \geq a_{d_n}\right)$ are obtainable given the distribution of A_n and A_{d_n}. The joint probability $P\left(A_n \geq a_n, A_{d_n} \geq a_{d_n}\right)$ requires a joint attenuation model. The ITU proposes a bivariate lognormal model, assuming A_n and A_{d_n} are lognormal, in [30, Section 2.2.4]. The recommendation also provides a method to approximate the distribution obtained with the ITU model with a lognormal model.

B.3 Summarized procedure

The process to compute $P\left(\bar{k}_n^{\text{ci}}\left((A_n, A_{d_n})\right) < k\right)$ can be summarized as follows:

1. Compute the lowest uplink attenuation $a_n^{\max}$ such that ${}^{\uparrow}k_n^{\text{ci}}\left((a_n^{\max}, 1)\right) < k$ with Algorithm 3.
2. Take $I > 2$ points $a_{n,i}$ from the segment $[1, a_n^{\max}]$, ordered increasingly, with $a_{n,1} = 1$ and $a_{n,J} = a_n^{\max}$.
3. For each $i \in \{2, \ldots, I\}$, do the following:
   (a) Compute the lowest downlink attenuation $a_{d_n,i}$ such that $\bar{k}_n^{\text{ci}}\left((a_{n,i}, a_{d_n,i})\right) < k$ (adapt Algorithm 3).
   (b) Compute $P\left(A_n < a_{n,i}, A_{d_n} < a_{d_n,i}\right)$, e.g. with ITU models.
   (c) Compute $P\left(A_n < a_{n,i-1}, A_{d_n} < a_{d_n,i}\right)$ in the same way.
   (d) Subtract 3.c) to 3.b) to get $P\left(a_{n,i-1} \leq A_n < a_{n,i}, A_{d_n} < a_{d_n,i}\right)$.
4. Sum all $P\left(a_{n,i-1} \leq A_n < a_{n,i}, A_{d_n} < a_{d_n,i}\right)$ to estimate $P\left(\bar{k}_n^{\text{ci}}\left((A_n, A_{d_n})\right) \geq k\right)$.
5. Compute $1 - P\left(\bar{k}_n^{\text{ci}}\left((A_n, A_{d_n})\right) \geq k\right)$ to get $P\left(\bar{k}_n^{\text{ci}}\left((A_n, A_{d_n})\right) < k\right)$.

Bibliography

[1] S. Varrette, P. Bouvry, H. Cartiaux, and F. Georgatos, "Management of an academic HPC cluster: The UL experience," in *Proc. of the 2014 Intl. Conf. on High Performance Computing & Simulation (HPCS 2014)*, Bologna, Italy: IEEE, Jul. 2014, pp. 959–967. DOI: 10.1109/HPCSim.2014.6903792.

[2] "The state of broadband: Accelerating broadband for new realities," International Telecommunication Union, United Nations Educational, Scientific, and Cultural Organization, Geneva, CH, ISBN: 9789261367510, Sep. 2022. [Online]. Available: https://unesdoc.unesco.org/ark:/48223/pf0000383330 (visited on 11/16/2023).

[3] "Measuring digital development: Facts and figures," International Telecommunication Union, Geneva, CH, ISBN: 9789261370115, 2022. [Online]. Available: https://www.itu.int/hub/publication/d-ind-ict_mdd-2022/ (visited on 11/16/2023).

[4] "Regulation of global broadband satellite communications," International Telecommunication Union, Geneva, CH, Thematic report, Apr. 2012. [Online]. Available: http://handle.itu.int/11.1002/pub/807b38cc-en (visited on 11/24/2023).

[5] "Consumer and enterprise broadband via satellite, 22nd edition," Northern Sky Research, Industry analysis, Sep. 2023. [Online]. Available: https://www.nsr.com/?research=consumer-and-enterprise-broadband-via-satellite-22nd-edition (visited on 11/16/2023).

[6] "Facing the challenges of broadband deployment in rural and remote areas," European Commission, Brochure, Apr. 2020. [Online]. Available: https://digital-strategy.ec.europa.eu/en/library/broadband-handbook-facing-challenges-broadband-deployment-rural-and-remote-areas (visited on 11/16/2023).

[7] "State of the satellite industry report," Satellite industry association, Industry analysis, Jun. 2022. [Online]. Available: https://sia.org/news-resources/state-of-the-satellite-industry-report/ (visited on 11/16/2023).

[8] G. Maral and M. Bousquet, *Satellite communications systems: systems, techniques and technology*, eng, Sixth edition. Hoboken, New Jersey: Wiley, 2020, ISBN: 9781119382072.

[9] B. R. Elbert, *Satellite Communication Applications Handbook.* eng, 1st ed. Norwood: Artech House, 2003, ISBN: 9781580538084.

[10] X. Vuong, F. Zimmermann, and T. Shimabukuro, "Performance analysis of Ku-band VSAT networks," *IEEE Communications Magazine*, vol. 26, no. 5, pp. 25–33, 1988. DOI: 10.1109/35.450.

[11] D. Hogg and T.-S. Chu, "The role of rain in satellite communications," *Proceedings of the IEEE*, vol. 63, no. 9, pp. 1308–1331, 1975. DOI: 10.1109/PROC.1975.9940.

[12] A. D. Panagopoulos, P.-D. M. Arapoglou, and P. G. Cottis, "Satellite communications at Ku, Ka, and V bands: Propagation impairments and mitigation techniques," *IEEE Communications Surveys & Tutorials*, vol. 6, no. 3, pp. 2–14, 2004. DOI: 10.1109/COMST.2004.5342290.

[13] H. Bischl, H. Brandt, T. de Cola, R. De Gaudenzi, E. Eberlein, N. Girault, E. Alberty, S. Lipp, R. Rinaldo, B. Rislow, J. A. Skard, J. Tousch, and G. Ulbricht, "Adaptive coding and modulation for satellite broadband networks: From theory to practice," *International Journal of Satellite Communications and Networking*, vol. 28, no. 2, pp. 59–111, 2010. DOI: 10.1002/sat.932.

[14] J. N. Pelton, S. Madry, and S. Camacho-Lara, *Handbook of Satellite Applications*, eng. New York, NY: Springer New York, 2013, ISBN: 9781441976710. DOI: 10.1007/978-1-4419-7671-0.

[15] H. Al-Hraishawi, H. Chougrani, S. Kisseleff, E. Lagunas, and S. Chatzinotas, "A survey on nongeostationary satellite systems: The communication perspective," *IEEE Communications Surveys & Tutorials*, vol. 25, no. 1, pp. 101–132, 2023. DOI: 10.1109/COMST.2022.3197695.

[16] A. Mallet, A. Anakabe, J. Sombrin, R. Rodriguez, and F. Coromina, "Multi-port amplifier operation for Ka-band space telecommunication applications," in *2006 IEEE MTT-S International Microwave Symposium Digest*, 2006, pp. 1518–1521. DOI: 10.1109/MWSYM.2006.249601.

[17] A. Le Pera, F. Forni, M. Grossi, M. Lucente, V. Palma, T. Rossi, and M. Ruggieri, "Digital transparent processor for satellite telecommunication services," in *2007 IEEE Aerospace Conference*, 2007, pp. 1–9. DOI: 10.1109/AERO.2007.352932.

[18] P. L. Sastri L. Kota Kaveh Pahlavan, *Broadband Satellite Communications for Internet Access*, eng, 1st ed. New York, NY: Springer New York, NY, Nov. 2003, ISBN: 978-1-4020-7659-6. DOI: 10.1007/978-1-4419-8895-9.

[19] "Satellite Earth stations and systems (SES); broadband satellite multimedia; part 1: Survey on standardization objectives," European Telecommunication Standard Institute, Sophia Antipolis, FR, Technical report ETSI TR 101 374-1 V1.2.1, Oct. 1998.

[20] "Satellite Earth stations and systems (SES); broadband satellite multimedia; part 2: Scenario for standardization," European Telecommunication Standard Institute, Sophia Antipolis, FR, Technical report ETSI TR 101 374-2 V1.1.1, Mar. 2000.

[21] "Satellite Earth stations and systems (SES); broadband satellite multimedia (BSM); services and architectures," European Telecommunication Standard Institute, Sophia Antipolis, FR, Technical report ETSI TR 101 984 V1.2.1, Dec. 2007.

[22] "Framework of a service level agreement," International Telecommunication Union, Geneva, CH, Standard ITU-T E.860, Jun. 20002.

[23] "General aspects of quality of service and network performance in digital networks, including ISDNs," International Telecommunication Union, Geneva, CH, Standard ITU-T I.350, Mar. 1993.

[24] "User group; quality of telecom services; part 2: User related indicators on a service specific basis," European Telecommunication Standard Institute, Sophia Antipolis, FR, Guide ETSI EG 202 009-2 V1.3.1, Dec. 2014.

[25] "Satellite Earth stations and systems (SES); broadband satellite multimedia (BSM); performance parameters," European Telecommunication Standard Institute, Sophia Antipolis, FR, Technical specification ETSI TS 102 673 V1.1.1, Nov. 2009.

[26] M. Guerster, "Revenue management and resource allocation for communication satellite operators," Ph.D. dissertation, Massachusetts Institute of Technology, Sep. 2020.

[27] E. Cianca, T. Rossi, A. Yahalom, Y. Pinhasi, J. Farserotu, and C. Sacchi, "EHF for satellite communications: The new broadband frontier," *Proceedings of the IEEE*, vol. 99, no. 11, pp. 1858–1881, Nov. 2011. DOI: 10.1109/JPROC.2011.2158765.

[28] C. Sacchi, T. Rossi, M. Murroni, and M. Ruggieri, "Extremely high frequency (EHF) bands for future broadcast satellite services: Opportunities and challenges," *IEEE Transactions on Broadcasting*, vol. 65, no. 3, pp. 609–626, Sep. 2019. DOI: 10.1109/TBC.2019.2892655.

[29] M. A. Samad, F. D. Diba, and D.-Y. Choi, "A survey of rain fade models for Earth–space telecommunication links—taxonomy, methods, and comparative study," *Remote Sensing*, vol. 13, no. 10, 2021, ISSN: 2072-4292. DOI: 10.3390/rs13101965.

[30] "Propagation data and prediction methods required for the design of Earth-space telecommunication systems," International Telecommunication Union, Geneva, CH, Recommendation ITU-R P.618-13, Dec. 2017.

[31] A. Petrolino, G. Codispoti, C. Riva, F. Massaro, M. Sigler, G. Bacci, L. Luini, G. Parca, and A. Vaccaro, "Using the Q/V-band Aldo Paraboni payload to validate future satellite systems: Test campaign and preliminary results of the QV-LIFT project," in *2018 2nd URSI Atlantic Radio Science Meeting (AT-RASC)*, 2018, pp. 1–3. DOI: 10.23919/URSI-AT-RASC.2018.8471633.

[32] "Digital video broadcasting (DVB); second generation DVB interactive satellite system (DVB-RCS2); part 2: Lower layers for satellite standard," European Telecommunication Standard Institute, Sophia Antipolis, FR, European standard ETSI EN 301 545-2 V1.2.1, Apr. 2014.

[33] E. Noussi, "A study of fade mitigation and resource management of satellite networks in rain condition," Ph.D. dissertation, University of Portsmouth, Jun. 2008.

[34] "Digital video broadcasting (DVB); second generation framing structure, channel coding and modulation systems for broadcasting, interactive services, news gathering and other broadband satellite applications," European Telecommunication Standard Institute, Sophia Antipolis, FR, European standard ETSI EN 302 307 V1.1.2, Jun. 2006.

[35] A. Aroumont, J. Radzik, M. Bousquet, and L. Castanet, "DVB-RCS return link radio resource management for broadband satellite systems using fade mitigation techniques at Ka band," in *2008 IEEE International Workshop on Satellite and Space Communications*, Nov. 2008, pp. 221–225. DOI: 10.1109/IWSSC.2008.4656792.

[36] G. Giambene, Ed., *Resource Management in Satellite Networks: Optimization and Cross-Layer Design*, eng. Boston, MA: Springer US, 2007, ISBN: 9780387539911.

[37] A. Aroumont, "Etude de techniques de gestion adaptative des ressources satellitaires pour les systèmes de télécommunication par satellite, tenant compte du canal de propagation et des flux de trafic," Ph.D. dissertation, Institut Supérieur de l'Aéronautique et de l'Espace, Jul. 2010.

[38] D. Serrano-velarde, E. Lance, H. Fenech, and G. E. Rodriguez-guisantes, "Novel dimensioning method for high-throughput satellites: Forward link," *IEEE Transactions on Aerospace and Electronic Systems*, vol. 50, no. 3, pp. 2146–2163, Jul. 2014. DOI: 10.1109/TAES.2014.120429.

[39] F. G. Ortiz-Gomez, R. Martínez, M. A. Salas-Natera, A. Cornejo, and S. Landeros-Ayala, "Forward link optimization for the design of VHTS satellite networks," *Electronics*, vol. 9, no. 3, 2020, ISSN: 2079-9292. DOI: 10.3390/electronics9030473.

[40] F. G. Ortiz-Gomez, M. A. Salas-Natera, R. Martínez, and S. Landeros-Ayala, "Optimization in VHTS satellite system design with irregular beam coverage for non-uniform traffic distribution," *Remote Sensing*, vol. 13, no. 13, 2021, ISSN: 2072-4292. DOI: 10.3390/rs13132642.

[41] A. Paraboni and F. Barbaliscia, "Multiple site attenuation prediction models based on the rainfall structures (meso or synotic-scales) for advanced TLC or broadcasting systems," in *Proc. Of XXVIIth General Assembly of the International Union of Radio Science*, Maastricht, Netherlands, 2002, pp. 1–4.

[42] J. Arnau, D. Christopoulos, S. Chatzinotas, C. Mosquera, and B. Ottersten, "Performance of the multibeam satellite return link with correlated rain attenuation," *IEEE Transactions on Wireless Communications*, vol. 13, no. 11, pp. 6286–6299, Nov. 2014. DOI: 10.1109/TWC.2014.2329682.

[43] N. Jeannin, L. Féral, H. Sauvageot, L. Castanet, and F. Lacoste, "A large-scale space-time stochastic simulation tool of rain attenuation for the design and optimization of adaptive satellite communication systems operating between 10 and 50 GHz," *International Journal of Antennas and Propagation*, vol. 2012, May 2012. DOI: 10.1155/2012/749829.

[44] K. Paulson, L. Luini, N. Jeannin, B. Gremont, and R. Watson, "A review of channel simulators for heterogeneous microwave networks," *IEEE Antennas and Propagation Magazine*, vol. 55, pp. 118–127, Oct. 2013. DOI: 10.1109/MAP.2013.6735480.

[45] C. Capsoni, L. Castanet, P. Gabellini, G. Gallinaro, F. Lacoste, N. Jeannin, L. Luini, A. Martellucci, and A. Paraboni, "Use of space-time channel models and data for design and control of adaptive SatCom systems," in *Proceedings of the 5th European Conference on Antennas and Propagation, EUCAP 2011*, May 2011, pp. 3389–3392.

[46] L. Luini, L. Emiliani, and C. Capsoni, "Planning of advanced SatCom systems using ACM techniques: The impact of rain fade," in *Proceedings of the 5th European Conference on Antennas and Propagation (EUCAP)*, Apr. 2011, pp. 3965–3969.

[47] C. Morel, P.-D. Arapoglou, M. Angelone, and A. Ginesi, "Link adaptation strategies for next generation satellite video broadcasting: A system approach," *IEEE Transactions on Broadcasting*, vol. 61, no. 4, pp. 603–614, Dec. 2015. DOI: 10.1109/TBC.2015.2470355.

[48] A. Kyrgiazos, B. Evans, P. Thompson, P. T. Mathiopoulos, and S. Papaharalabos, "A terabit/second satellite system for European broadband access: A feasibility study," eng, *International journal of satellite communications and networking*, vol. 32, no. 2, pp. 63–92, 2014, ISSN: 1542-0973. DOI: 10.1002/sat.1067.

[49] X. Alberti, J. M. Cebrian, A. Del Bianco, Z. Katona, J. Lei, M. A. Vazquez-Castro, A. Zanus, L. Gilbert, and N. Alagha, "System capacity optimization in time and frequency for multibeam multi-media satellite systems," in *2010 5th Advanced Satellite Multimedia Systems Conference and the 11th Signal Processing for Space Communications Workshop*, 2010, pp. 226–233. DOI: 10.1109/ASMS-SPSC.2010.5586902.

[50] B. Gremont and M. Filip, "Spatio-temporal rain attenuation model for application to fade mitigation techniques," eng, *IEEE transactions on antennas and propagation*, vol. 52, no. 5, pp. 1245–1256, 2004, ISSN: 0018-926X. DOI: 10.1109/TAP.2004.827501.

[51] V. Pranjic, B. S. Mysore, N. Mazzali, and L. Emiliani, "Return link optimized resource allocation for satellite communications in the Ku/Ka-band," in *Proceedings on the 22nd Ka and Broadband Communications Conference and the 34th AIAA International Communications Satellite Systems Conference (ICSSC)*, Oct. 2016.

[52] "Maximum permissible levels of off-axis e.i.r.p. density from Earth stations in geostationary-satellite orbit networks operating in the fixed-satellite service transmitting in the 6 GHz, 13 GHz, 14 GHz and 30 GHz frequency bands," International Telecommunication Union, Geneva, CH, Recommendation ITU-R S.524-9, Apr. 2006.

[53] M. Padberg, *Linear Optimization and Extensions*, eng, 2nd ed. Berlin, Heidelberg: Springer Berlin, Heidelberg, Jun. 1999, ISBN: 9783540658337. DOI: 10.1007/978-3-662-12273-0.

[54] L. Wolsey, *Integer Programming*, 2nd ed. Wiley, Sep. 2020, ISBN: 9781119606536. DOI: 10.1002/9781119606475.

[55] M. Jünger, G. Reinelt, and S. Thienel, "Practical problem solving with cutting plane algorithms in combinatorial optimization," in *Combinatorial Optimization*, vol. 20, American Mathematical Society, 1993, ISBN: 978-1-4704-3978-1. DOI: 10.1090/dimacs/020.

[56] M. Smolnikar, A. Aroumont, M. Mohorcic, T. Javornik, and L. Castanet, "On transmission modes subset selection in DVB-S2/RCS satellite systems," in *2008 IEEE International Workshop on Satellite and Space Communications*, 2008, pp. 263–267. DOI: 10.1109/IWSSC.2008.4656808.

[57] H. Al-Hraishawi, E. Lagunas, and S. Chatzinotas, "Traffic simulator for multibeam satellite communication systems," in *2020 10th Advanced Satellite Multimedia Systems Conference and the 16th Signal Processing for Space Communications Workshop (ASMS/SPSC)*, 2020, pp. 1–8. DOI: 10.1109/ASMS/SPSC48805.2020.9268831.

[58] R. Booton, "Improving satellite bandwidth utilization by applying combinatorial optimization to the integrated waveform (DAMA UHF SatCom)," in *MILCOM 2008 - 2008 IEEE Military Communications Conference*, 2008, pp. 1–7. DOI: 10.1109/MILCOM.2008.4753481.

[59] S. J. Maher, T. Fischer, T. Gally, G. Gamrath, A. Gleixner, R. L. Gottwald, G. Hendel, T. Koch, M. E. Lübbecke, M. Miltenberger, B. Müller, M. E. Pfetsch, C. Puchert, D. Rehfeldt, S. Schenker, R. Schwarz, F. Serrano, Y. Shinano, D. Weninger, J. T. Witt, and J. Witzig, "The SCIP Optimization Suite 4.0," Zuse Institute Berlin, ZIB-Report 17-12, Mar. 2017. [Online]. Available: http://nbn-resolving.de/urn:nbn:de:0297-zib-62170 (visited on 11/27/2023).

[60] J. Forrest, T. Ralphs, S. Vigerske, LouHafer, B. Kristjansson, jpfasano, EdwinStraver, M. Lubin, H. G. Santos, rlougee, and M. Saltzman, "Coin-or/CBC: Version 2.9.8," version releases/2.9.8, 2018. DOI: 10.5281/zenodo.1317566.

[61] A. W. Marshall, *Inequalities: Theory of Majorization and Its Applications*, eng, 2nd ed., ser. Springer Series in Statistics. 2011, ISBN: 9780387682761.

[62] O. Burdakov, C. Kanzow, and A. Schwartz, "Mathematical programs with cardinality constraints: Reformulation by complementarity-type conditions and a regularization method," *SIAM Journal on Optimization*, vol. 26, Oct. 2015. DOI: 10.1137/140978077.

[63] J. L. Gearhart, K. L. Adair, J. D. Durfee, K. A. Jones, N. Martin, and R. J. Detry, "Comparison of open-source linear programming solvers," Sandia National Laboratories (SNL-NM), Albuquerque, NM (United States), Tech. Rep. SAND2013-8847, Oct. 2013. DOI: 10.2172/1104761.

[64] "Characteristics of precipitation for propagation modelling," International Telecommunication Union, Geneva, CH, Recommendation ITU-R P.837-7, Jun. 2017.

[65] L. Luini and C. Capsoni, "MultiEXCELL: A new rain field model for propagation applications," *IEEE Transactions on Antennas and Propagation*, vol. 59, no. 11, pp. 4286–4300, 2011. DOI: 10.1109/TAP.2011.2164175.

[66] L. Luini, "A comprehensive methodology to assess tropospheric fade affecting Earth–space communication systems," *IEEE Transactions on Antennas and Propagation*, vol. 65, no. 7, pp. 3654–3663, Jul. 2017. DOI: 10.1109/TAP.2017.2700883.

[67] [Dataset] Center for International Earth Science Information Network - CIESIN - Columbia University, *Gridded population of the world, version 4 (GPWv4): Population density adjusted to match 2015 revision UN WPP country totals, revision 11*, 2018. DOI: 10.7927/H4F47M65.

[68] Great Britain, Parliament, "The electronic communications (universal service) (broadband) order 2018," Mar. 2018. [Online]. Available: https://www.legislation.gov.uk/uksi/2018/445/contents/made (visited on 11/27/2023).

[69] M. Grant and S. Boyd, *CVX: Matlab software for disciplined convex programming, version 2.1*, Mar. 2014. [Online]. Available: http://cvxr.com/cvx (visited on 11/27/2023).

[70] M. C. Grant and S. P. Boyd, "Graph implementations for nonsmooth convex programs," in *Recent Advances in Learning and Control*, V. D. Blondel, S. P. Boyd, and H. Kimura, Eds., London: Springer London, 2008, pp. 95–110, ISBN: 978-1-84800-155-8. DOI: 10.1007/978-1-84800-155-8_7.

[71] "Satellite Earth stations and systems (SES); broadband satellite multimedia (BSM); services and architectures; BSM traffic classes," European Telecommunication Standard Institute, Sophia Antipolis, FR, Technical specification ETSI TS 102 295 V1.1.1, Feb. 2004.

[72] "End-user multimedia QoS categories," International Telecommunication Union, Geneva, CH, Standard ITU-T G.1010, Nov. 2001.

[73] G. Maral, *VSAT networks*, eng, 2nd ed., ser. Wiley series in communication and distributed systems. Wiley & Sons, 2004, ISBN: 9780470866863.

[74] "Network performance objectives for IP-based services," International Telecommunication Union, Geneva, CH, Standard ITU-T Y.1541, Dec. 2011.

[75] "Method for the determination of performance objectives for satellite hypothetical reference digital paths using adaptive coding and modulation," International Telecommunication Union, Geneva, CH, Recommendation ITU-R S.2131-1, Jan. 2022.

[76] X. Vuong and S. Vuong, "Satellite link margin and availability issues," in *Proceedings of MILCOM '96 IEEE Military Communications Conference*, vol. 1, 1996, 11–16 vol.1. DOI: 10.1109/MILCOM.1996.568575.

[77] "Prediction method of fade dynamics on Earth-space paths," International Telecommunication Union, Geneva, CH, Recommendation ITU-R P.1623-1, Mar. 2005.

[78] C. Lemieux, *Monte Carlo and Quasi-Monte Carlo Sampling*, eng, 1st ed., ser. Springer Series in Statistics. New York, NY: Springer New York, 2009, ISBN: 9780387781655. DOI: 10.1007/978-0-387-78165-5.

[79] C. Capsoni, A. Paraboni, C. Riva, E. Matricciani, L. Luini, G. Gallinaro, G. Nicola, and J. Castro, "Verification of propagation impairment mitigation techniques," European Space Agency, Contract ESTEC20887, Jan. 2011.

[80] N. Jeannin, X. Boulanger, L. Féral, L. Castanet, and F. Lacoste, "Inter-annual variability, risk and confidence intervals associated with propagation statistics. Part I: Theory of estimation," *International Journal of Satellite Communications and Networking*, vol. 32, no. 5, pp. 407–421, 2014. DOI: 10.1002/sat.1060.

[81] H. Dong and M. K. Nakayama, "A tutorial on quantile estimation via Monte Carlo," in *Monte Carlo and Quasi-Monte Carlo Methods*, B. Tuffin and P. L'Ecuyer, Eds., Cham: Springer International Publishing, 2020, pp. 3–30, ISBN: 978-3-030-43465-6.

[82] "B-ISDN ATM layer specification," International Telecommunication Union, Geneva, CH, Standard ITU-T I.361, Feb. 1999.

[83] International Telecommunication Union (ITU), *Handbook on Satellite Communications*, eng, 3rd ed. Geneva, CH: Wiley, 2002, ISBN: 9780471221890.

[84] R. Peters, P. Woolner, and E. Ekelman, "Analytic calculation of noise power robbing, NPR, and polarization isolation degradation," in *26th International Communications Satellite Systems Conference (ICSSC)*, Jun. 2008. DOI: 10.2514/6.2008-5509.

[85] *Radio regulations*, eng, Edition of 2016. Geneva, CH: International Telecommunication Union, 2016, ISBN: 978-92-61-17791-1.

[86] A. J. Erich Lutz Markus Werner, *Satellite Systems for Personal and Broadband Communications*, eng, 1st ed. Berlin, Heidelberg: Springer Berlin, Heidelberg, 2002, ISBN: 9783642597275. DOI: 10.1007/978-3-642-59727-5.

[87] O. Vidal, "Next generation high throughput satellite systems: Advanced interference based system techniques," Ph.D. dissertation, Institut Supérieur de l'Aéronautique et de l'Espace, Oct. 2014.

[88] R. E. Collin, *Antennas and radiowave propagation*, eng, ser. McGraw-Hill series in electrical engineering. New York: McGraw-Hill, 1985, ISBN: 0-07-011808-6.

[89] C. Paoloni, D. Gamzina, R. Letizia, Y. Zheng, and N. C. Luhmann, "Millimeter wave traveling wave tubes for the 21st century," eng, *Journal of electromagnetic waves and*

applications, vol. 35, no. 5, pp. 567–603, 2021, ISSN: 0920-5071. DOI: 10.1080/09205071.2020.1848643.

[90] "Application for fixed satellite service by SES-17 S.a R.L.," Federal Communications Commission, Technical Report SATPPL2019030500014, Mar. 2019.

[91] "Probability distributions relevant to radiowave propagation modelling," International Telecommunication Union, Geneva, CH, Recommendation ITU-R P.1057-6, Aug. 2019.

[92] D. I. L. de Villiers and R. Lehmensiek, "Rapid calculation of antenna noise temperature in offset gregorian reflector systems," *IEEE Transactions on Antennas and Propagation*, vol. 63, no. 4, pp. 1564–1571, 2015. DOI: 10.1109/TAP.2015.2399933.

[93] "Time series synthesis of tropospheric impairments," International Telecommunication Union, Geneva, CH, Recommendation ITU-R P.1853-2, Aug. 2019.

[94] T. A. Manteuffel, "An incomplete factorization technique for positive definite linear systems," *Mathematics of Computation*, vol. 34, pp. 473–497, 1980. DOI: 10.1007/BF01740546.

[95] S. Kotz, N. Balakrishnan, and N. Johnson, *Continuous Multivariate Distributions, Volume 1: Models and Applications*, ser. Continuous Multivariate Distributions. Wiley, 2004, ISBN: 9780471654032. DOI: 10.1002/0471722065.

[96] C. Cortes and V. N. Vapnik, "Support-vector networks," *Machine Learning*, vol. 20, pp. 273–297, 1995. DOI: 10.1023/A:1022627411411.

[97] I. del Portillo, B. Cameron, and E. Crawley, "Ground segment architectures for large LEO constellations with feeder links in EHF-bands," in *2018 IEEE Aerospace Conference*, 2018, pp. 1–14. DOI: 10.1109/AERO.2018.8396576.

[98] L. M. Tomaz, C. Capsoni, and L. Luini, "Model to scale rain attenuation time series with link elevation angle for LEO satellite based systems," *Radio Science*, vol. 58, no. 1, e2022RS007551, 2023. DOI: 10.1029/2022RS007551.